12-1-2012

Plasma test on Industrial Diamond Powder in Hydrogen and Air for Fracture Strength Study

Rohit Asuri Sudharshana Asuri Sudharshana Chary
University of Nevada, Las Vegas, asurisud@unlv.nevada.edu

Follow this and additional works at: https://digitalscholarship.unlv.edu/thesesdissertations

Part of the Materials Science and Engineering Commons, and the Mechanical Engineering Commons

Repository Citation

PLASMA TEST ON INDUSTRIAL DIAMOND POWDER IN HYDROGEN AND AIR

FOR FRACTURE STRENGTH STUDY

By

Rohit Asuri Sudharshana Chary

Bachelor of Technology in Mechanical Engineering

Jawaharlal Nehru Technological University, India

May 2009

A thesis submitted in partial fulfillment

of the requirements for the

Master of Science in Mechanical Engineering

Department of Mechanical Engineering

Howard R. Hughes College of Engineering

The Graduate College

University of Nevada, Las Vegas

December 2012

THE GRADUATE COLLEGE

We recommend the thesis prepared under our supervision by

Rohit Asuri Sudharshana Chary

entitled

Plasma Test on Industrial Diamond Powder in Hydrogen and Air for Fracture Strength Study

be accepted in partial fulfillment of the requirements for the degree of

Master of Science in Mechanical Engineering
Department of Mechanical Engineering

Zhiyong Wang, Committee Chair

Brendan O'Toole, Committee Member

Vellore Venkatesh, Committee Member

Venkatesan Muthukumar, Graduate College Representative

Thomas Piechota, Ph. D., Interim Vice President for Research and Graduate Studies and Dean of the Graduate College

December 2012

ABSTRACT

PLASMA TEST ON INDUSTRIAL DIAMOND POWDER IN HYDROGEN AND

AIR FOR FRACTURE STRENGTH STUDY

by

Rohit Asuri Sudharshana Chary

Dr. Zhiyong Wang, Examination Committee Chair

Associate Professor of Mechanical Engineering

University of Nevada, Las Vegas

Diamonds are the most precious material all over the world. Ever since their discovery, the desire for natural diamonds has been great; recently, the demand has steeply increased, leading to scarcity. For example, in 2010, diamonds worth $50 billion were marketed. This increased demand has led to discovering alternative sources to replace diamonds. The diamond, being the hardest material on earth, could be replaced with no other material except another diamond. Thus, the industrial or synthetic diamond was invented. Because of extreme hardness is one of diamond's properties, diamonds are used in cutting operations. The fracture strength of diamond is one of the crucial factors that determine its life time as a cutting tool.

Glow discharge is one of the techniques used for plasma formation. The glow discharge process is conducted in a vacuum chamber by ionizing gas atoms. Ions penetrate into the atomic structure, ejecting a secondary electron. The objective of this study is to determine

the change in fracture strength of industrial diamond powder before and after plasma treatment. This study focuses mainly on the change in crystal defects and crushing strength (CS) of industrial diamond powder after the penetration of hydrogen gas, air and hydrogen-air mixture ions into the sample powder.

For this study, an industrial diamond powder sample of 100 carats weight, along with its average fracture strength value was received from Engis Corporation, Illinois. The sample was divided into parts, each weighing 10-12 carats. At the University of Nevada, Las Vegas (UNLV), a plasma test was conducted on six sample parts for a total of 16 hours on each part. The three gas types mentioned above were used during plasma tests, with the pressure in vacuum chamber between 200 mTorr and 2 Torr. The plasma test on four sample parts was in the presence of hydrogen-air mixture. The first sample had chamber pressures between 200 mTorr and 400 mTorr. The remaining three samples had chamber pressures between 600 mTorr and 1 Torr. The fifth sample part underwent plasma in the presence of atmospheric air, due to accidental closing of the hydrogen valve, at pressure levels 200 mTorr to 400 mTorr. On the last sample, the plasma test was carried out in hydrogen gas at pressures of 1 and 2 Torr. X Ray Diffraction (XRD) was conducted at UNLV before and after plasma tests. The samples were shipped back to Engis Corporation to test the difference in CS after plasma treatment.

 The XRD results revealed that plasma experiment had no significant change in lattice constants on diamond powder. However, the crystal defect concentrations increased due to change in full width half maximum (FWHM), but the samples are in a highly crystalline state since the change is very small. FWHM after plasma is higher than that before plasma. This confirms a change in defect concentration after plasma. The plasma

test conducted in hydrogen gas increased the CS of diamond powders by 0.4%. The CS of the plasma treated sample in air was 1.4% above the average crushing strength. From the four plasma samples of hydrogen-air mixture, the plasma performed at pressures of 200 mTorr to 400 mTorr had a higher CS than the average value by 4.4%. The other three samples had CS between 49-50% which was lower than the average value.

These experiments suggest that the plasma test conducted in pure hydrogen gas proved to increase the crushing strength of diamond powders. However, it is possible that limiting the pressure values below 400 mTorr during plasma experiment in pure hydrogen could give better crushing strength results. Plasma test performed in hydrogen- air mixture yielded better CSI results compared to plasma tests conducted in only hydrogen or only air.

ACKNOWLEDGEMENTS

I deeply express my sincere gratitude to my advisor Dr. Zhiyong Wang for trusting my abilities to work on this project. His invaluable guidance, suggestions and thoughts throughout the entire course of this research work is priceless. It has been very rewarding and satisfying experience to be able to work with him. I am also grateful to the Department of Mechanical Engineering, University of Nevada, Las Vegas for providing me the opportunity to pursue my master degree. I would like to thank Dr. Brendan O'Toole, Dr. V.C. Venkatesh and Dr. Venkatesan Muthukumar for their time in reviewing the prospectus, participation in defense of the thesis as committee members.

This thesis has been a challenging experience and was accomplished with the help of many people. I would to like to thank Dr. Robert Schill, for all his help and kindness to allow me to use the experimental apparatus in his laboratory. I would like to thank Dr. Thomas Hartmann for all his guidance during XRD. I would like to thank Kevin Nelson for his help during machining. I would like to appreciate and thank graduate students, Sean Andersen and Shaoru Garner for their support throughout the experiments. I would like to extend my thanks to Srikanth Madala, Ph.D. student, for all his support.

Last but not the least, I thank my parents, family, friends, and all the other people whom I have not mentioned above but have helped me in some way throughout the completion of my master degree. I would like to take this opportunity to express my gratitude to those who have helped me bring this thesis to a successful end with their knowledge, help and co-operation.

Table of Contents

LIST OF TABLES

LIST OF FIGURES

CHAPTER 1

INTRODUCTION

Diamond has been one of the fascinating items to mankind since centuries. In a lecture "On Diamonds" seventy-five years ago Professor Maskelyne said, "The diamond is a substance which transcends all others in certain properties to which it is indebted for its usefulness in the arts and its beauty as an ornament. Thus, on the one hand, it is the hardest substance found in nature or fashioned by art. Its reflecting power and refraction energy, on the one hand, exceed those of all other colorless bodies, while it yields to none in the perfection of its pellucidity "[1]. Due to high hardness, diamond is a useful tool in cutting operations. Wear resistance of diamonds determine their life as cutting tool [2]. High fracture toughness or Impact strength of diamond increases their wear resistance, which in turn increases their tool life [3].

1.1. Background

The word diamond comes from the Greek word adámas, meaning adamant or unbreakable [4]. Diamonds have history backed to over 3,000 years ago in India. Mostly found in a region from central India towards the Deccan plateau, major diamond mines were said to be located in the kingdom of Golconda ruled by Nizam [1]. These diamonds were sold to major continents for their use. As years passed by, the craving for diamonds increased with people familiar with its advantages in various fields. In 2010, the requirement was worth 50 billion dollars [5]. Diamond became scare. As a result, methods to produce industrial or synthetic diamonds were developed.

1

During 1800s, scientists experimenting on all the possible discoveries came with various stones of diamond. J. Ballantine Hannay credited with making the first synthetic diamond in 1880 by applying high heat and pressure to coal [6]. Evalyn Walsh McLean man-made diamonds have taken the place of natural diamonds. According to a news column, "My Say" written for the Washington Times- Herald, their use in drills could "open up untold wealth for the country" [6]. However, it was not until 1950s, the countries during World War II invented various methods of destructive violence, used diamond in nuclear weapons. After repeated struggle by diamond industries over years created history as Synthetic diamond was patented in 1954 by scientists of General Electric. The patent was kept secret until it was revealed to the world on February 15, 1954. Figure 1.3 shows a 1/1000th of a carat weight first jewelry diamond produced in New York by General Electric Company[2][7]. It is of the size 1/16th of an inch. Figure 1.1 shows the apparatus for producing the first artificial diamond used by General Electric Company. The machine weighs 1,000 tons applying a pressure of 100,000 atmospheres at 1.6 million pounds per square inch [4].
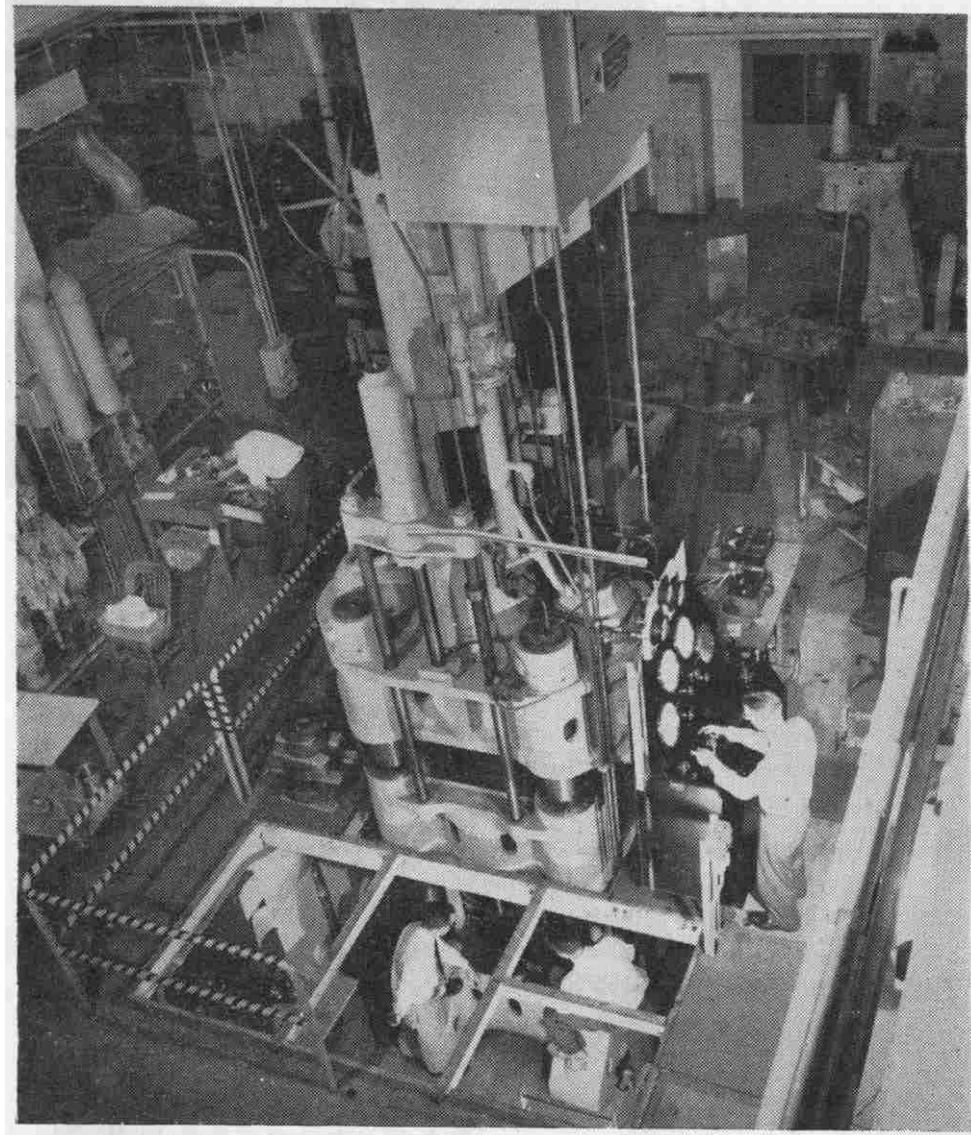
Figure 1.1. First manmade diamond apparatus [8]

Synthetic or artificial diamonds are produced by process involving catalytic high pressure and high temperature synthesis. The pressure and temperature applied determines the growth rate and nucleation. These are directly related to the mechanical strength of the crystal. The greater the crystal defects the less is the strength of the crystal [9]. Impurities and crystalline structure are important factors for fracture characteristics. Impurities weaken structural bonds leading to high defects during crystal growth. Due to uniform

3

expansion formed by atomic strains, the uniform distribution of impurities does not generate macro stresses; otherwise, leading to large elastic stresses [10].

Research experiment done by Dr H. P. Bovenkerk et.al [11] from the Chemistry Research Department-at the General Electric Research Laboratory in Schenectady, New York, used the idea of various methods of diamond formation. The direct transition of graphite to diamond was their first experimental work. The process of vaporization of carbon requires high heat (more than 100 k.cal./gm. mol.) indicates the need for high temperatures before much recrystallization of the carbon can occur. The usual temperatures for graphite formation industrially from petroleum-coke are between 1,800-2,400ºC. This research team performed tests in the laboratory on the graphitization of diamond at 0.1 and 20,000 atm. The test results showed graphitization beginning at 1,500-2,000ºC. Temperatures of a higher range were necessary to graphitize diamond at 20,000 atm compared to 0.1 atm.

The research group also stated that experiments in which graphite was heated at high pressure, where its density became nearly identical to the theoretical density of graphite, no diamond was formed even after a pressure of 120,000 atm [11].This was due to strong bonding between the sheets of atoms in the graphite, which requires much higher pressure. The required pressure is in the region of 200,000 atm. However, experiments with such high pressures have never been conducted. Figure 1.2 shows a photomicrograph image of diamond crystals prepared during experimentation.

Many other chemical systems were studied with respect to diamond synthesis involving carbon and oxygen, salt-like carbides, and other chemical reactions. The following results were derived:

1) Temperature and pressure of the diamond should be relatively stable throughout.

2) Many catalytic metals can be used for the effective growth of small diamond crystal. A few examples are rhodium, palladium, osmium, iridium or platinum, chromium, manganese, iron, cobalt, nickel, ruthenium. Among these Tantalum is very powerful metal as catalyst.

3) The rate of growth of diamond crystals can be as high as 0.1mm/min

4) The transformation from carbon to diamond occurs at a very thin layer. This can be possible only with the presence of catalyst.

5) The amount of solubility of carbon in the catalyst and also the temperature of the mixture are both major factors in diamond formation.

6) Any foreign particle present in the carbon will not hinder diamond formation. Thus the catalyst has to be in powder form, thoroughly mixed without any impurities.

7) Diamond forming cannot always be guaranteed. Even graphite that is rich in carbon, when pressed under high temperature and pressure, may not convert into diamond.

8) Diamond crystals of good quality can be formed only from regular graphite. Materials like carbon black and sugar charcoal may not yield good results.

9) Diamond crystal color varies when formed at different temperatures. Low temperature give black in color which changes to dark green, light green, yellow and white at high temperature. Green and yellow indicates imperfect crystal formation.
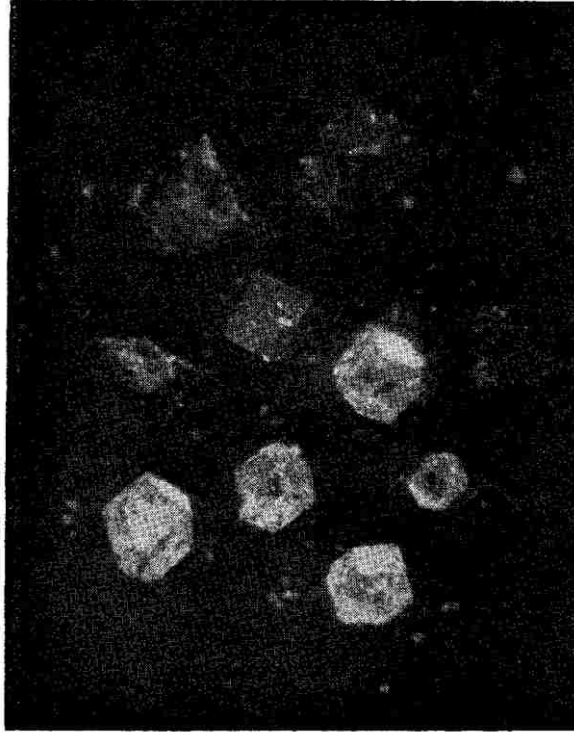
Figure 1.2: Artificial Diamond crystals [11]
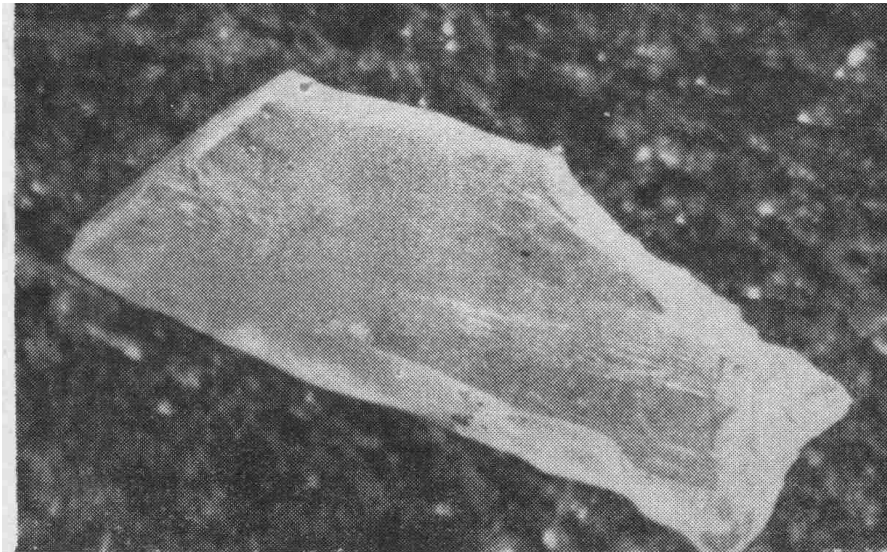
Figure 1.3: Largest artificial diamond formed. It is 1/16thof an inch lengthwise [8]

1.2. Difference between Natural and Industrial Diamonds

Natural diamonds that are mined under the earth's surface have been formed many thousands of years ago. They are available in various sizes. When polished professionally, the expensive glowing gemstone results. Diamonds are the hardest substance on Earth with a Mohr's scale reading of 10 [12]. Diamonds are crystal clear gems having high thermal conductivity, however not good conductors of electricity. They tend to have various colors, depending on their percentage and type of trace impurities. Boron and nitrogen are the major kinds of impurities found in diamonds [12]. Single dissolved nitrogen, boron or hydrogen atoms cause the surrounding diamond lattice to expand by 40%, 33.7% and 31%, respectively [10]

1.2.1. Types of Diamond

Diamonds are categorized into various types with respect to the impurity percentage of nitrogen. [12].

Ia: These have nitrogen percentage of up to 0.3, the most commonly found diamond.

Ib: These have 550ppm of nitrogen. Industrial diamonds commonly fall under this category.

IIa: These have a very little nitrogen content in them. This type of diamond is very rare to find. [13].

IIb: These are very rare ones too, which have even less nitrogen than type IIa.

The other forms of impurities in synthetic diamond result from nickel, iron, and cobalt. These are the most commonly used components of catalysts. YueMeng et.al [14] concluded that cobalt related impurities can be found when crystal is annealed to a high temperature of 1800^0C, however they found no iron components. X-Ray Fluorescence (XRF) microanalysis on a diamond crystal layer showed nickel impurities dispersed and incorporated, but not present as a separate phase, iron whereas is present in a oxidized form. Figure 1.4 shows the diamond crystal used for experiment on impurities.
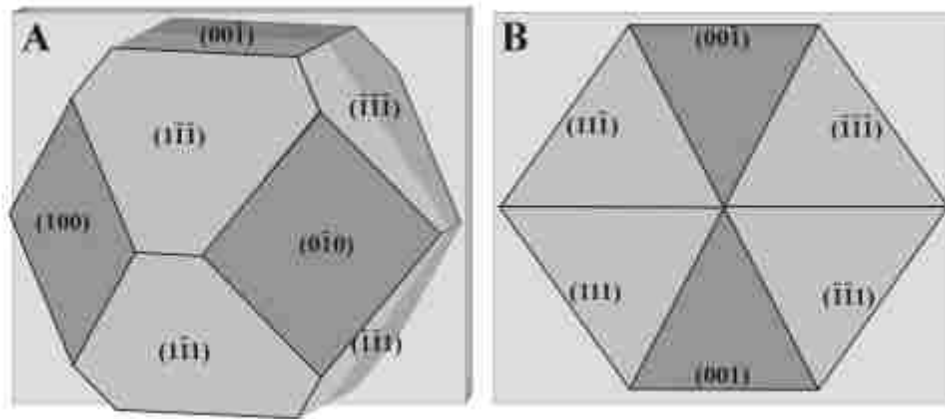
Figure 1.4: Diagram of diamond crystal used for impurities experiment [14]

Industrial diamonds are formed by synthesis. The graphite, along with catalyst, is placed in a container, which undergoes high pressure and high temperature (HPHT) over a specific period. The pressure is around 53,000 times more than atmospheric pressure and the temperature is greater than 5000^0F [8].This results in the formation of diamond a few millimeters in size. These cannot be used in jewelry due to many flaws in structure; however they can be used as cutting tool. With the current increase in technology, these flaws can be removed to the point that in recent years, the difference between natural and industrial diamond is hard to determine with naked eye. They can be distinguished only

with a high technology machine used to determine the difference in crystal structure. One such machine is patented by De Beers [15]

1.2.2. Microstructure Difference

Comparison of the microstructure between natural and industrial diamonds cannot be made easily. The recent technological developments have been made to reproduce an artificial diamond that is same as a natural in appearance. According to detailed study by De et.al[16] Carbonado was used as a comparison for natural diamond as author defines it the hardest diamond found, exhibiting good hardness and high thermal conductivity. The wear of carbonado is uniform as compared to a single- crystal diamond, which varies in crystallographic orientation. The diamond- diamond bonding is very tight which made it the first choice to reproduce it by artificial sintering. A diamond powder sample of average grain size 5-7 μm was selected to experiment supplied by General Electric Company Super abrasives.

The experiment was conducted on a multi- anvil press at Geophysical Laboratory, at the Carnegie Institution in Washington, D.C. The diamond powder was sealed in molybdenum capsules without a catalyst. Pressure of 1GPa/hr was applied and temperature of 80°C/min. A series of experiments was conducted to determine the right temperature, pressure and time required.

Powder was initially sintered at 6GPa at temperatures varying between 1200°C, 1600°C and 1800°C for 6, 3, 3, hours, respectively. The highest temperature of 1800°C was clear failure as the product that was formed showed a completely different texture. Both at

1200°C and 1600°C temperatures, the crystal had a good bonding; however the internal

structure of 1600°C had a higher pore space. The second experiment was conducted to

determine the right pressure. Two pressures were used, 6GPa and 8GPa. The higher

pressure yielded good results with low dislocation densities, shown in Figure 1.5. These

experiments proved that the grain boundaries of artificial and natural diamonds were

similar. By varying the time from 2, 3, and 6 hours there was no comparable variation in

the product. The higher sinter time had a higher dislocation.
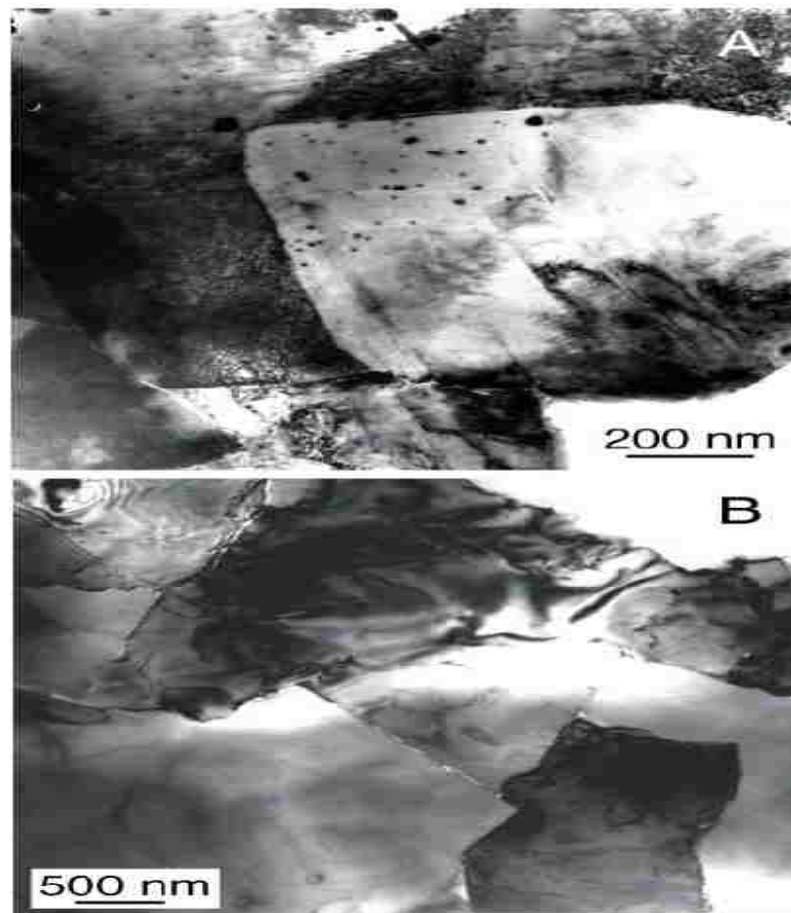
Figure 1.5: Transmission Electron Microscope (TEM) image showing low dislocation

densities a) grain boundary of an artificially sintered diamond and b) grain boundary of a

natural diamond[16]

By using the optimum numbers for temperature (1200°C), pressure (8GPa), and time (2hrs), the sinter technique did not reproduce similar to natural diamond. However, there were a few matches in properties, for example, the diamond grain orientation, which was same in both the crystals. Even so, the artificial diamond showed significant gaps, and small crystals formed between the large grains indicated that the toughness is not matched. Figure 1.6 shows the grain boundaries in sintered and natural diamond.
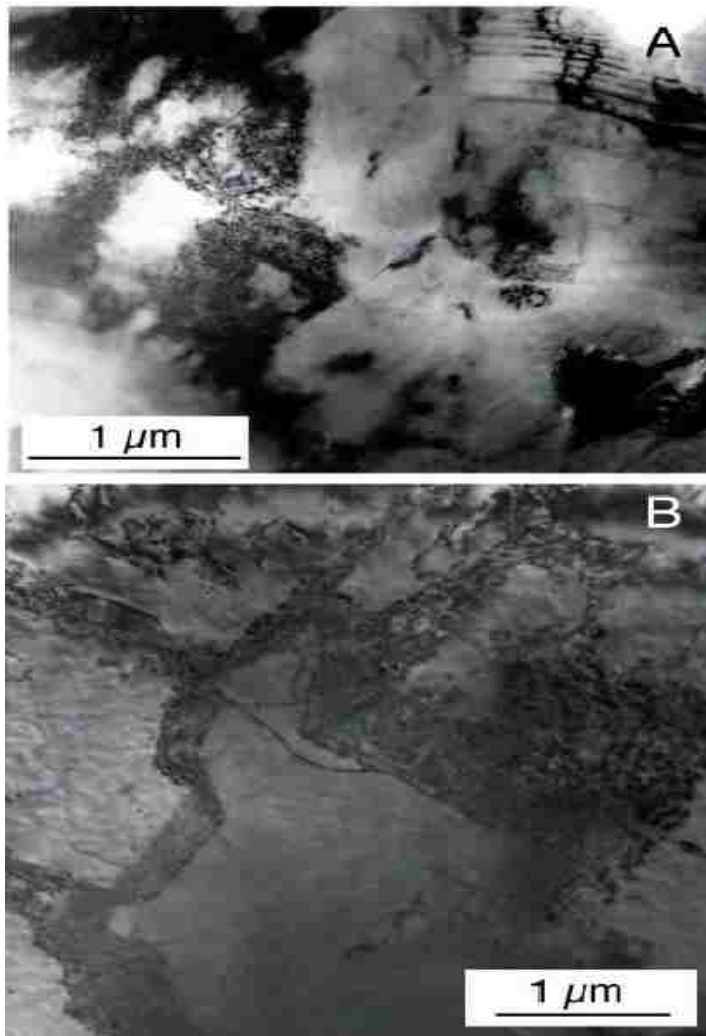
Figure 1.6: Grain boundaries in a) a sinterd at 8GPa and 1200°C b) a natural carbonado diamond [16]

1.3. Cutting Tool

Diamonds are insulating material and thermally stable which makes them useful at high temperatures. This led to providing thin film coating of diamond on material for various cutting tool operations [17]. About 250 tons of industrial diamonds are being consumed each year around the world in cutting tool industries [18]. Cutting tools for metal cutting have many shapes. Each tool shape has a specific purpose in metal cutting. Diamond cutting was penetrating into Europe from India in 1456.A lapidary Louis Van Berquen, a Belgian living in the city of Bruges, was believed to be the first to discover the art of cutting and polishing diamonds by their powder. But this information has no proper reference [1].

Wentorf Jr. et al.[19] indicated that polycrystalline diamond was more effective than natural diamond as a cutting tool for wheel dressers and cut-off wheels. This is due to its high strength and resistance to shock wave. This research group invented the diamond tool as a mass of crystals bonded together for cutting instead of making a single point cutting tool. Various experiments have proved that single point tool is not very effective in high stress conditions which led to this invention [20]. The metallic substances in the form of powder are mixed thoroughly, with diamond crystals embedded. These are subjected to high temperature and pressure to sinter about the diamond. These are brazed on to the tool holder.

Diamonds are used for various cutting operations for a smooth finish and low cost. They are used in grinding wheels and dental instruments for increased productivity. A good diamond cutting tool is determined by the characteristics that result during hard press.

The amount of pressure and temperature applied during formation reveals its strength as a cutting tool. Weak bonding of atoms might result in cracks. The size of the chemical composition affects the binding strength between diamond and surrounding metal matrix [21][22]. The life of diamond tool depends on its bonding strength to the base metal. Steel is a commonly used base metal as a diamond holder. A metal matrix includes nickel, cobalt and magnesium. Figure 1.7 shows images of diamond bonded to base by metal matrix. Electrolyte and electroless coatings are used for nickel and cobalt metals. An electrolyte coating has low hardness $300H_v$ and cannot be applied on complex shapes. In comparison an electroless coating allows controlled plating thickness to be possible on all complex structures; it also has a hardness of 1000 H_v after post plating heat treatment[21].

Figure 1.7: Scanning electron microscope (SEM) image of a diamond and metal matrix [22][23]

Bert Brenner et.al [24] patented the preparation of a diamond tool. This group kept in mind a few conditions such as uniform distribution, non-dislocation from initial position, cracks, and bruises throughout the life cycle of the diamond. An initial test was conducted by coating with gold or silver and re-coating with copper. This did not prove to be an effective method, as large air gaps were formed, leading to cracks. A second trial

experiment of platinum coating containing chloroplatinic acid (6% by weight) was added

with solvents Ethyl alcohol (57% by weight) and Ethyl Ether (32% by weight) along with

turpentine (5% by weight) as used as the wetting agent. These were combined in a tub

along with diamond crystals. The tub was heated to a high enough temperature such that

the acid broke down and solvent vaporized, leaving platinum form as a thin layer over the

diamond. These crystals were reheated so that the platinum layer adhered firmly to the

surface of the diamond.

Coated diamonds are put in an electrolytic tub, with nickel as a bonding metal, evenly

distributed along the base metal, which is stainless steel. Electrolysis was used to deposit

the nickel as the base metal so that the diamond was not dislocated, even after repeated

use as a cutting tool. Brenner discovered that a platinum coating has more advantages

than silver or gold, as there was no air gaps formed. During the operation, the

temperature of the cutting tool was raised to around 800^0C, above the range of silver and

gold, causing displacement in the tool.

1.4. Applications

The major criteria for a metal-cutting industry were to improve performance and reduce

cost. The increase in inventions and discoveries has paved the way for a high quality

standard of the product. Recent inventions have various complex designs creating a need

for precision cutting tools. With advancements in science and technology, applications of

cutting-tool components have increased. Such features as high speed and dry machining

increased the use of polycrystalline diamond as a cutting tool. These tools have high

hardness, good toughness, and extreme thermal conductivity. Molds and dies made from

ferrous materials are good examples, and their major applications are in the field of optics

and lenses. Aluminum scanner mirrors, the aluminum substrate drum used in

photocopying machines, and the computer memory disk were major products produced

during 1980's. The diamond tools were used for high precision finish of tens of

nanometer [25]. Other advantage is the high quality of surface finish. Figure 1.8 and 1.9

show X-Ray telescope mirrors and cylindrical mirrors for Synchrotron orbital Radiation

(SOR) as examples.
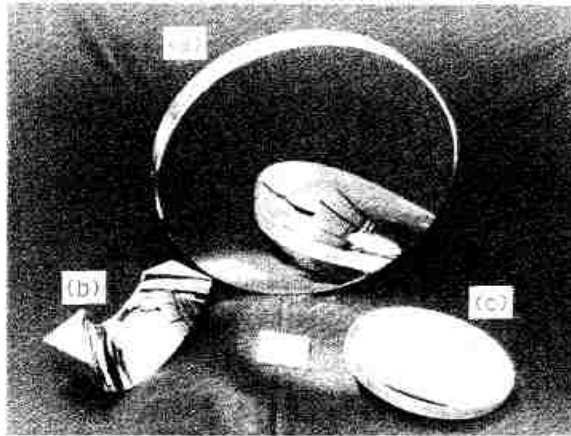
Figure 1.8: Diamond turned curved mirrors [25]

a) Large concave mirror, 600mm; b) Off- axis parabolic mirror; and

c) Concave mirror, 300mm
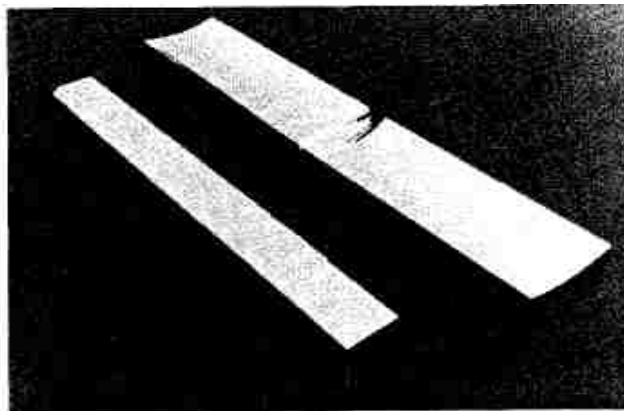
Figure 1.9: Toroidal mirror for Synchrotron Radiation [25]

15

As indicated by Scott et.al [26] the polycrystalline diamond cutter was developed around 1973, when General Electric Company introduced the Compax diamond drill blanks for oil and gas drill bits. This was a carbide disc 0.330 in (8.38 mm) diameter by 0.110 inc (2.8 mm) thick, with a 0.020 in (0.5 mm) thick PDC layer that was un-chamfered. Figure 1.10 shows a diagram image of cutter. A tungsten carbide insert (TCI) bit by the Hughes Tool Company was introduced, paving way for increased tool life and machinability. Taking the ideas and suggestions from many key customers and entrepreneurs, a tool was first introduced in December 1776 [26]. This was 13 mm with good impact resistance as compared to older version of 8mm.
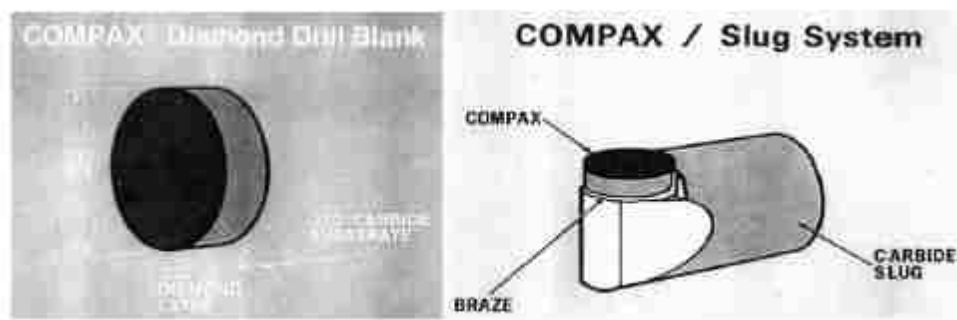
Figure 1.10: Polycrystalline diamond cutter diagram – COMPAX [26]

Since then, many inventions have taken place through late 1980's in the field of drilling practices, bit designs, hydraulics, and cutters. These carved way for improved cutter technology, helped by means of the commercial success of the polycrystalline diamond (PCD) cutter. Competition in the cutter field and a growing bit market helped drive the technology forward. There was rapid growth in drilling activity in the late 1970's and early 1980's, and a subsequent rapid fall, due by surplus supply and low oil prices in the mid 1080's [26].From 1990's on, there has been a vast improvement in these tools.

16

Cutters over 4mm thick have been introduced, raising the ranges for durability, wear resistance, consistency as well as extending the types of applications for these tools.

Saw industry also has a wide range of applications for diamond tools. This industry accounts for one-third of the total world consumption of diamond tools [18]. The major application is in construction industry for use with hard materials, such as concrete and rocks. These substances require large grits of a cubo-octahedral shape produced only by 3 companies in the world: General Electric Company USA, De Beers and Iljin in South Korea. Saws come in three shapes; circular, frame and wire. . Figures 1.11 shows the different shapes and sizes of a diamond saw. The wire-shaped is the most popularly used type due its flexibility of using in manufacturing complex shape parts. Sawing can be done in the holes and inner surfaces using wire. High speed, long life, and low cost are the major requirements of a good saw. These can be achieved by properly placing the diamond at a good distance from each other so as to not create an overload of grit as seen in figures 1.11 and 1.12.

Figure 1.11: Various types of diamond saws [18]
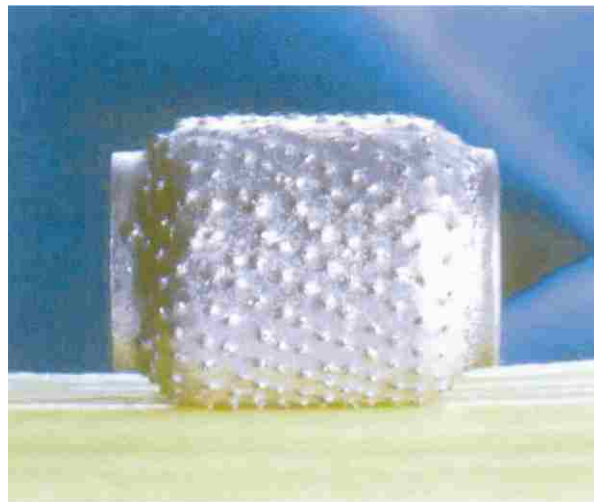
Figure 1.12: Planned grit placement of diamond saw[18]

CHAPTER 2

PLASMA

Plasma is defined as a state similar to solids, liquids and gases that has charged particles. This term was first used in 1927 by Irvine Langmuir [27]. Plasma is formed by the ionization of atoms [28].The difference between the states of matter can be distinguished by the strength of bonding between the atoms. The binding in solids is the strongest compared to liquids, which is stronger compared to the gaseous state [29].The phase after gaseous state is plasma formed by applying an external force to dissipate the molecular bonding [30].

Plasma does not contain any defined shape. Plasma contains free electrons and ionized atoms that move around within the area where the plasma is formed. These are attracted towards each other by electrostatic, or coulombic force. Plasma is formed by providing an external source that increases the temperature of a substance. When the temperature rise reaches a maximum limit, the atoms are ionized. Plasma can be used to increase the strength of a material and reduce crystal defects by implanting gas ions[31][32].The plasmic source can be formed naturally or artificially[30].

2.1. Types of Plasma

Plasma is divided into two types as natural and artificial plasma.

2.1.1. Natural Plasma

Research has determined the existence of plasma formed naturally in the universe. Since the plasma occurs at high temperatures, an abundance of plasma can be at the sun [28].The major gases present in the sun are hydrogen and helium, which generate vast amounts of energy by means nuclear fusion [33].The high temperature does not allow the atoms to bond, resulting in plasma. The solar atmosphere around the sun consists of three regions around it [34][35].

The sun we observe from the Earth is one of the regions, referred to as the photosphere. This is the region from which the white light is emitted to the earth's surface. The layer surrounding the sun is called the chromosphere. This is formed around the photosphere, emitting gases. The outer most region is called the corona extending itself into the outer space. This region, best viewed during solar eclipse is in the form of hot plasma formed by solar magnetic field [36]. Figure 2.1 shows the magnetic field. Figures 2.2 and 2.3 shows the regions of the sun.

Figure 2.1: Magnetic field on the surface of the sun [37]
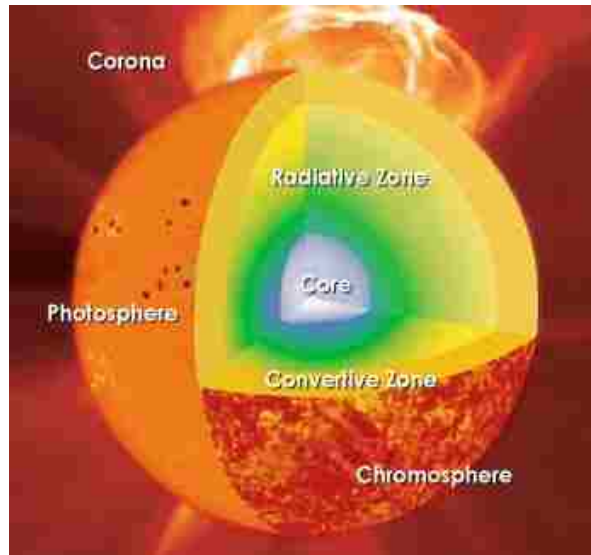
Figure 2.2: Structure of Sun [38]

The corona and the solar magnetic field extend to a far off distance into the space; this is known as a solar wind, and contains electrons and protons emitted by the sun reacting with the Earth's Magnetosphere [29].

Figure 2.3: Corona [36]

2.1.2. Artificial Plasma

Artificial or laboratory plasma is divided into two types: High- temperature plasma also called as fusion plasma, low temperature or gas discharge plasma.

Artificial plasmas are created mainly in two ways [30].

1) Photo ionization, which occurs by electro-magnetic radiations interacting with the gases resulting in breaking the atoms into electrically charged particles. Ionization can be produced by X-Ray or Gamma Rays which absorbs the photons.

2) Gas discharge process has a high potential difference applied across the electrodes in the chamber. Plasma glow discharge has three particles or species: electrons (negative charge), ions (positive) and neutral atoms. The potential difference breaks the gas in the chamber into ions and electrons. The free electrons energize and collide with other atoms.

   The various types of gas discharges are:[39]

   a. Direct current (d.c) glow discharge.

      If the potential difference in the chamber is constant, it results in a constant direct current called as d.c glow discharge.

   b. Capacitive coupled discharge, using Radio frequency.

   The potential difference applied is varied by time. The target is bombarded by ions and electrons alternatively for each half-cycle. This process does not charge to be built at one electrode. It is best used when working with dielectric films. During plasma the electrodes get covered with insulating

material. An alternating voltage power is supplied in radio frequency range at 13.56 MHz [39].

Gas discharges are further classified into a local thermal equilibrium and a non-local thermal equilibrium based on pressure in the plasma. Thermal equilibrium refers to equal temperatures of all the species in localized areas of the plasma. At high pressure, the energy exchange between species is efficient due to a large number of collisions, leading to equal temperatures. However, low pressure results in only a few collisions, leading to inefficient energy transfer and causing variable temperatures of different species. Thermal equilibrium occurs at high temperatures, from 4000 K for cesium (Cs) to 20000 K for Helium. Equilibrium temperatures are applicable for cutting, spraying, and welding; non-equilibrium temperatures are used for etching and film deposition processes [39] .Figure 2.7 shows the V-I characteristics of Direct Current glow discharge. The first section is the dark discharge region. In this region there is no glow as the energy is low since ionization begins as a natural process. The rate of ionization increases with applied voltage and reaches a breakdown point. At this point glow discharge region begins due to breakdown of gas atoms in the vacuum chamber. Figure 2.5 shows various regions in a glow discharge. Arc discharge has high current density which may damage the electrodes [27] .
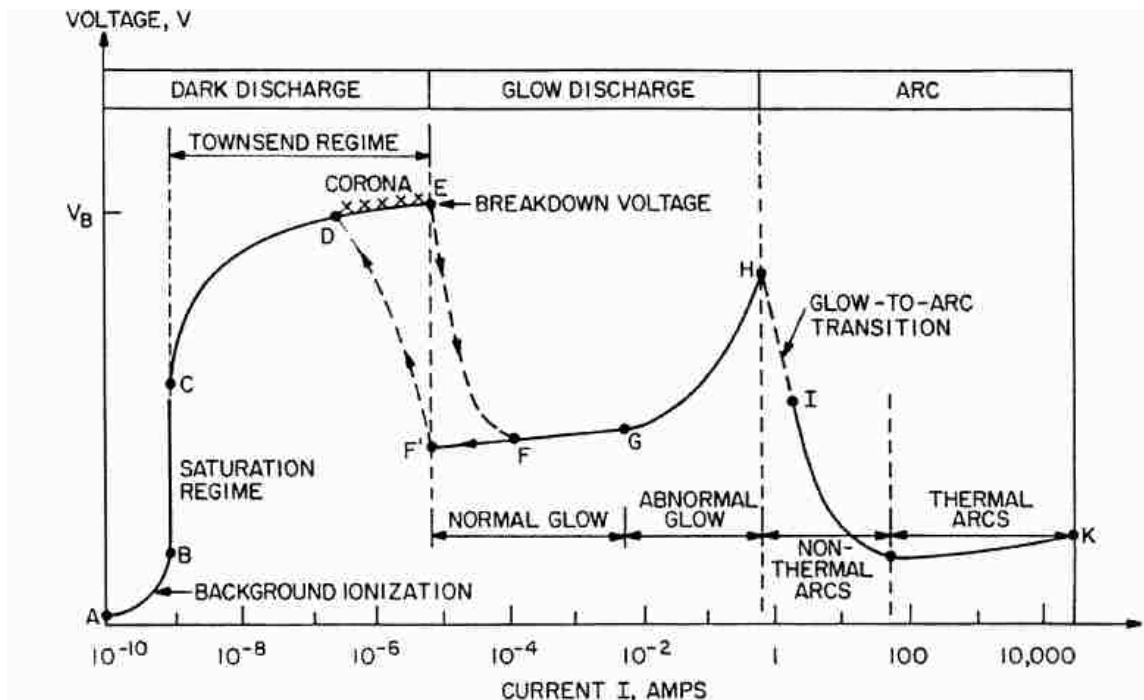
Figure 2.4: V– I Characteristics of DC glow discharge [27]

2.2. Plasma Process

Glow discharge is maintained in plasma by Ionization. The degree of ionization varies from 100% for fully ionized gases to $10^{-4} - 10^{-6}$ for partially ionized gases [39] . When an atom is hit by a primary electron, it removes the electron from the bond, creating two electrons and one ion. The electric field accelerates the electrons, which creates more ions. Ionization potential is the minimum energy required to break the atom, measured in terms of electron volts. Ionization potential can be explained by the potential difference applied in volts between two points to accelerate the electron multiplied by electron charge e, indicated as eV. Recombination of an electron with a positive ion forms a neutral atom. But this is not possible in a single step. The ions and electrons are combined to maintain the ratio of particles by applying an external source [27].

24

Excitation does not remove the electron from the atom, as compared to ionization. It only moves the electron to a higher level within the atom absorbing the energy. Hence, the primary electron loses kinetic energy and gets deflected. The light glow in a plasma discharge is due to relaxation of the electron after excitation [30]. Excited electrons have a very small life time, only a few nanoseconds. Due to its instability, an excited electron returns back to its original form, and emits photon of a specific energy (ΔE). The density of electrons and ions are equal, but less than the density of neutral atoms [30].

2.3. Plasma Apparatus

Plasma is attained at a pressure level around 10 Torr or less [40]. This is created in a closed plastic tube between two electrode plates on either end. The ionization and excitation processes are the major source of glow in the negative region. Positive glow fills a major percentage of space between the electrodes. Glow discharge or plasma is the negative column formed close to the cathode. Between the glow regions is the Faradays dark space. Figure 2.5 shows the various glow regions.
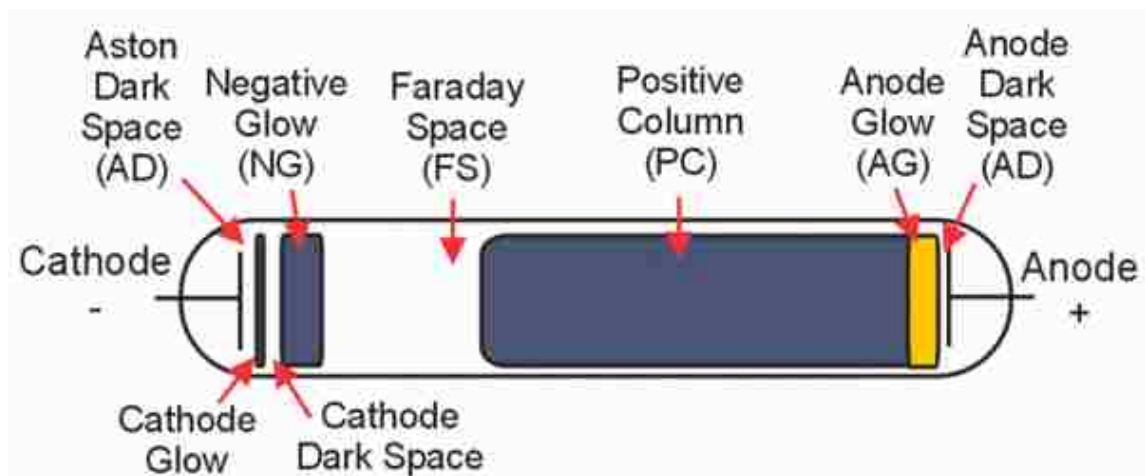
Figure 2.5: Electric Glow Discharge tube [41]

Hundreds of volts of direct current (DC) are applied across the electrodes, with the chamber filled with gas. The gas atoms in the chamber initially are ionized by the collision process. Electrons also are emitted from the cathode with energy of 1eV [42]. Since opposite charges attract, electrons are pulled towards the anode, and ions move towards the cathode. If these ions hit the neutral atoms on the way, the neutral atoms break into ions and secondary electrons; if the ions hit the cathode, the cathode emits secondary electrons[39]. Electrons that have been accelerated in the cathode region to high speeds produce ionization; slower electrons that already have inelastic collisions, cause excitations. The negative glow is predominantly generated by the slow electrons. It is the region where most exciting and ionizing collision processes occur because of the high density for both negative and positive charged particles [41].Dark space region surrounds the cathode and anode [40].
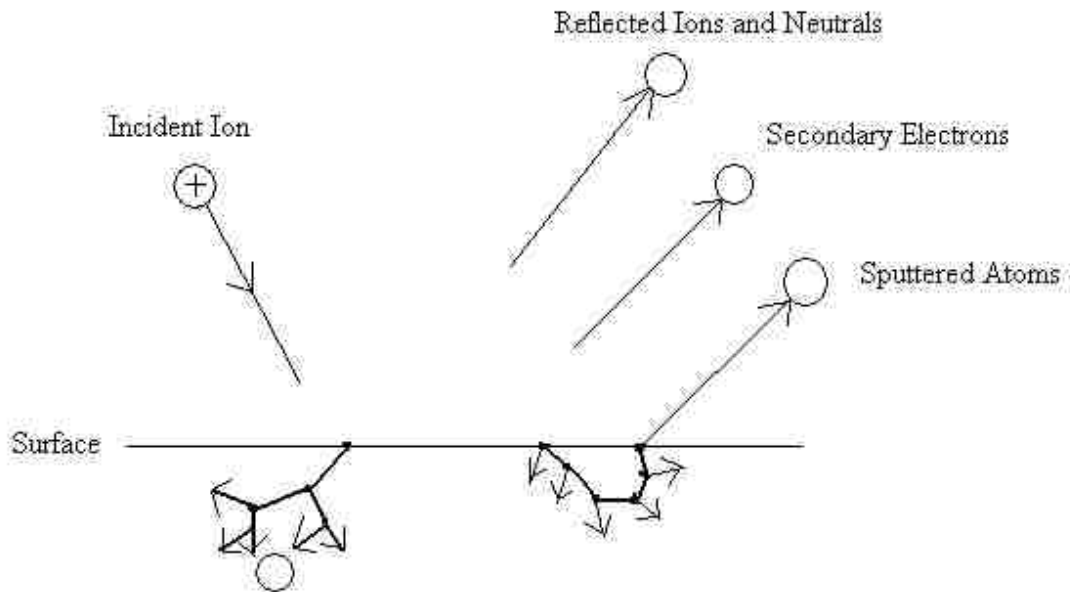
Figure 2.6: Reactions in a plasma chamber

Figure 2.6 shows three possible reactions that might take place [40]:

1) The ion can be reflected back, causing it to neutralize. This is called ion scattering spectroscopy.

2) The ion can hit an electron on the surface, causing it to eject out. These electrons are called secondary electrons, and are the main source of maintaining the glow.

3) The ion can be implanted or buried in the target. This is called ion-implantation. When this happens, an atom from the surface will be ejected out.

There is no specific ratio of which these possibilities may occur. However, the second and third possibility is the most effective phenomenon and may be responsible for change in crystal defects in the target. Minor changes include missing atoms and atoms out of position, while the major change are lattice defects, for example, change in relative proportion (stoichiometry) or a change in electrical charge levels. Thus, the term sputtering is related to the ejection of an atom from the target after colliding with various other atoms within the target material [40].

2.4. Glow discharge system

The glow discharge system apparatus is as shown in the schematic in Figure 2.7:
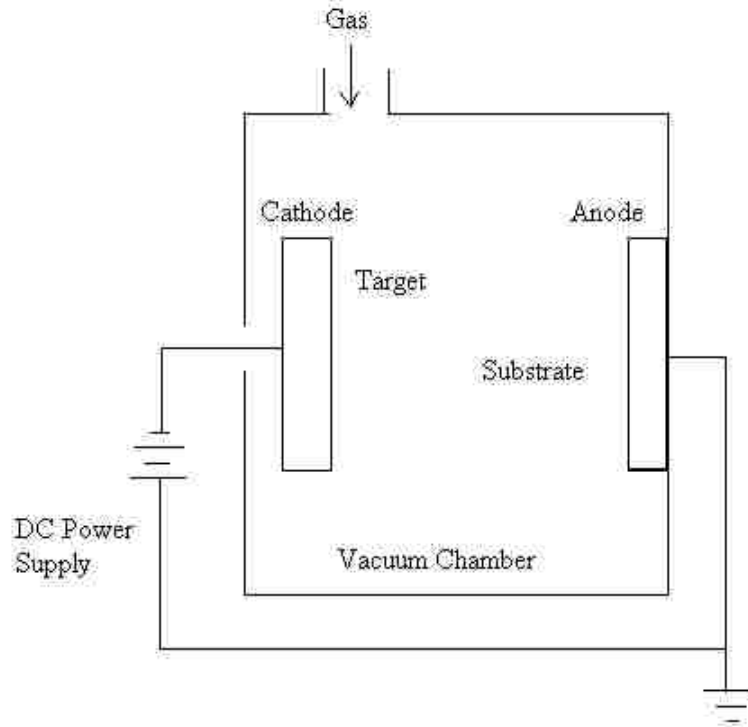
Figure 2.7: Schematic Diagram of a glow discharge System

The target material that has to sputter is made the cathode. This is put in a vacuum

chamber which is connected to a DC power supply. Gas is pumped into the chamber to

maintain the required pressure. The electric field excites the atoms of the gas which

collide with each other to form ions and electrons. Ions move towards cathode and hit the

target. These ions either sputter atoms of the target or eject secondary electrons. Atoms

move towards the anode with high energy, which is supplied by the electric field applied

to the chamber. Secondary electrons are used in maintaining the glow discharge.

CVD technique was first invented for providing thin film coating by plasma [43]. But this

proved a costly leading to the invention of the sputtering technique for diamond films by

Akio Hiraki et al. [43]. Nanometer thick diamond film was formed by supplying DC

current to hydrogen filled chamber. Pressure was reduced to 0.5 Torr. Graphite was used

to sputter on target material. This invention led to formation of uniform films of varying thickness.

2.5. Gases used in Plasma

Discharge plasma is generated in a vacuum chamber using DC current to ionize various gases. These gases play a vital role in the deposition process. Noble gases, such as neon (Ne), Xenon (Xe), Argon (Ar) and helium (He) are useful in certain experiments, compared to reactive gases like nitrogen (N_2), oxygen (O_2), hydrogen(H_2), methane (CH_4), silane (SiH_4), and silicon tetrafluoride (SiF_4). A mixture of noble-noble, reactive-reactive, and noble-reactive gases works best in testing the properties of the target material. In addition, atmospheric air can be combined with either a noble or reactive gas [44].

Hydrogen and argon gases not only are used in deposition but also in layer removal off the surface, a technique was patented by Joe W. Zhao et.al in 1977 [45]. The target material used was an integrated circuit, formed by the deposition process. Each layer of deposition was patterned by coating a layer of photoresist polymer. This layer was removed off before the deposition of the second layer. Cleaning with oxide solutions causes a reaction with the circuit, which leads to damage of sensitive parts. An experiment conducted on plasma cleaned with argon gas removes the layer from the surface; however, there is a risk of photo resist polymer layer getting stuck on the walls of circuit. Thus, cleaning with both argon and hydrogen gas was invented, which converts the polymer coating to a gaseous state. The polymer in the gaseous state then is blown off the chamber.

CHAPTER 3

X-RAY DIFFRACTION

3.1. Background

The study of crystalline solids, and the principles that govern their growth, external shape and internal structure is called crystallography. X-ray diffraction is used to identify minerals and crystalline materials [46]. X- rays are electromagnetic waves with a wavelength of 1.54Å, shorter than the wavelength of light[47]. Wilhelm Conrad Rontgen discovered X- rays accidentally in 1895, while working on the effects of high tension electric discharges in a glass tube [48]. The experiment involved cathode ray production in a sealed discharge tube wrapped in black paper. When the electron beam hit the glass of the discharge tube, it produced low - intensity radiations. This radiation caused nearby material to glow in the dark; however, many unsolved questions about this radiation caused it to be named as X-radiation. Since its discovery, X-rays have been used in many fields of application [48].

Max Von Laue from the University of Munich suggested the use of X-rays for crystal study in 1912 [48]. Von Laue, a lecturer in Professor Sommerfield's department, was working on interface phenomena. Sommerfield also was interested in the nature and excitation of X-Rays, which led them to work together. They were assisted by Paul Heinrich Groth, a leading crystallographer, at the University of Munich. In 1912, Paul Edward, worked under Sommerfield on scattering of light waves passing through a crystal [48]. Paul wanted to measure the wavelength and interatomic space of X-rays which had not been successfully achieved during Rontgen's research [48]. He assumed a

fixed value for either the wavelength or interatomic space to determine the value of the other. Also in 1912, Williams Henry Bragg and Williams Lawrence Bragg, father and son, developed a generalized equation known as the Braggs Equation[49].

The Braggs equation explains the concept of X-ray diffraction in terms of reflection of X-rays by sets of lattice planes [50]. Diffraction patterns are caused by irregular surface patterns on the material. The roughness pattern on the surface describes the diffraction. When the distance between the roughness is regular and equal to wavelength of light, it forms as diffraction [51]. Figure 3.1 shows a diffraction pattern.
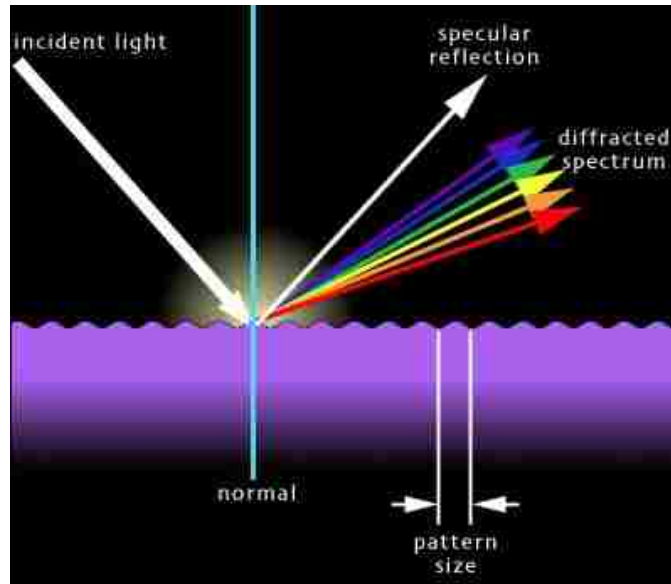
Figure 3.1: Diffraction phenomenon on a rough surface [51]

Crystal structure is the arrangement of atoms in an order to form a lattice [52]. These atoms are bonded together to form periodic unit cells. Lattice planes are explained as using one unit cell, as shown in Figure 3.2. X, Y, Z axes are determined for the unit cell. The lengths of the edges of the unit cell are called as lattice parameters (a, b, c). The

joined intercepts on the parameters form a lattice plane. The inverse of the plane

intercepts gives the values of Miller Indices (h, k, l) [53].
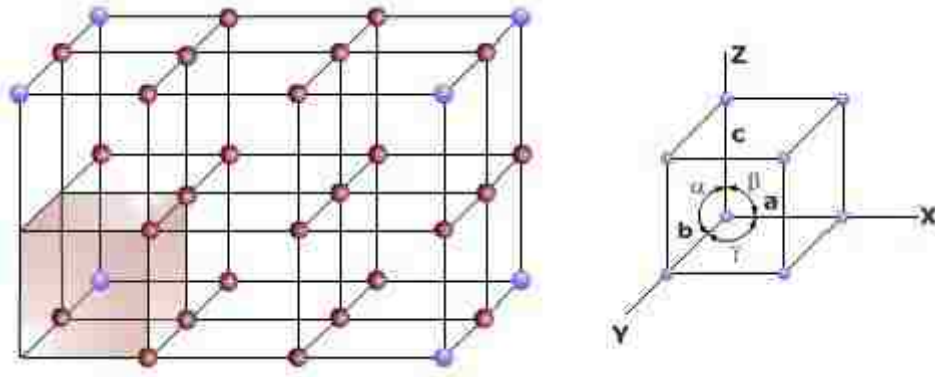
Figure 3.2: Diagram of a unit cell [54]

Real time images of the lattice planes are shown in Figure 3.3 in a scanning electron

micrograph (SEM) photo of niobium carbide dendrite.

Figure 3.3: Scanning electron microscope figure of niobium carbide dendrite [55]

A unit cell has lattice planes with varying (h, k, l) values. Parallel planes have the same

indices value. They are separated from each other by a distance of d, represented d_{hkl}[53].

3.2. Bragg's Equation

Bragg's law was derived by using the concept of having an incident ray and a reflected ray at the same angle [56]. An X- ray machine sends in multiple beams which are parallel and in phase to each other. As seen in Figure 3.4 (a) below, as the first ray strikes an atom P at an angle θ, the second ray continues to move into the crystal, striking at atom B on the inner lattice plane. Both the rays are reflected back at an angle similar to their incident rays. In the same angle, the second beam travels an extra distance of AB+BC. The extra distance is considered as a multiple n (n=1, 2,..n) to the wavelength λ.
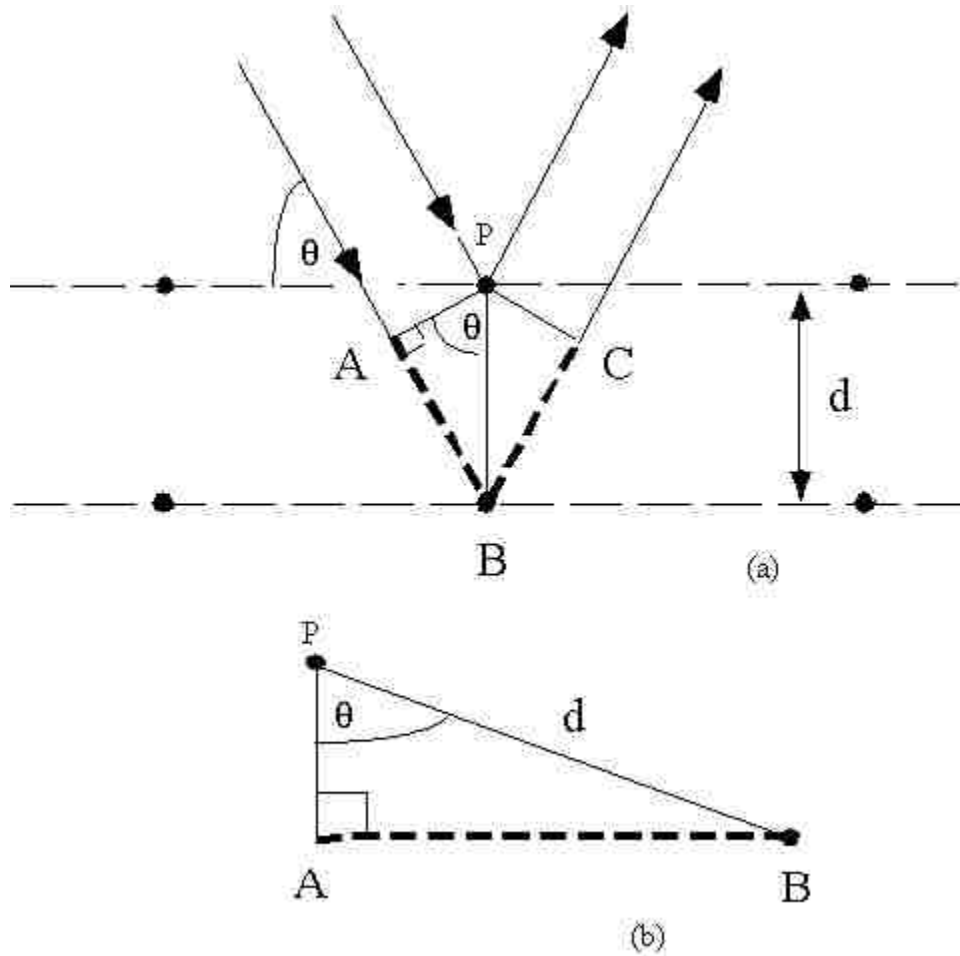
Figure 3.4: Illustration of derivation geometry for Bragg's Law [56]

They determined that the wave attains constructive interference only if:

$$n\lambda = AB + BC \text{ --------------------- (1)}$$

With d as the hypotenuse of the right triangle ABP, as shown from Figure 3.4 (b), we can use trigonometry to relate d to the distance (AB + BC). The distance AB is opposite θ, so,

$$AB = d\sin\theta \text{ -- (2).}$$

Because AB = BC, Eq. (1) becomes:-

$$n\lambda = 2AB \text{ --- (3)}$$

Substituting Eq. (2) in Eq. (3), we have,

$$n\lambda = 2\,d\sin\theta \text{ --(4)[56]}$$

3.3. Powder Method

The powder method of X- ray investigation was discovered due to a lack of precision orientation in crystals. The internal structure of a crystal is sometimes not clearly formed leading to difficulties during an X- ray diffraction (XRD) study. The specimen is made to a fine powder and mixed with an amorphous material [50]. The powder is mounted onto a rotating plate. The particles on the plate are mixed properly to have random orientation. When a beam of monochromatic rays strike the plate, it creates diffraction rays at random angles. The interatomic spacing (d), and the incident angle should satisfy Bragg's Law [48]. Thus, a different set of spacing values (d) is satisfied by different angles of

34

incidence. The rays, when viewed on a photographic plate (Figure 3.5) looks like concentric circles.
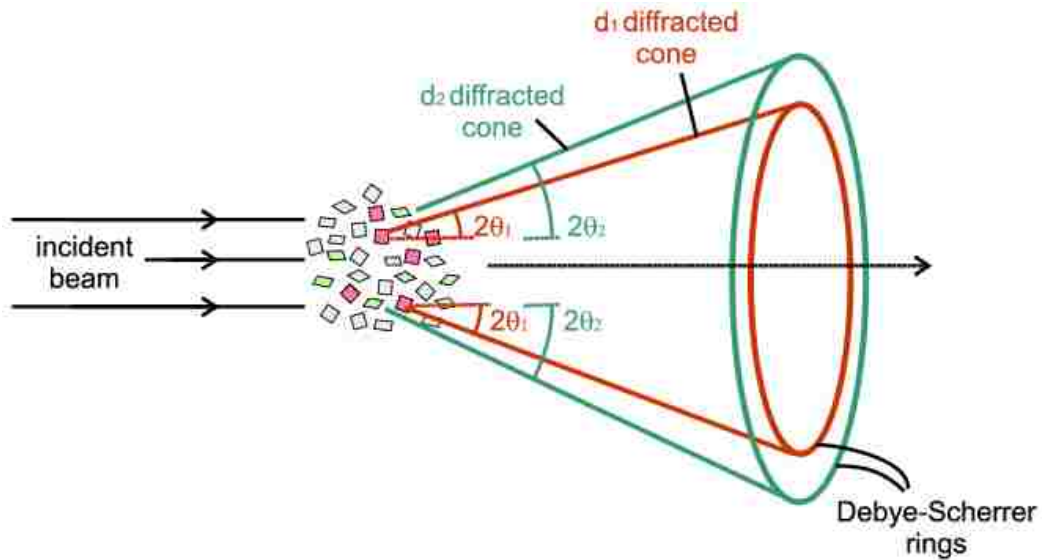
Figure 3.5: Powder diffraction [57]

The formation of concentric circles is explained by the Debye – Scherrer method [58]. In powder diffraction, the powder is mounted on a flat plate. Each particle has different orientation angles. Consider a single particle on which the X-ray beam is incident, as in Figure 3.6. The nth order reflection occurs only at an angle of θ. (Fig.3.6a). The plate is rotated on an axis at an angle perpendicular to the beam. The angle chosen should be such that it satisfies Bragg's law. This forms as a cone reflected as a circle on the photographic plate (Fig. 3.6b). This is for one set of crystals with a constant "d" value. The plate is rotated on other axes for circles of other d values. Since three rotations result in the crystal being oriented in every possible position in space, it is equivalent to using powdered crystals which, because of their random orientation, are already oriented in every possible direction. Fig. 3.6c and d shows cone reflections for different orders and

separation distance. To further ensure randomization, the powder sample mounting is

rotated by an external motor.
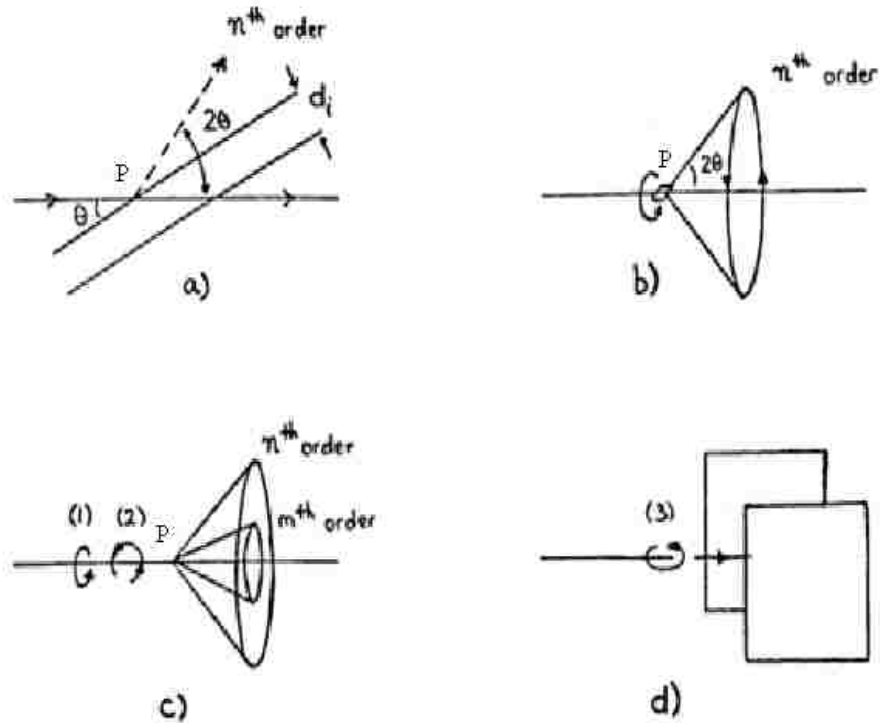
Figure 3.6: Debye –Scherrer method explained [58]

3.4. X ray Diffraction Apparatus

X- ray diffraction apparatus consists of three major components

1) An X- ray source,

2) An X- ray detector, and

3) A sample holder

These are sub categorized and each sub- category has applications depending on the type of result required.

3.4.1. X- Ray Source

a) In –house or laboratory source

An in-house or laboratory source produces X-Rays using either an evacuated tube or a rotating anode. This method uses the old type of production discovered by Rontgen [59].
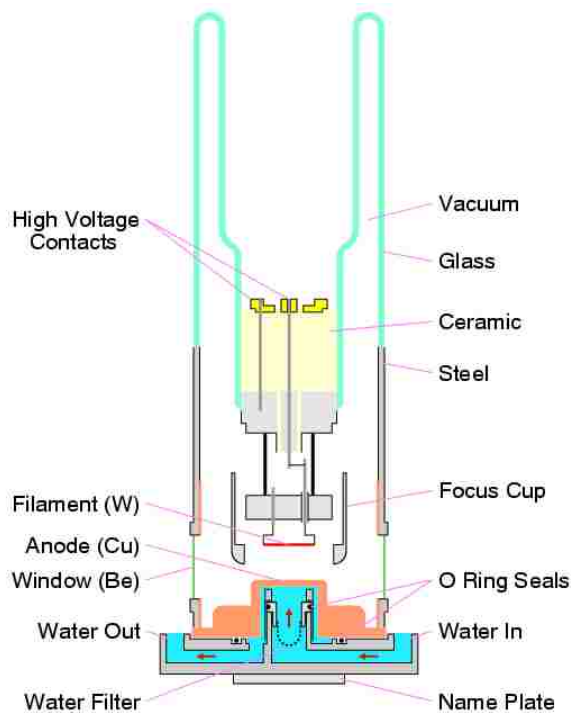
Figure 3.7: Laboratory X- ray tube diagram [60]

The X rays are produced in a vacuum chamber. X-Ray tube consists of a filament that acts as a cathode. Electrons are emitted by the hot cathode and accelerated by a voltage of several kilowatts across the vacuum chamber towards the anode. The anode consists of a metal target made of a characteristic material, usually copper and chromium [61].

As the electron beam impacts the anode, the kinetic energy of the electrons is converted during deceleration into X-rays. The divergent rays exit the chamber through the Beryllium opening. The energy of the electrons hitting the anode gets converted into heat which dissipates into the anode. This is cooled by the water stored at the bottom of the chamber [60] .

Figure 3.8: Laboratory X- ray source [60]

b) Synchrotron X- ray Source

A synchrotron source is more advantageous than a laboratory source. Synchrotron sources are used for measuring high quality powder diffraction. The wavelength can be

varied from a short wavelength, in order to penetrate through absorbing samples, to a larger wavelength for scattering phenomena. Synchrotron radiation is emitted when the charged particles change velocity by following a curved trajectory due to a magnetic field [47]. The invention of synchrotron was a gradual process. During the 1920's, the radiation from circulating electrons proved to fail as they were losing energy. This led physicists to develop a magnetically induced electron accelerator machine, known as the Betatron [62].

The first Betatron to operate successfully was a 2.3-MeV device built in 1940 by Donald William Kerst at the University of Illinois. General Electric Company followed with a 20-MeV first and then a 100-MeV machine to produce high-energy X- rays for nuclear research [63]. These machines were not very efficient, as the energy radiating away from the circulating particles needed to be replaced.

During 1944, research by J. Blewett raised the need of radio frequency to counter the radiation losses due to low energy. The radio frequency initially was set to a fixed frequency [64]. However, in 1945 Edwin McMillan from the U.S and V.I.Veksler from the Soviet Union independently proposed decreasing the frequency of the RF voltage as the energy increases to keep the voltage and the particle in synchronous[62]. Keeping these ideas in mind Herb Pollock, Robert Langmuir, Frank Elder, and Anatole Gurewitsch from General Electric Company tested a 70 MeV synchrotron on April 24, 1947 [65]. Figure 3.9 shows the first synchrotron radiation indicated by an arrow.
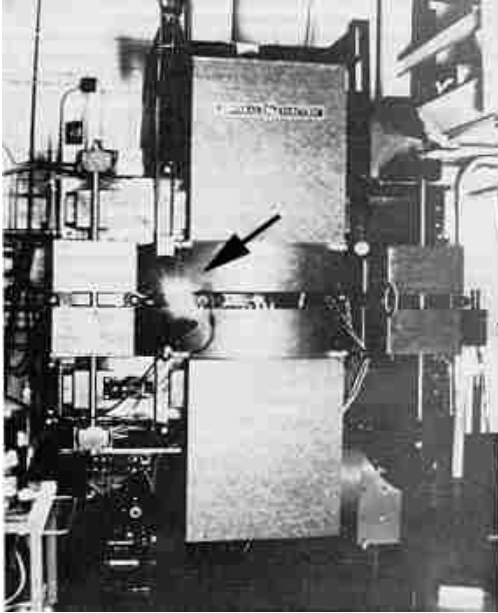
Figure 3.9: Radiation (indicated by an arrow) of a synchrotron built by General Electric

Company [63].

Figure 3.10 shows a schematic diagram of a synchrotron source. Electrons are produced

in a small electron gun, and are pre-accelerated in the booster ring. The electrons then are

injected into the ring. The electron beam current in the booster ring flows in a clock-wise

direction. The radio frequency cavity, or generator compensates the energy losses of the

circulating electrons and keeps them at constant speed and energy [66].
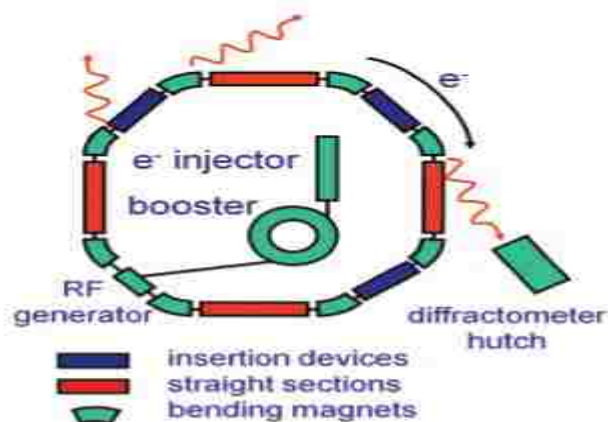
Figure 3.10: Schematic diagram of a synchrotron source [66]

3.4.2. X- Ray Detector

X-Ray detectors are of three types: Scintillation or Point Detectors; Gas-filled Detectors; and Position- Sensitive Detectors.

a) Scintillation or Point Detector

These are two stage detectors. In the first stage, X-ray photons collide with a phosphor screen, and a thallium-doped sodium iodide crystal. Photons are emitted in the blue region, and converted to voltage pulses by the photomultiplier tube attached. The number of electrons ejected by the photocathode is proportional to the number of visible photons which strike it; this in turn is proportional to the energy of the original X-ray photon [47]. Since the energy resolution is poor, it cannot determine between the kα and kβ photons. This type of detector is useful mainly in measuring the intensity at a point [67].

b) Gas-filled Detector

The principle behind this is that X-ray photons ionize a noble gas forming it into an electron, and an ion pair. Since the energy required for ionization is low(10-20 eV) compared to X-Ray photon energy (8KeV), a large number of gas atoms can be ionized [47]. A wire placed inside the detector is set to a potential of about 1,000 V [68]. This potential accelerates the electrons of the ion pair towards the wire causing further ionization and an enhanced signal by gas amplification. The burst of electrons on the wire is converted into a voltage pulse, which then is shaped and counted by the electronics. Gas-filled detectors have a better energy resolution than scintillation detectors; however the disadvantage is that they lose linearity at high count rates [47].

41

c) Position- Sensitive Detector (PSD)

This is a more advanced form of a gas detector. This type has a long anode wire that has high voltage applied at both ends. The pulse moves towards both ends of the wire simultaneously. By measuring the rate at which the pulse arrives at both ends of the wire, it is possible to determine where on the wire the pulse originated. The pulses are stored in a multi-channel analyzer (MCA) device according to the pulse position on the wire. This enables PSDs to record data over a whole range of scattering angles, which can be useful where speed of acquisition is crucial [68].

3.4.3. Sample Holder

The sample holder for each type of instrument geometry varies. Reflection geometry uses a sample holder having a flat-plate base [47]. These make it easy to transfer the sample onto the holder, and are most widely used in samples of small quantities. Flat plates are difficult to work with at vertical angles which can lead to samples falling off the holder [47].

Figure 3.11: Types of sample holders for reflection geometry [69]

Glass capillaries are used for transmission geometry. These are manufactured in various standard sizes of diameter depending on the nature of the sample. The most common diameter values are 0.2, 0.3, 0.5, 0.7, and 1.0 mm [69]. The tube is sealed to prevent sample loss. This type is most useful during low temperature studies. Glass capillaries are useful in diffraction measurement of air –sensitive samples that cannot be determined in flat plate samples. These are not widely used due to the following reasons [47]:

1) X- rays from the source diffuse through the walls.
2) Filling the tube is time consuming
3) The tube axis needs proper care in alignment to the diffractometer.

Figure 3.12 shows a 1 mm diameter glass capillary tube connected to a Brass metal holder. The sample was an organic substance white in color which has turned to yellow due to X- Ray.

Figure 3.12: Glass capillary tube [60]

3.5. Monochromator

An X- ray beam can be characterized for diffraction, reflection or absorption by using optical elements. A monochromator crystal is used in diffraction to select a particular wavelength [70]. Filters are used to absorb unwanted radiations in the laboratory X-ray source. A uniform thin sheet of monochromator crystal is placed in the path of the beam. They are used to separate the Cu $K\alpha_1$ rays from unwanted Cu $K\alpha_2$ and Cu K_β [71]. $K\alpha_1$

and Kα$_2$ overlap each other almost throughout the diffraction pattern. Figure 3.13 shows Kα$_1$and Kα$_2$ overlapping each other. At lower angles the number of places of overlap on the graph plot is greater, compared to higher angles [70]. Mirrors are used to focus an X-ray beam onto the irregularly shaped sample material closely- parallel to it.

Monochromators are used to reflect the diffracted beam by the wavelengths that satisfy Bragg's equation [47]. These are set to a particular orientation angle θ. In a synchrotron, two monochromators are used to select the required wavelength from the polychromatic beam. In general, a double layered monochromator is used to maintain the direction of the incidence beam all through [47].
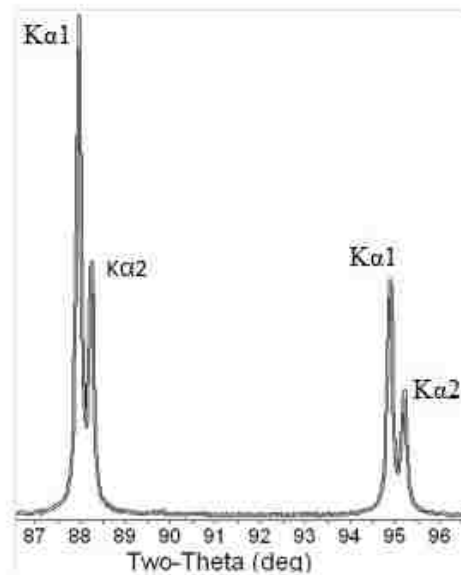
Figure 3.13: Overlap of kα1 and kα2 rays [70]

Pyrolytic graphite and silicon are the two most commonly used materials as monochromators [71]. They are usually in the form of single crystals aligned in an orientation to form a mosaic. Pyrolytic graphite and silicon are used as broad band and

narrow band monochromators respectively, represented by $\Delta\lambda/\lambda$. Figure 3.14 shows $\Delta\lambda/\lambda$ in pyrolytic graphite and silicon. In pyrolytic graphite, the mosaic spread alignment is relatively broad in contrast to silicon which is near perfect [71].

(a)   (b)
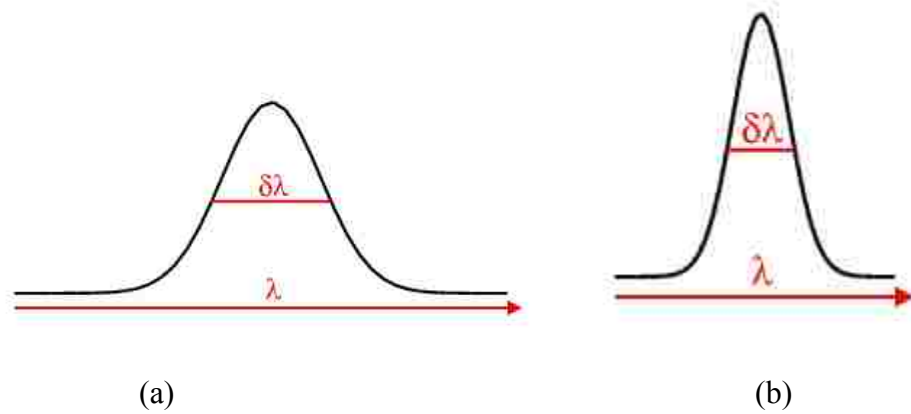
Figure 3.14: ($\Delta\lambda/\lambda$) in   a) pyrolytic graphite and   b) silicon [71]

In a laboratory copper X-ray source, monochromator crystals with a narrow band pass will separate the $K\alpha_1$ and $K\alpha_2$ wavelengths. A wide band width will allow both $K\alpha$ wavelengths, but not $K\beta$, which has a different Bragg angle [71]. The other types of materials that can be used for narrow width are silicon, germanium, and quartz. Monochromators can be used as a pre-sample or a post-sample. Generally, graphite is used for a post-sample, while quartz or germanium is used as a pre-sample monochromator [32].

3.6. Instrumental Geometry

Reflection and transmission geometry are the two types of instrumental geometry.

3.6.1. Reflection Geometry

Reflection geometry is the most common principle used in academic and industrial experiments [47]. In reflection geometry the sample is loaded onto a flat plate. Flat plate diffractometers have good peak intensities and high resolution due to focusing of the diffracted beam [72]. According to Dinnebier and Billinge "The divergent incident beam is reflected off the surface of the sample and converges at fixed radius from the sample position. This geometry is referred as Bragg- Brentano" [47][67].The ratio of incident and reflected ray angle is $\theta : 2\theta$. Figure 3.15 shows Bragg- Brentano geometry.
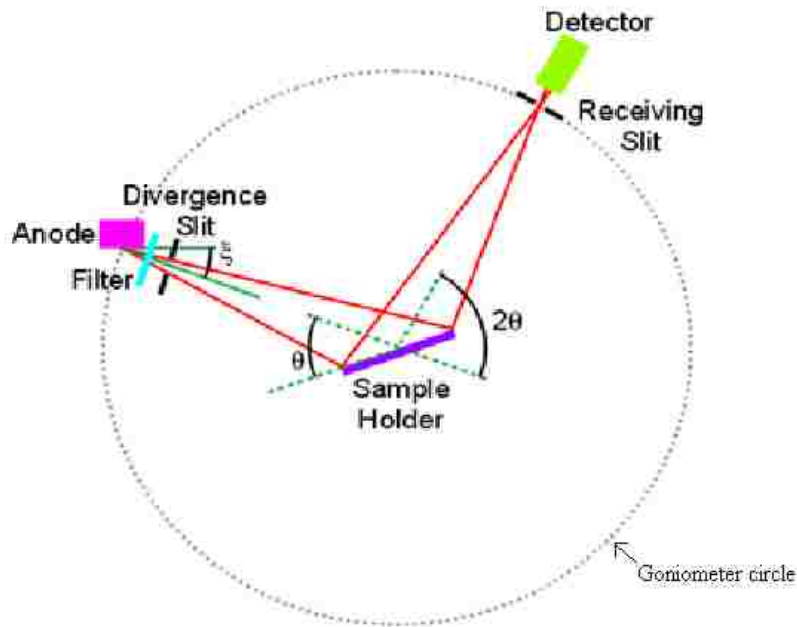
Figure 3.15: Bragg- Brentano Geometry [72]

As shown in Figure 3.15, the cathode ray tube is aligned to the anode in a way that it forms an angle ξ. One or more divergence slits are placed after the source, to control the divergence of the beam. Filters are placed to the source beam when no pre or post sample

46

monochromators are used. Figure 3.16 shows a post sample monochromator XRD. Graphite is used as it has a low degree of crystalline perfection. A flat crystal of graphite is adequate for this purpose. In Figure 3.17, a pre-sample monochromator uses quartz or germanium crystals. These are near perfect crystals which give a better result in the separation of $k\alpha_1$ and $k\alpha_2$ rays[47]. After striking the curved monochromator crystal, $K\alpha_2$ rays after striking the curved monochromator crystal deviates its path from $k\alpha_1$. Slits placed after the source removes $k\alpha_2$ before it reaches the sample. In Bragg- Brentano reflection geometry, the source is fixed at an angle, while the sample and detector rotate at angles of θ and 2θ, respectively. Alternatingly, the sample is fixed, rotating the source and detector by $-\theta$ and θ angles, respectively [47].
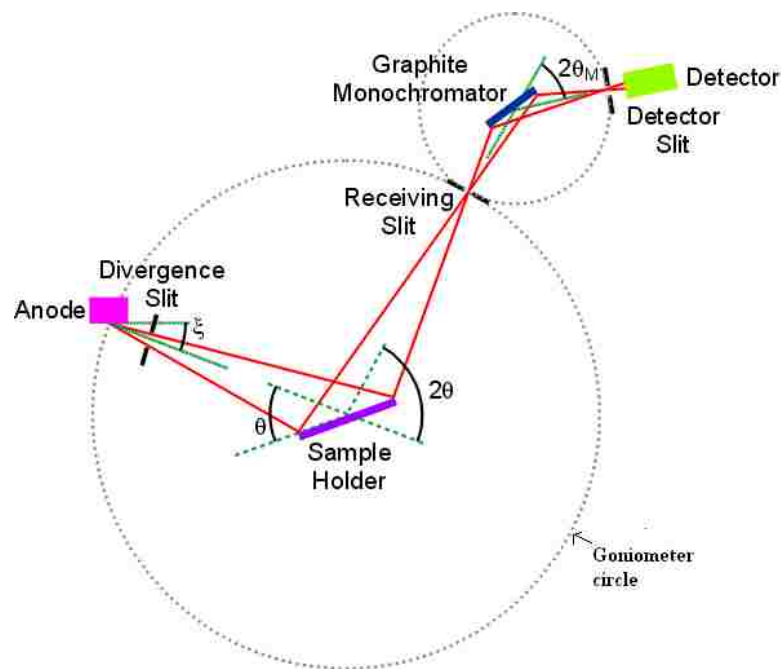
Figure 3.16: Post- Sample Monochromator [72]

47
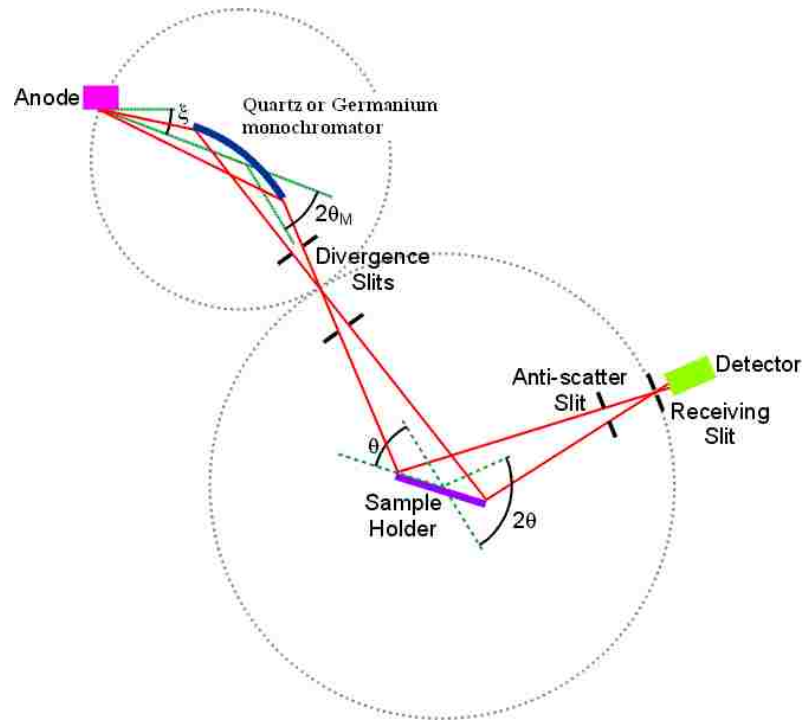
Figure 3.17: Pre-sample Monochromator [72]

3.6.2. Transmission Geometry

The transmission powder diffractometer is based on the Debye- Scherrer camera geometry technique. A thin foil or glass capillary is used as a sample holder. The divergent beam from the source does not stop at the sample but goes beyond onto a curved PSD to collect efficient data. The sample holder is spun about its own axis to get good diffraction peaks. Figure 3.18 shows this type of instrumental geometry.
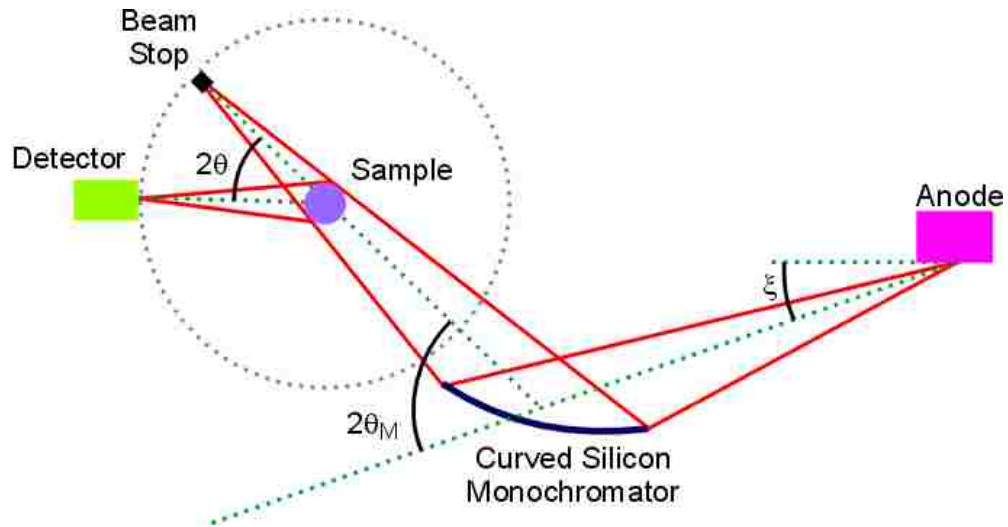
Figure 3.18: Transmission Geometry [72]

3.7. Standard Samples

Standard samples are used to check the reliability of the diffractroemter. They give details about alignment, calibration and resolution. Standard samples used in X-Ray diffraction are silicon(Si), lanthanum hexaboride(LaB6), nickel(Ni), zinc oxide (ZnO), titanium dioxide (TiO2), cerium oxide (CeO2), alumina (Al2O3), chromium III oxide(Cr2O3), and yttrium oxide (Y2O3). A single type of standard sample does not give complete information on all the details about the sample powder. Figure 3.19 shows the types of containers to mix samples and standard samples. These containers are called mortars and pestles.

Figure 3.19: Containers to mix samples and standard samples [60]

3.8. Applications

X-ray powder diffraction is most widely used for the identification of crystalline materials. This includes minerals and inorganic compounds [73]. Determination of the unknown solids is critical to studies in geology, environmental science, material science, engineering and biology.

XRD is advantageous in:

1) Characterizing thin film samples by determining lattice mismatch between film and substrate and to inferring stress and strain

2) Determining dislocation density and quality of the film by rocking curve measurements

3) Identification of fine-grained minerals such as clays and mixed layer clays that are difficult to determine optically

4) Determine dimensions of a unit cell

5) Determining the characterization of crystalline materials

6) Crystal structures determination using Rietveld refinement

7) Making textural measurements, such as the orientation of grains, in a polycrystalline sample

3.9. Strengths and Limitations

Strengths

- XRD is a powerful and rapid tool for unknown mineral identification in almost less than 20 minutes [74].

- XRD provides an unambiguous mineral determination.

- Data interpretation is easy.

- Surface texture can be measured extremely fast. An XRD system collects texture data and background values simultaneously for multiple poles and multiple directions [75].

Limitations

- Must have access to a standard reference such as d-spacings or hkl's of inorganic compounds

- Requires tenths of a gram of material, which must be ground into a powder.

- Indexing of patterns for non-isometric crystal systems is complicated for unit cell determinations.

CHAPTER 4

PLASMA EXPERIMENT

Plasma experiment is conducted implementing the concept of gas discharge. As seen in the previous chapter gas discharge is the major source of plasma formation due to transfer of electrons at high energy. The particles of gas after ionization tend to move close to the electrodes. The electrons move towards the anode (positive charge), ions move towards the cathode having a negative charge. When these fast moving ions are hindered by a substance (diamond in our experiment) they tend to either implant into it, causing change in crystal defects, or reflect off the surface.

The experiment is conducted on two different samples. This is to see the difference after the plasma experiment on each sample separately. The first experiment was conducted on industrial diamond crystals they were of 21 counts. The second sample was from Engis Corporation, Illinois, in the form of diamond powder. A total weight of 100 carats with a sample size ranging 15-25 micron was imported from the company. The sample is divided into 8 parts, each part weighing 10-12 carats. The plasma experiment on each sample was conducted for total of 16 hours.

4.1. Experiment on Diamond Crystals

Plasma test is performed on Diamond crystals to determine the change in crystal defects before and after plasma.

4.1.1. Apparatus

1)   Turble molecule vacuum pump

2)   Convectron Gauge (controller and sensor)

3)   Tygon tube

4)   Experiment chamber or vacuum chamber

5)   Hydrogen cylinder

6)   Direct Current (DC) Voltage source

7)   Teflon stand

8)   Vacuum Grease

9)   Grounding Stick

10)   Latex Glove

Figure 4.1: Plasma Experiment

4.1.2. Experimental setup

Schematic diagram of setup is shown in figure 4.2. A vacuum pump is connected to the vacuum chamber. The chamber is connected to a Resistor of 10 Ω. The Resistor is connected to Keithley High DC voltage supply. The voltage supply has a maximum voltage of 5000V and maximum 5 mA current. The vacuum pump and chamber are in the series connection. DC supply and vacuum chamber are connected in parallel. Two connections are drawn between the vacuum pump and the experiment chamber. The first connection is to a convectron gauge. The gauge is connected to a digital controller which displays the pressure inside the chamber throughout the experiment. The second connection is to the hydrogen cylinder. All the connections are made through Tygon tubes which supply hydrogen gas throughout.

54

Figure 4.2: Schematic diagram of Plasma Connections

The vacuum chamber or experimental chamber is the heart of the experiment. This chamber was designed by the students of UNLV. The setup has a hollow glass tube closed on both sides by plastic plates. Through the Centre of the glass tube runs two hollow brass tube from both sides, connected to aluminum plates on one end. The aluminum plates and brass rods act as conductors of voltage supplied. Between the aluminum plates is a Teflon stand on which the diamond crystals are placed, as shown in figure 4.3 and 4.4. Crystals are stuck to the stand in an order of proper rows and columns with the help of vacuum grease.
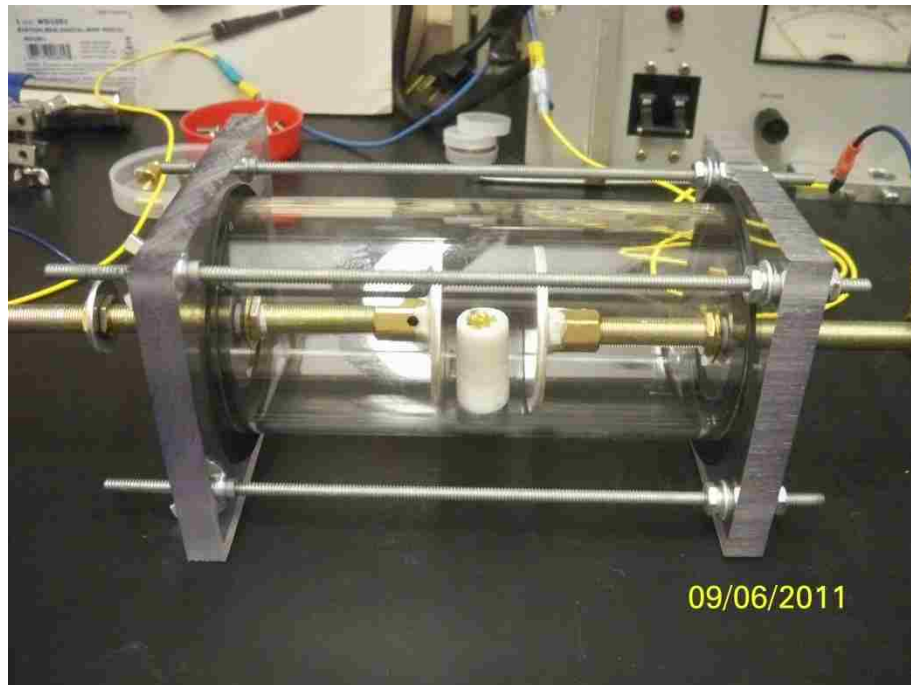
Figure 4.3: Vacuum chamber for experiment

Figure 4.4: Diamond crystals for experiment

4.1.3. Procedure

The crystals are initially weighed and stuck to the stand using vacuum grease. The crystals are arranged in the order of rows and columns. This arrangement is easier to pick the four which were closer to the cathode. The stand placed between the cathode and anode plates, is placed more towards the cathode where plasma glow is largely concentrated. The chamber is sealed tight, not allowing air to enter through any possible gaps. The vacuum pump is switched on to suck the air inside the closed chamber. The pump is run continuously for 5-6 hours till the pressure inside is less than 300 mTorr. After reaching the desired pressure with the vacuum pump running, voltage and hydrogen gas is simultaneously supplied to the chamber. Initial voltage is set to 500 Volts and current supplied 0.15 mA. Plasma is formed inside the chamber between the aluminum plates as shown in figure 4.5.

Figure 4.5: Plasma formed between the electrodes

The voltage and current are varied accordingly to have continuous plasma. High current can cause an arching effect on the glass plastic, which can melt the plastic cylinder down if run for long hours. Thus a continuous check has to be done throughout the experiment.. Grounding the current in the chamber by grounding stick is necessary before touching the apparatus to avoid current shock.

This concludes the first day of experiment. The same procedure is repeated for 5 days for a total of 16 hours. Collect the crystals close to cathode after each day experiment in a bag to check the weight. Care should be taken not to touch the Teflon stand with bare hands as finger prints and dirt on it may not give appropriate results. Latex gloves should be worn while placing or removing the crystals.

The variations in current, pressure and voltage during the experiment each day is recorded in tables.

Table 4.1: Diamond crystals, Day 1

Time	Voltage (V)	Current (mA)	Pressure (mTorr)
10-11 AM	470	0.21	84
11AM-12PM	470	0.27	120
12-1 PM	470	0.4	132
1-2 PM	470	0.05	140
2-3 PM	470	0.055	150
3-4 PM	470	0.06	180
4-5 PM	470	0.085	206

Table 4.2: Diamond crystals, Day 2

Time	Voltage (V)	Current (mA)	Pressure (mTorr)
9-10 AM	500	0.05	150
10-11 AM	470	0.055	160
11AM-12PM	480	0.055	163
12-1 PM	480	0.06	170
1-2 PM	480	0.06	176
2-3 PM	490	0.07	181
3-4 PM	500	0.072	185
4-5 PM	500	0.07	176

Table 4.3: Diamond crystals, Day 3

Time	Voltage (V)	Current (mA)	Pressure (mTorr)
9-10 AM	480	0.05	246
10-11 AM	480	0.052	250
11AM-12PM	480	0.045	230
12-1 PM	490	0.045	235
1-2 PM	480	0.037	220
2-3 PM	480	0.052	240
3-4 PM	480	0.057	265
4-5 PM	480	0.050	250

Table 4.4: Diamond crystals, Day 4

Time	Voltage (V)	Current (mA)	Pressure (mTorr)
9-10 AM	470	0.15	290
10-11 AM	475	0.2	320
11AM-12PM	470	0.1	280
12-1 PM	470	0.095	260
1-2 PM	470	0.095	253
2-3 PM	472	0.1	279
3-4 PM	470	0.1	270
4-5 PM	470	0.1	265

Table 4.5: Diamond crystals, Day 5

Time	Voltage (V)	Current (mA)	Pressure (mTorr)
9-10 AM	510	0.08	248
10-11 AM	510	0.06	290
11AM-12PM	510	0.07	270
12-1 PM	510	0.07	265
1-2 PM	510	0.065	252
2-3 PM	510	0.065	240
3-4 PM	510	0.05	210
4-5 PM	515	0.052	230

Table 4.6: Diamond crystals weight before plasma

Diamond sample No	Weight (gm)
1	0.0054
2	0.0050
3	0.0051
4	0.0042
5	0.0051
6	0.0054
7	0.0062
8	0.0068
9	0.0083
10	0.0067
11	0.0038
12	0.0042
13	0.0050
14	0.0045
15	0.0039
16	0.0055
17	0.0057
18	0.0080
19	0.0089
20	0.0057
21	0.0052

Table 4.7: Diamond crystals weights after experiment

Diamond sample No	Weight of sample after each day experiment in grams(gm)				
	Day 1	Day 2	Day 3	Day 4	Day 5
1	0.0054				
2	0.0050				
3	0.0051				
4	0.0042				
5	0.0051	0.0050			
6	0.0054	0.0054	0.0054		
7	0.0062	0.0062	0.0063	0.0063	
8	**0.0068**	**0.0068**	**0.0068**	**0.0069**	**0.0067**
9	0.0083	0.0083			
10	0.0067	0.0067	0.0067		
11	0.0038	0.0037	0.0037	0.0037	
12	**0.0042**	**0.0042**	**0.0043**	**0.0042**	**0.0040**
13	0.0050	0.0050			
14	0.0045	0.0044	0.0044		
15	0.0039	0.0040	0.0040	0.0041	
16	**0.0055**	**0.0057**	**0.0057**	**0.0058**	**0.0056**
17	0.0057	0.0058			
18	0.0080	0.0080	0.0079		
19	0.0089	0.0089	0.0089	0.0088	
20	**0.0057**	**0.0057**	**0.0057**	**0.0057**	**0.0056**
21	**0.0052**	**0.0053**	**0.0054**	**0.0053**	**0.0053**

Result

The crystals after each day experiment are taken to check weight using physical balance. The weights before and after plasma are tabulated as shown in Tables 4.6 and 4.7. The crystals in bold were soaked in plasma for all five days. The plasma run on it for hours, had no change on the atoms which can be seen from the table below showing no change in weight of the crystals.

4.2. Plasma experiment on diamond powder

The plasma test on diamond powder was conducted on six parts to determine the change in crystal defects and crushing strength. Each part weighed 10-12 carats. Each sample part was designated by the following names

1) S5902
2) S5926
3) S6012A
4) S6012B
5) S6012C
6) S6012D

4.2.1. Apparatus

1) Turble molecule vaccum pump

2) Convectrongauge (controller and sensor)

3) Tygon tube

4)   Experimental chamber

5)   Hydrogen cylinder

6)   Direct Current(DC) Voltage source

7)   Hollow plastic cylinder.

8)   Vacuum Grease

9)   Grounding stick

10)   Latex Glove

4.2.2. Experimental Setup

A vacuum pump is connected to the vacuum chamber. The chamber is connected to a

Resistor. The Resistor is connected to Keithley High DC voltage supply. The voltage

supply has a maximum voltage of 5000V and maximum 5mA current. The vacuum

pump and chamber are in the series connection. DC supply and vacuum chamber are

connected in parallel. Two connections are drawn between the vacuum pump and the

experiment chamber. The first connection is to a Convectron gauge. The gauge is

connected to a digital controller which displays the pressure inside the chamber

throughout the experiment. The second connection is to the hydrogen cylinder. All the

connections are made through Tygon tubes which supply hydrogen gas throughout.

Figure 4.2 shows a schematic diagram of the setup.

The sample used here is in powder form as compared to the previous experiment which

was in crystals. Since the experiment was done in vacuum care had to be taken not

allowing sample to get sucked by the vacuum pump. Thus a box had to be built which prevents sample from being blown off, at the same time allows plasma to pass through it. Many options were considered before getting the right box.

The first sample holder made was a hollow container plastic box with aluminum plate on one end, the other end covered by filter paper to allow air to be sucked from the box. But this did not prove to be useful as the pressure inside the chamber did not drop below 2 Torr, even after long hours of suction. The design was taken back to the drawing board. The filter paper was replaced by a 5 micron sieve. The sieve was a failure too, as getting a sieve of required diameter and mesh size was a costly affair. The container plastic was later discarded as the plastic was oozing gases which were hard to remove after running the pump for long time. After consulting Professors at UNLV, an idea was conceived to use a hard hollow plastic box tightly fitted between the electrode plates. A hard hollow plastic cylinder was machined at UNLV machine shop for the experiment.

But this was not efficient in the beginning since the air inside was stuck, not allowing plasma to form. Holes were punched in the surface to allow air suction. The first design was to have an aluminum base for the box, for easy placement of the sample between the electrodes. The idea was an initial failure because the aluminum plate base for the box was not allowing the plasma to be formed inside the box. All the plasma was formed to the sides of the box on the electrodes. A lot of taping and wiring took place which had no positive result. The final setup without an aluminum base proved to do the job. Figure 4.7 shows the hollow cylinder.

Figure 4.6: Diamond powder on cathode plate

Figure 4.7: Diamond powder covered by hollow cylinder

As the apparatus was used earlier in the experiment, Burrs were formed on the electrode plates. These burrs created a lot of arching in the plasma. These had to be sanded down regularly for smooth finish to have a good plasma glow. Since the diamond powder is very fine grained size, care has to be taken not to lose them.

4.2.3. Experiment Procedure

Diamond powder is divided into 8 parts, each weighed on a physical balance measuring up to 2.4 grams (10-12 carats). Out of eight, seven parts are taken. One is used for XRD test before plasma, and others for plasma experiment. The powder of each part had to be carefully placed on the cathode plate before covering it with the plastic box so that the sample is inside the box. This has to be covered by the plastic cylinder and sealed, so that the chamber will not allow air leaks. Figure 4.6 and 4.7 shows steps in sealing the diamond powder between the electrodes inside the cylinder for experiment.
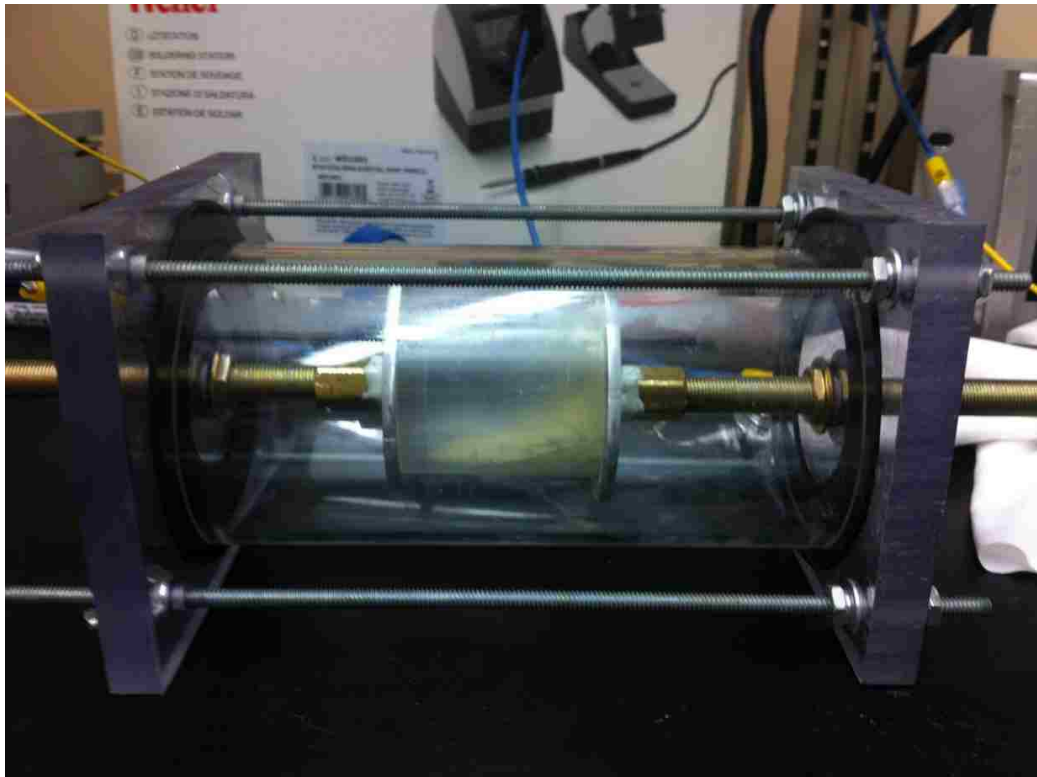
Figure 4.8: Diamond powder inside the hollow cylinder

The vacuum pump is switched on and left running until the pressure drops to around 250 mTorr. Keeping the pump switched on, hydrogen is purged into the chamber along with

DC current. The current bombards the hydrogen changing it to plasma. This is continued for a total of 16 hours before removing for the XRD Test.

Figure 4.9: Violet color plasma seen in dark room

4.3. Inlet Gases for plasma

Pure hydrogen was used for the first diamond powder sample part. In order to check the reliability of the plasma experiment, test was performed on the second part of the sample. Although the hydrogen pump was turned off accidentally, it did not affect the plasma formation. Air leaks were suspected in the vacuum chamber helping in maintaining the required pressure. The experimental setup too did not prove to be as efficient as expected. The hydrogen gas inlet to the chamber was connected to the main line next to the vacuum pump, figure 4.2. This led most of the hydrogen gas to be sucked by the pump even before reaching the vacuum chamber. Thus leaks into the chamber were confirmed, which are maintaining the pressure.

Three types of gases were used for plasma test. The tables below indicate the values selected for voltage, current and pressure for each gas type. The readings are noted for each hour. The pressures fluctuated in an hour, thus an average value was taken for that hour. The samples are designated by a particular number starting with an alphabet given by Engis Corporation.

4.3.1. Hydrogen- air mixture

All the samples were not tested in the same batch. Figures 7.3 and 7.13 indicate the samples in each batch.

Table 4.8: S5902, Day 1

Time	Voltage (V)	Current (mA)	Pressure (mTorr)
9-10 AM	700	0.1	208
10-11 AM	700	0.3	360
11AM-12PM	750	0.2	300
12-1 PM	800	0.3	350
1-2 PM	775	0.3	330
2-3 PM	650	0.15	270
3-4 PM	725	0.4	360
4-5 PM	700	0.5	354

Table 4.9: S5902, Day 2

Time	Voltage (V)	Current (mA)	Pressure (mTorr)
9-10 AM	650	0.15	280
10-11 AM	660	0.37	310
11AM-12PM	660	0.3	315
12-1 PM	700	0.3	368
1-2 PM	660	0.4	346
2-3 PM	680	0.4	330
3-4 PM	680	0.45	325
4-5 PM	680	0.5	320

Table 4.10: S6012B, Day 1

Time	Voltage (V)	Current (mA)	Pressure (average)
2-3 PM	700	2	900 mT
4-5 PM	700	2	950 mT
5-6 PM	700	2	975 mT
6-7 PM	700	2	820 mT
7-8 PM	700	2	800 mT
8-9 PM	700	2	950 mT
9-10 PM	700	2.5	1 T

Table 4.11: S6012B, Day 2

Time	Voltage (V)	Current (mA)	Pressure (average)
11.30- 12.30 PM	700	2.5	870 mT
12.30-1.30 PM	700	2.5	800 mT
1.30-2.30 PM	700	1.5	660 mT
3.30-4.30 PM	700	2	900 mT
4.30-5.30 PM	700	2	900 mT
5.30-6.30 PM	700	2	830 mT
6.30-7.30 PM	700	2	900 mT
7.30-8.30 PM	700	2	880 mT

Table 4.12: S6012C, Day 1

Time	Voltage (V)	Current (mA)	Pressure (average)
11.30- 12.30 PM	700	2	850 mT
12.30-1.30 PM	700	2	800 mT
1.30-2.30 PM	700	2	920mT
2.30-3.30 PM	700	2	800 mT
3.30-4.30 PM	700	2	900 mT
4.30-5.30 PM	700	2	950 mT
5.30-6.30 PM	700	2	950 mT
6.30-7.30 PM	700	2	950 mT
7.30-8 PM	700	2	950 mT

Table 4.13: S6012C, Day 2

Time	Voltage (V)	Current (mA)	Pressure (average)
10-11 AM	700	2	800 mT
11AM-12PM	700	2	920 mT
12-1 PM	700	2	950 mT
1-2 PM	700	2	1 T
3-4 PM	700	2	800 mT
4-5 PM	700	2	970 mT
5-6 PM	700	2	810 mT

Table 4.14: S6012D, Day 1

Time	Voltage (V)	Current (mA)	Pressure (average)
7-8 PM	700	2	700 mT
8-9 PM	700	2	900 mT
9-10 PM	700	2	850 mT
10-11 PM	700	2	870 mT

Table 4.15: S6012D, Day 2

Time	Voltage (V)	Current (mA)	Pressure (average)
10.30-11.30 AM	700	2	850 mT
11.30- 12.30 PM	700	2	630 mT
12.30-1.30 PM	700	2	680 mT
1.30-2.30 PM	700	2	670 mT
2.30-3.30 PM	700	2	675 mT
3.30-4.30 PM	700	2	700 mT
4.30-5.30 PM	700	2	690 mT
5.30-6.30 PM	700	2	850 mT
6.30-7.30 PM	700	2	826 mT
7.30-8.30 PM	700	2	847 mT
8.30-9.30 PM	700	2	860 mT
9.30-10.30 PM	700	2	880 mT

4.3.2. Hydrogen gas

Table 4.16: S6012A, Day 1

Time	Voltage (V)	Current (mA)	Pressure (average)
12-1 PM	700	2	2T
1-2 PM	700	2	2T
2-3 PM	700	2	1T
3-4 PM	700	3	2T
4-5 PM	700	3	2T
5-6 PM	700	3	2T

Table 4.17: S6012A, Day 2

Time	Voltage (V)	Current (mA)	Pressure (average)
1-2 PM	800	2	2T
8-9 PM	700	3	2T
9-10 PM	700	3	2T

Table 4.18: S6012A, Day 3

Time	Voltage (V)	Current (mA)	Pressure (average)
1-2 PM	700	3	2 T
2-3 PM	700	3	2 T
3-4 PM	650	2	1 T
4-5 PM	650	2	820 mT
5-6 PM	650	2	950 mT
6-7 PM	680	2	980 mT

4.3.3. Air

Table 4.19: S5926, Day 1

Time	Voltage (V)	Current (mA)	Pressure (mTorr)
9-10 AM	630	0.9	270
10-11 AM	640	1.2	350
11AM-12PM	660	1.2	330
12-1 PM	700	1	300
1-2 PM	660	1	370
2-3 PM	670	1.1	360
3-4 PM	680	1.1	351
4-5 PM	680	1.2	360

Table 4.20: S5926, Day 2

Time	Voltage (V)	Current (mA)	Pressure (mTorr)
9-10 AM	630	0.8	220
10-11 AM	640	1	320
11AM-12PM	660	1.2	340
12-1 PM	700	1.1	327
1-2 PM	660	1.2	370
2-3 PM	670	1.2	366
3-4 PM	680	1.2	361
4-5 PM	680	1.1	300

CHAPTER 5

X-RAY DIFFRACTION RESULTS

As seen in the previous chapter diamond powder was separated into different parts. One part was used for XRD before plasma and others for plasma test.

5.1. XRD at UNLV

X-ray diffraction analysis were performed on a Bruker AXS D8 Advance Vario using a Johansson-type primary pre-sample monochromator (lambda = 1.54063 Å) and a LynxEye silicon strip detector. Bragg-Brentano type measurements were performed in the 2 theta range 20-125 °2theta with step sizes of 0.008 °2theta and step time of 1 s. The X-ray diffraction pattern were quantified using Rietveld structure refinement (Topas 4.2)

Figure 5.1: Picture of XRD at UNLV

5.2. XRD Results

Appendices 5.1 to 5.7 show the XRD results of all the samples.

Table 5.1: Comparison of lattice constants

Sample	Lattice Constant
Before plasma	3.5675070(92)
S5902	3.567452 (15)
S5926	3.567540 (51)
S6012A	3.567555 (10)
S6012B	3.567301 (11)
S6012C	3.567300 (11)
S6012D	3.567243 (14)

Table 5.2: Comparison of Full Width Half Maximum (FWHM)

Sample	Full Width half Maximum (FWHM)
Before plasma	0.05782°2θ
S5902	0.07286°2θ
S5926	0.07134°2θ
S6012A	0.0845°2θ
S6012B	0.0623°2 θ
S6012C	0.08386°2 θ
S6012D	0.0617°2 θ

Table 5.3: Comparison of strain

Sample	Strain
Before plasma	L- 0.00097(53)
	G- 0.08713(82)
S5902	L- 0.0002(25)
	G- 0.0700(21)
S5926	L- 0.0004(17)
	G- 0.0662(63)
S6012A	L- 0.0005(22)
	G- 0.0150(77)
S6012B	L- 0.0001(23)
	G- 0.0616(17)
S6012C	L- 0.0031(20)
	G- 0.0208(67)
S6012D	L- 0.0001(27)
	G- 0.0584(22)

CHAPTER 6

CRUSHING STRENGTH INDEX

The diamond powder sample after XRD was shipped to Engis Corporation, Illinois for Particle Size Distribution (PSD) and Crushing Strength Index (CSI). Engis Corporation is an American Company that provides super abrasive finishing systems. They provide products for grinding, honing, lapping and polishing techniques, since they have a wide experience in industrial diamonds. Engis produce products like "diamond slurries, engineered diamond compound and electroplated grinding wheels of superior quality" [76].

The properties of mechanical strength and fracture mechanism determine the characteristics and performance of the crystal as an abrasive [9]. Crystals are used as abrasives in various operations like grinding, polishing and lapping. Defects in the crystal can lead to easy and early wear of tools. High stresses caused during operation may lead to damage of the work piece. The crystal powder fracture strength is determined by applying the similar conditions during the lapping process. Lapping is the most common application of a diamond tool whose abrasive diameter is between 5 to 40 microns [9].

Static or dynamic methods do not have a strict procedure or technique to determine the strength. Benea et.al [9] from Engis Corporation invented a method for determining the strength of micron powder (<40 microns) by subjecting it to crushing under conditions replicating lapping process conditions. "The method comprised determining an initial particle size distribution for particles, subjecting abrasive to crushing force; determining a post- crushing particle size distribution for the particles; and comparing the initial and

80

post crushing particle size distribution". This is evaluated by the particles which resist to crushing under applied load. The ratio of particles resisting to crushing after an applied load for a fixed time to particles before crushing determines the crushing strength also called resistance to crushing [9].

This has led to inventing an apparatus by Benea et.al for determining the crushing strength of micron super abrasive materials [9]. From figures 6.1, 6.2 and 6.3, the numbers in parenthesis indicate parts of the apparatus.
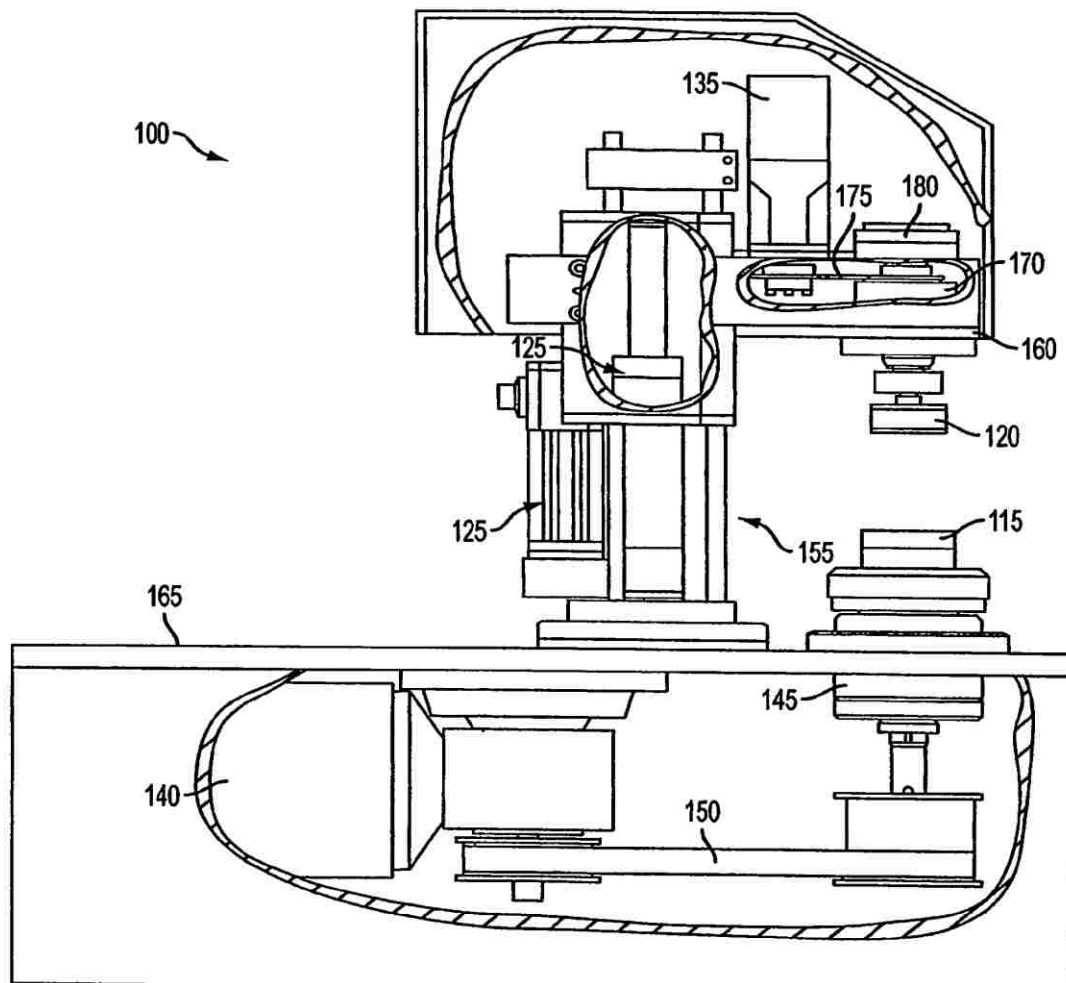
Figure 6.1: Schematic diagram of crushing strength apparatus

This apparatus uses kinematics of lapping to determine the crushing strength for particles with diameter as low as 10 microns. The testing apparatus is comprised of a steel cup (115), figure 6.3, and a steel piston (120), figure 6.2, rotating independently by gear motors (135) and (140) measured in RPM. The motors move in opposite direction with maximum speed of 200 RPM, figure 6.1. The linear actuator (125), with pneumatic or hydraulic cylinder is connected to piston (120) to apply the desired load to the cup. The cup is connected to spindle (145) which is connected to gear motor (140) by a belt (150). The piston is coupled to spindle (170), which is connected to gear motor (135) by chain (175). The gear motor (135) is mounted on an anti-rotational assembly (155). The linear actuator, piston, and anti-rotational assembly are all fixed to the platform (160). The cup, spindle (145), gear motor (140) and anti-rotational assembly are supported by the base (165).
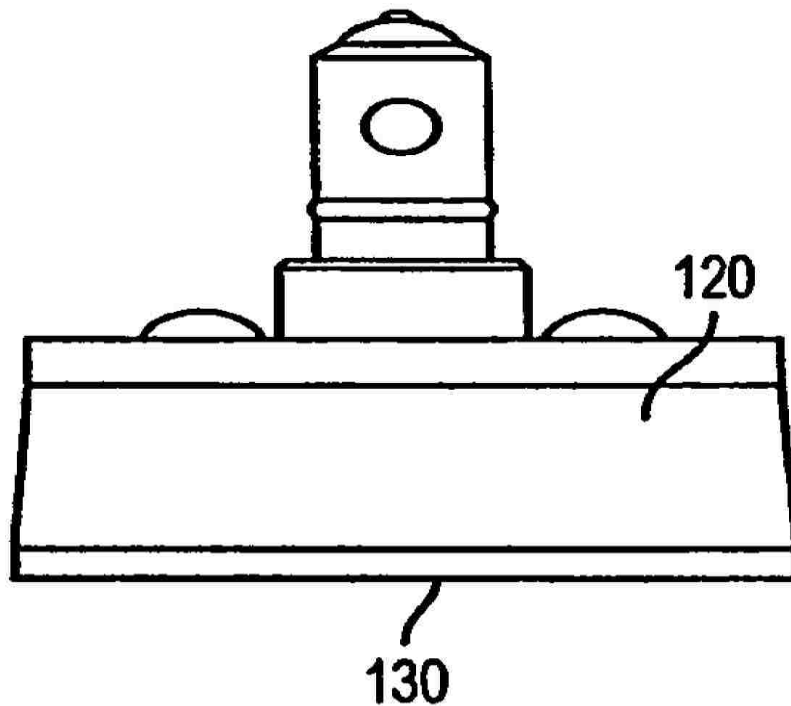
Figure 6.2: Schematic diagram of piston

82

As shown in figures 6.2 and 6.3, both piston and base cup metal are lined by

polycrystalline diamond compact (PCD) discs (130). This is to prevent the eroded steel

parts from contaminating the powder sample and to ensure precise test results.
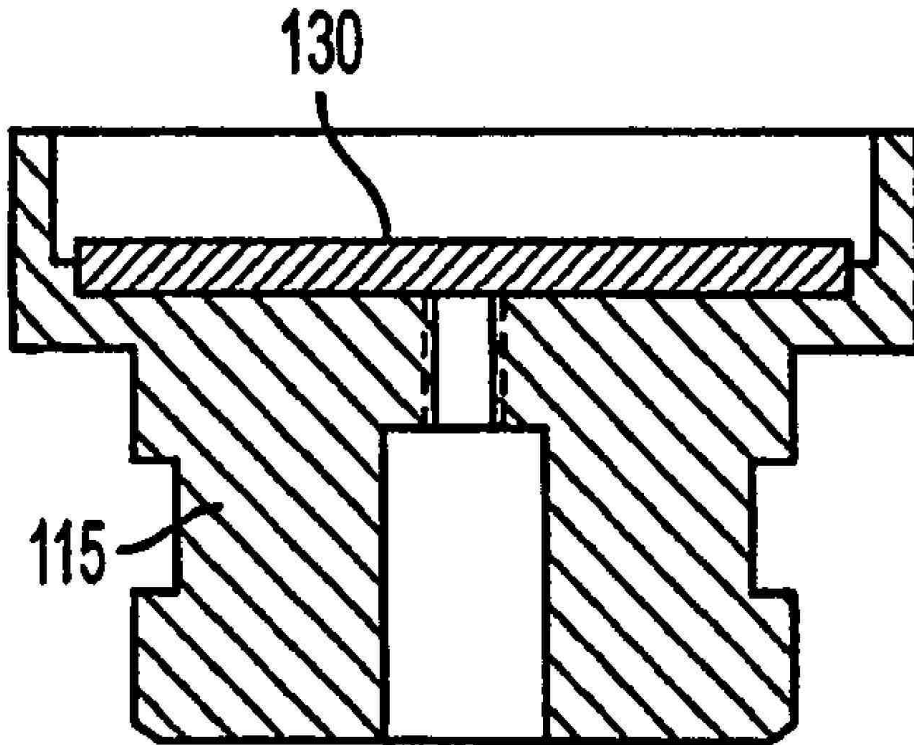
Figure 6.3: Schematic diagram of base cup

The sample powder is evenly distributed over the surface of the PCD disc. The piston

(120) is lowered into the cup (115) such that it touches the abrasive powder, pushing the

load transfer rod (190). This presses the load cell (180) causing it to produce a signal. The

signal is sent to the actuator (125) to produce the preset force for crushing. After

numerous experiments, it was determined that for particles below 40 microns, rotation is

at 10 RPM with a load of 13.4 lbs for 1 minute. As the load is evenly applied on the

abrasive powder, the cup and piston are rotated simultaneously in opposite directions at

the necessary speed for the entire duration of the crushing. At the end of the crushing time, rotations are stopped and piston is retrieved back. For further tests, powder is collected by cleaning the piston and cup with de-ionized water. This completes the crushing cycle.

The particles present in the sample vary according to their mass, size, count, surface area, etc. These particles are sorted into sections depending on them. The most common measurable property is the size of the particle. The particle size range varies between two values in microns. The number of particles in each size range is counted. Particle size distribution (PSD) is the important factor to look at before sintering process. The particles which are subjected to high pressure and temperature need to be in a specific ratio depending on their size, or else it might lead to formation of large pores after sintering, in turn lowering the strength of the component. If the ratio of large and medium particles is high, they do not pack together close enough which leads to gaps. These gaps should be filled up by small size particles sealing the sample air tight. The most common method of quantity measurement is by laser diffraction, a volume based technique. This technique determines the volume of particles of a particular size [77]. These values are used to plot a particle size distribution graph. X-axis represents the diameter in microns; Y-axis represents the frequency distribution of particles in each size range by percentile.

At Engis, the particle size distribution is done by an Electrozone sensing technique using Beckman- Coulter Multisizer III. Since the particle is present in a liquid, volume and diameter are measured by Coulter Principle [76]. The minimum (5%), mean (50%), 95% and maximum (99.9%) sizes of the particles are determined before and after crushing. These values are put in the form of a table.

The Crushing Strength Index depends on the On-Size particles in starting powder (OSS), On-Size particles in the resulting powder (OSR). "The cumulative percentile of particles between 50% and 95% of frequency distribution prior to crushing is OSS. The cumulative percentile of particles between 50% and 95% of frequency distribution after crushing is OSR. The Crushing Strength Index (CSI) is the ratio of On-size particles in resulting powder to On-size particles in starting powder" [9].

$$CSI = (OSR/OSS) * 100$$

To obtain a precise value of CSI, three trials are run on the sample determining 5%, 95% and mean values for each trial. In addition to crushing strength, fracture characteristics can also be determined by taking micrographs of the abrasive under a Scanning Electron Microscope (SEM) and Field Emission Scanning Electron Microscope (FESEM) before and after crushing.

CHAPTER 7

CSI RESULTS

Engis provided Dr. John Wang of the University of Nevada, Las Vegas with a sample of 30879 15-25 MA3 micron diamond powder. Powder treated by plasma/heat in an attempt to increase crushing strength and the sample was returned to Engis for testing.

Engis tested the powder sample designated S5902 with the following techniques:

- Particle Size Distribution

- Crushing Strength Index
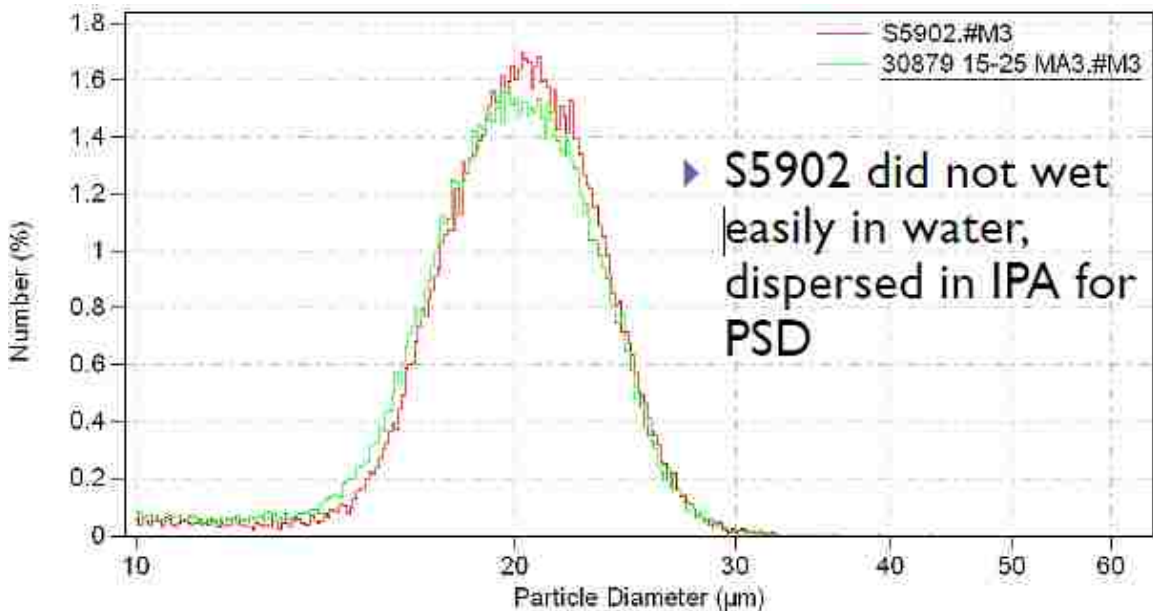
Figure 7.1: Particle size distribution

Table 7.1: Diameter on %(µm)

	Diameter on %(µm)			
Sample	5%	50%	95%	99.9%
S5902	15.69	20.27	25.20	30.71
30879	14.82	19.95	25.10	30.58
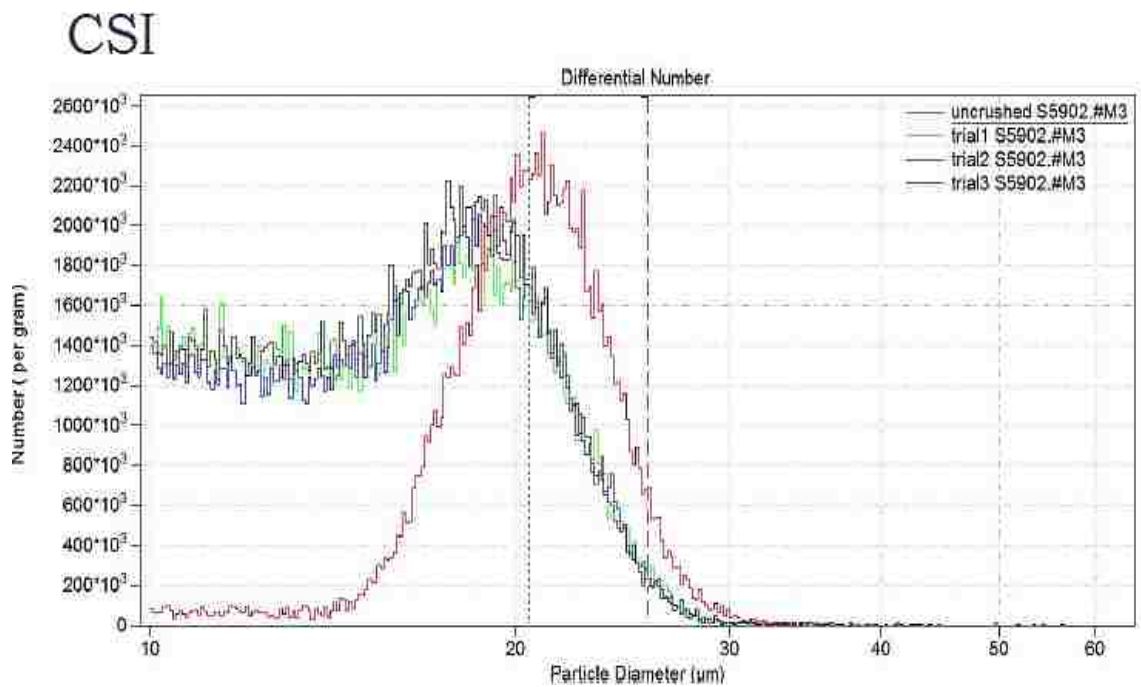
Figure 7.2: Crushing Strength Index

Table 7.2: CSI Percentage

	Range, μm		CSI				
Sample	50%	95%	Trial1	Trial2	Trial3	Average	Std dev
S5902	20.5	25.7	54.90%	55.70%	55.80%	55.50%	0.50%
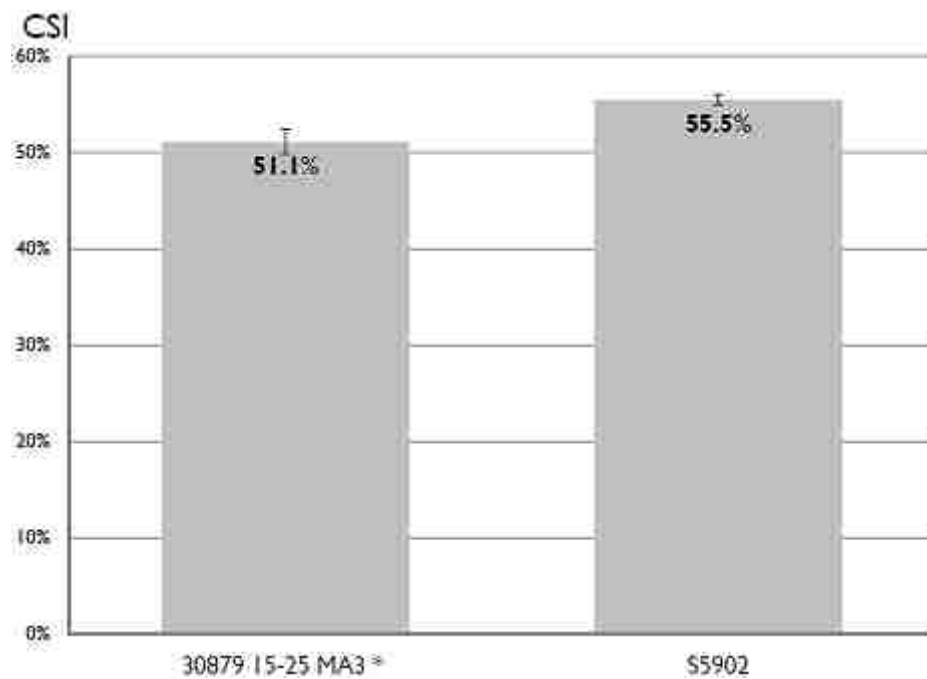
* - average of all results for 2012

Figure 7.3: CSI Summary

Plasma/heat treatment of micron diamond powder for strength enhancement by

UNLV – S5902 and S5926

Engis R&D

March-April 2012

Powder treated by plasma/heat in an attempt to increase crushing strength. 2 samples
were returned to Engis for testing:

 1 sample designated as S5902

2 sample designated as S5926
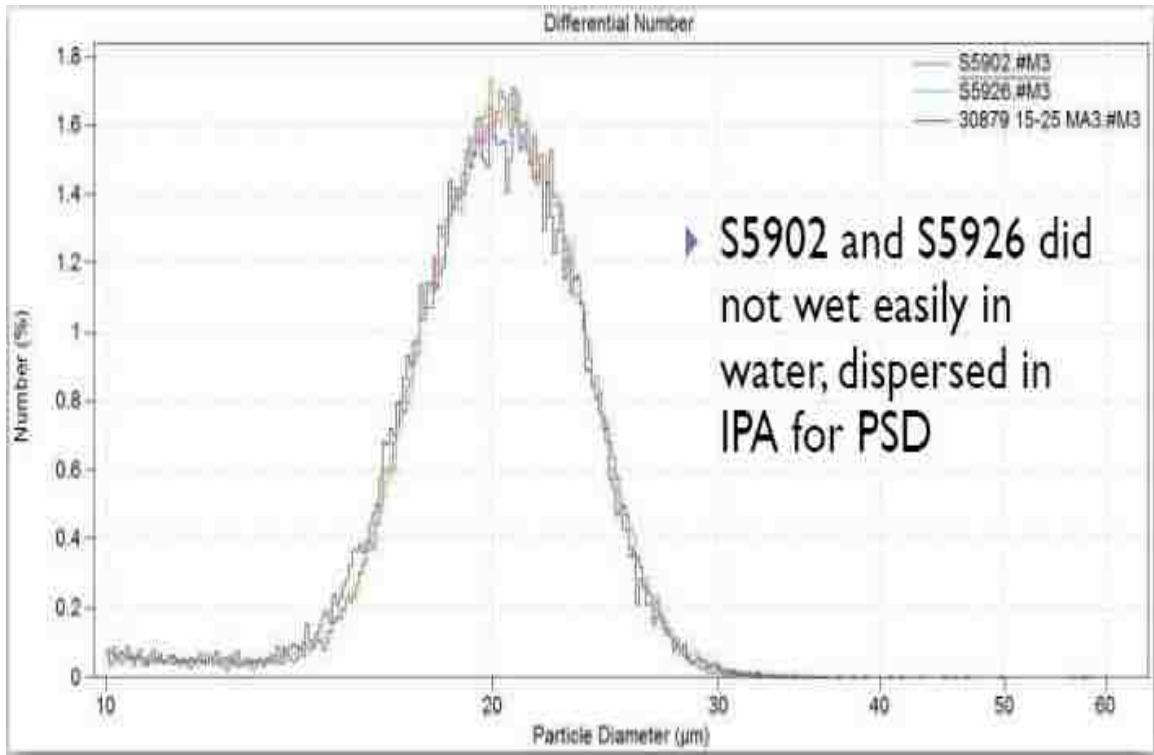
Figure 7.4: Particle Size Distribution

Table 7.3: Diameter on % (µm)

	Diameter on % (µm)			
Sample	5%	50%	95%	99.9%
S5902	15.69	20.27	25.20	30.71
S5926	15.56	20.29	25.37	32.02
30879	15.10	20.08	25.13	31.75
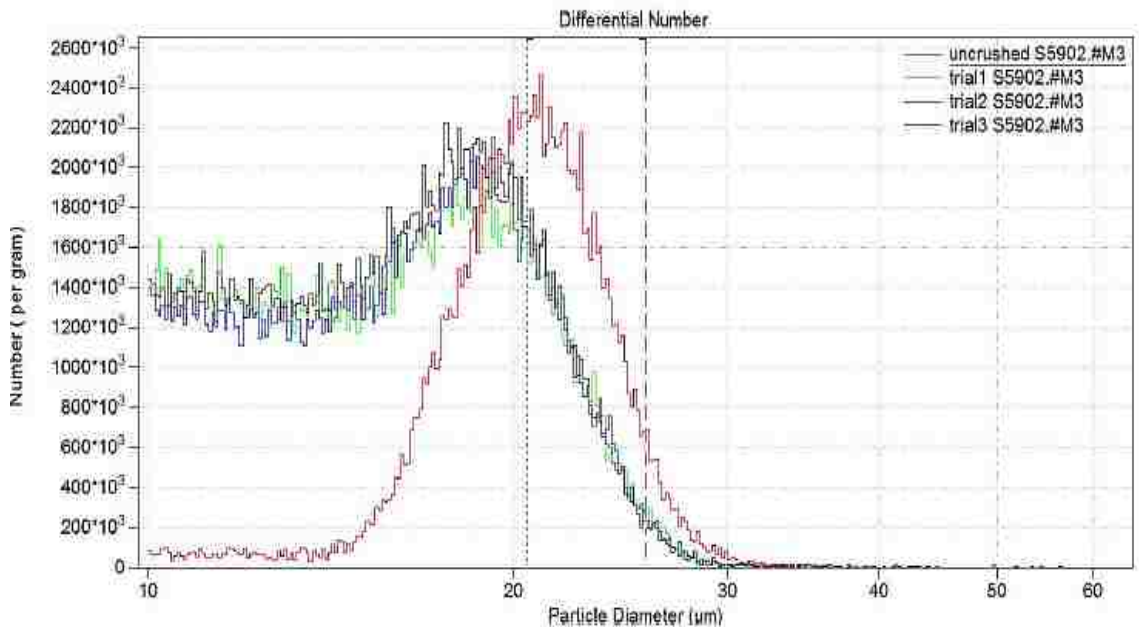
Figure 7.5: Crushing Strength Index of S5902

Table 7.4: CSI Percentage

	Range, μm		CSI				
Sample	50%	95%	Trial1	Trial2	Trial3	Average	Std dev
S5902	20.5	25.7	54.90%	55.70%	55.80%	55.50%	0.50%
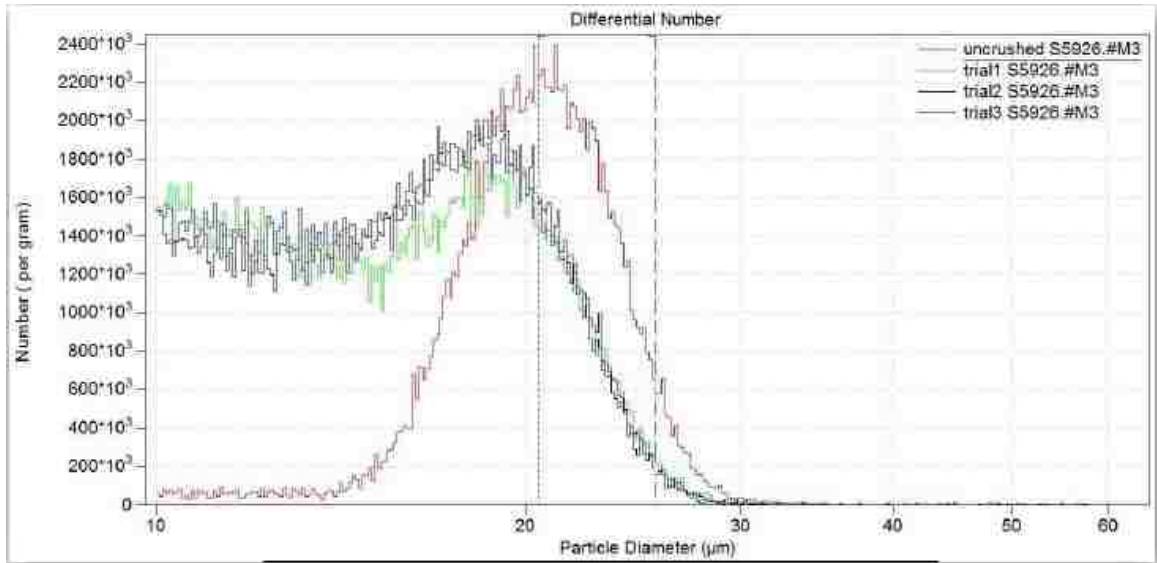
Figure 7.6: Crushing Strength index of S5926

Table 7.5: CSI Percentage

	Range, µm		CSI				
Sample	50%	95%	Trial 1	Trial 2	Trial 3	Average	Std dev
S5926	20.5	25.5	52.9%	53.3%	51.5%	52.5%	0.9%
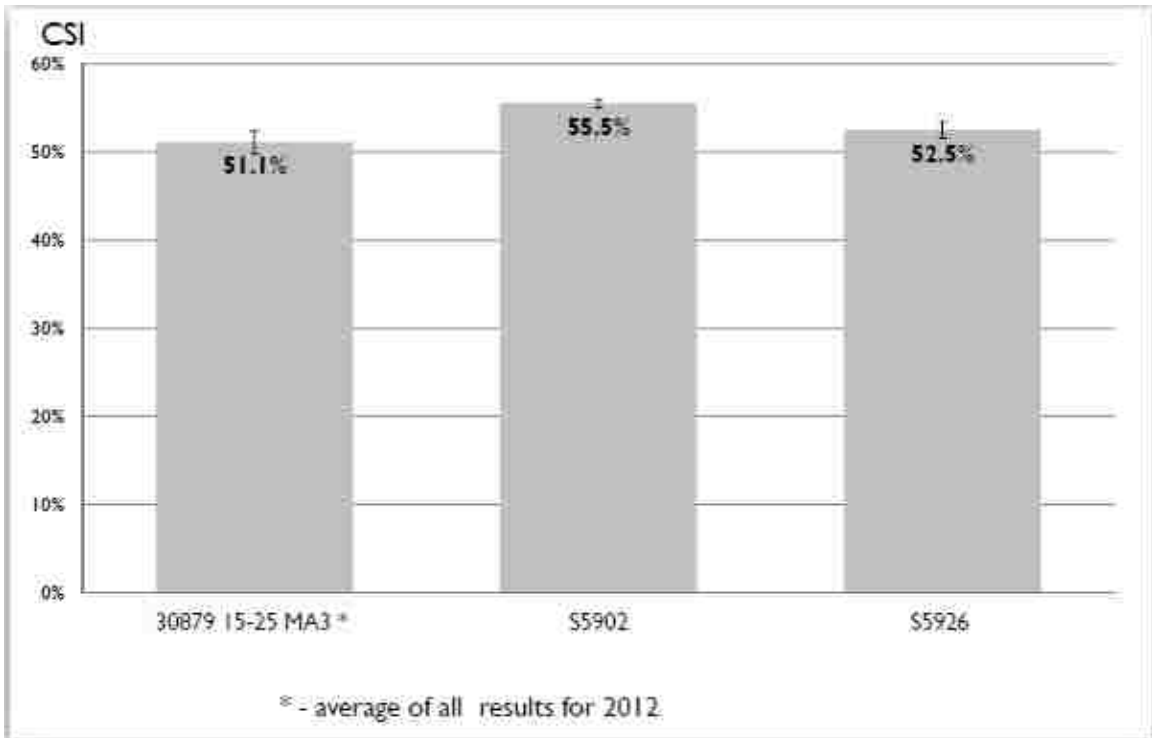
Figure 7.7: CSI Summary

Plasma/heat treatment of micron diamond powder for

strength enhancement by UNLV:

S6012A, S6012B, S6012C, S6012D

EngisR&D

June 2012

The samples were designated as:

1. sample (5/20/2012) -S6012A

2. sample (5/22/2012) -S6012B

3. sample (5/24/2012) -S6012C

4. sample (5/25/2012) -S6012D

Engis tested received diamond powders with the following techniques:

➢ Particle Size Distribution (PSD)

➢ Crushing Strength Index (CSI)
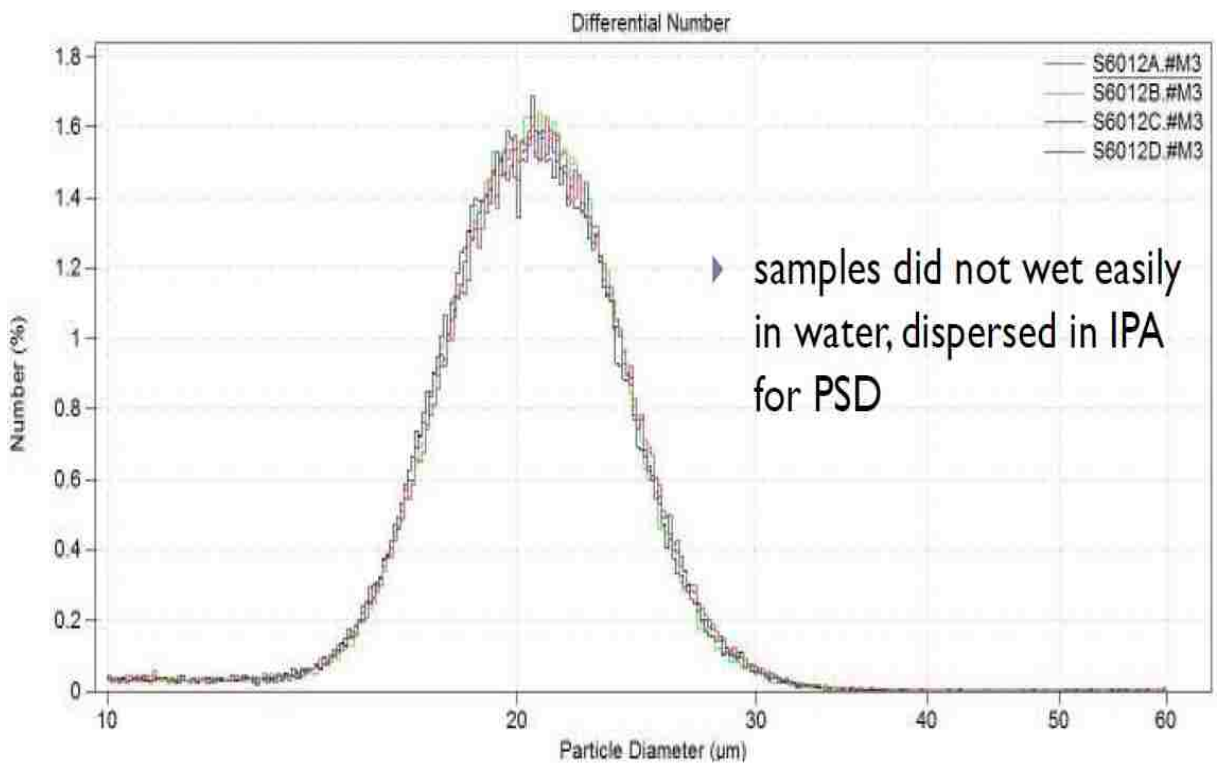
Figure 7.8: Particle size distribution

Table 7.6: Diameter on % (µm)

Diameter on % (µm)				
Sample	5%	50%	95%	99.9%
S6012A	15.86	20.58	26.25	41.26
S6012B	15.95	20.50	25.92	47.96
S6012C	15.83	20.51	26.16	36.91
S6012D	15.82	20.39	25.97	40.76
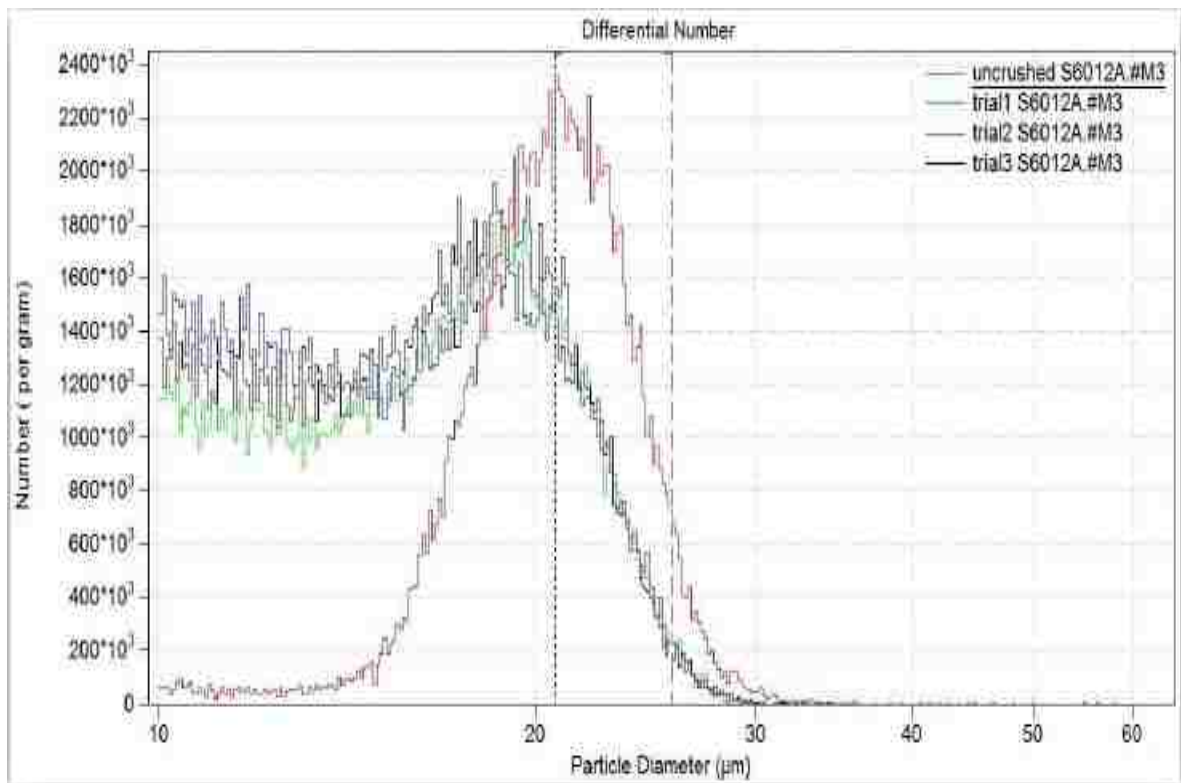
Figure 7.9: PSD- S6012A

Table 7.7: CSI Percentage

	Range, µm		CSI				
Sample	50%	95%	Trial 1	Trial 2	Trial 3	Average	Std dev
S6012A	20.7	25.7	51.6%	50.7%	52.1%	51.5%	0.7%
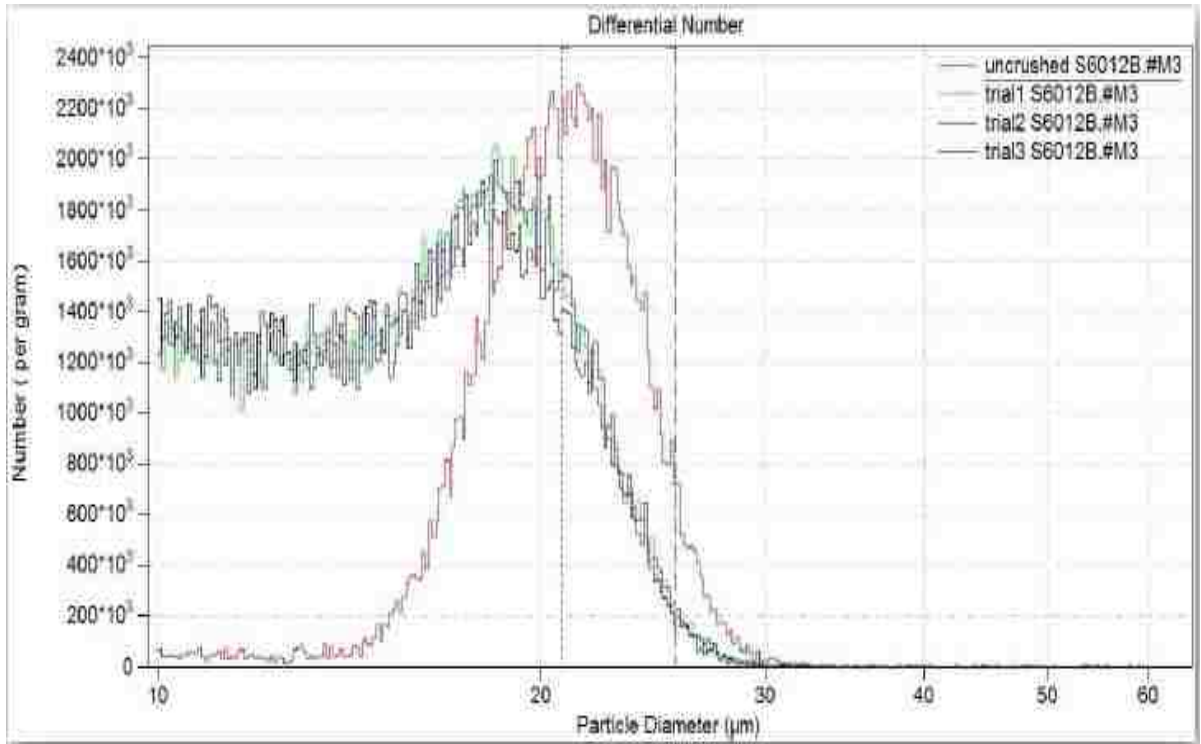
Figure 7.10: PSD S6012B

Table 7.8: CSI Percentage

	Range, µm		CSI				
Sample	50%	95%	Trial 1	Trial 2	Trial 3	Average	Std dev
S6012B	20.7	25.5	50.7%	51.0%	47.5%	49.7%	1.9%
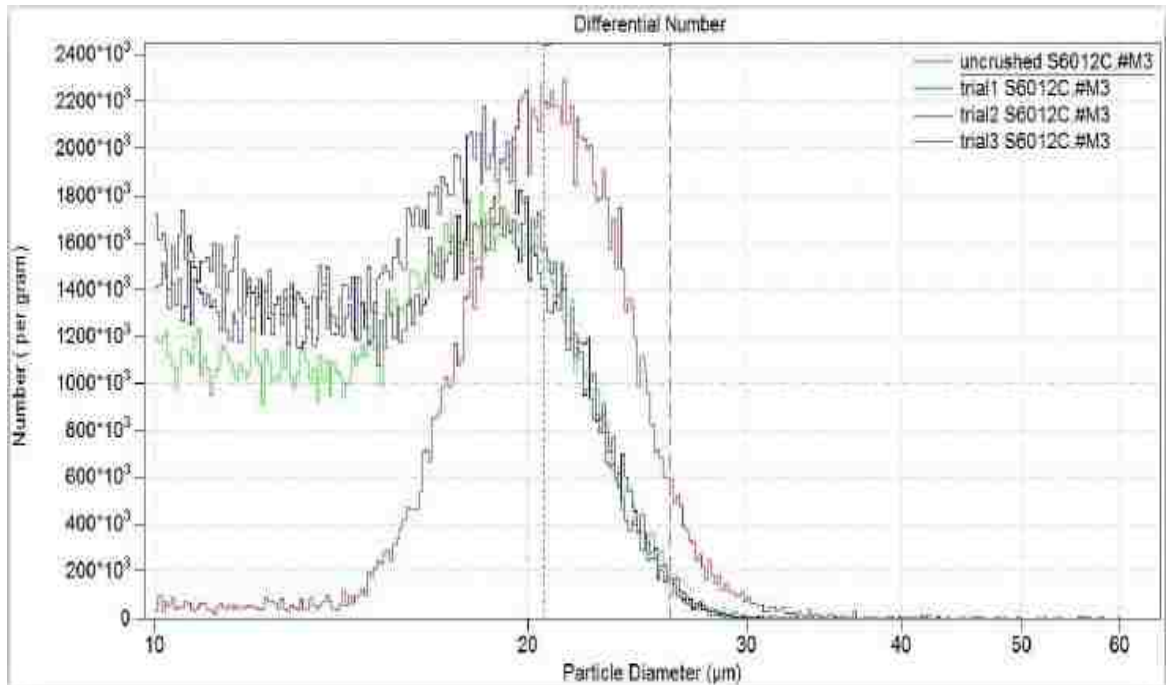
Figure 7.11: PSD S6012C

Table 7.9: CSI Percentage

	Range, μm		CSI				
Sample	50%	95%	Trial 1	Trial 2	Trial 3	Average	Std dev
S6012C	20.6	26.1	49.7%	49.0%	49.5%	49.4%	0.4%
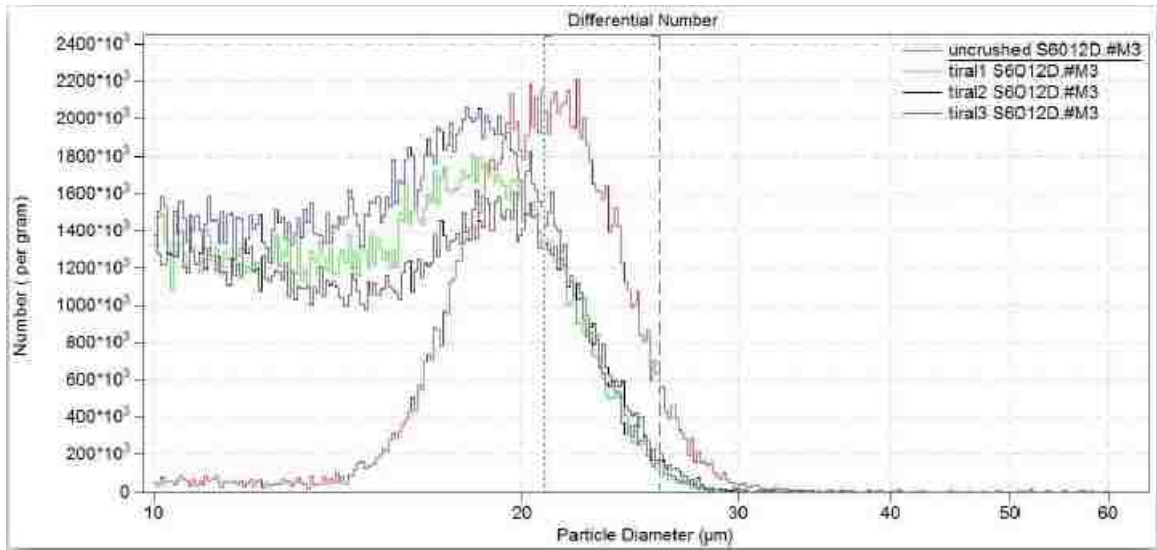
Figure 7.12: PSD S6012D

Table 7.10: CSI Percentage

	Range, µm		CSI				
Sample	50%	95%	Trial 1	Trial 2	Trial 3	Average	Std dev
S6012D	20.7	25.8	46.4%	50.3%	50.7%	49.1%	0.4%
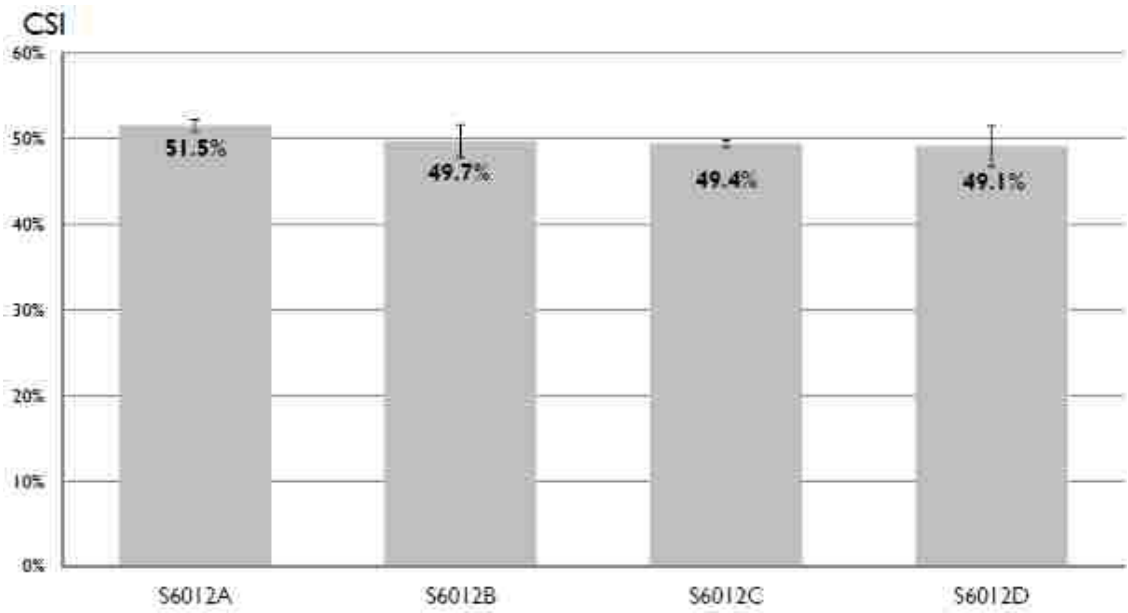
Figure 7.13: CSI Summary

CHAPTER 8

CONCLUSION AND FUTURE WORK

8.1. Conclusion

By analyzing the results of the crushing strength index the following can be concluded:

1) Comparing the Full Width Half Maximum (FWHM) values and CSI results shows no predominant relation between the two.

2) From Figure 7.13, pure hydrogen gas used in the plasma test for S6012A has proved to increase the crushing strength of diamond powders by 0.4%.

3) Conducting a plasma test on diamond powders at pressures less than 400 mTorr and for a time range higher than 16 hours in the presence of pure hydrogen gas could result in a higher crushing strength (CS).

4) From figure 7.7, the plasma test in hydrogen- air mixture (S5902) has a higher CS than plasma test in air (S5926) by 3%.

5) Comparing Figures 7.7, 7.13 and Tables 4.8-15, pressures below 400 mTorr should be maintained while performing plasma test in hydrogen-air mixture for better crushing strength results.

A detailed explanation for the conclusion is given below.

The diamond samples after plasma treatment for 16 hours total underwent XRD test to check for change in stress, strain and lattice parameters. XRD results from Chapter 5 showed no significant change in lattice parameters. The change in the full width half

maximum (FWHM) indicates a slight increase in defect concentration in crystal structures after the plasma tests. Since the change is minor, the sample is in a high crystallized state. Future tests performed on the samples could confirm it.

Table 8.1: FWHM and CSI relation

Sample name	FWHM	Crushing Strength Index (%)
S5902	0.07286°2θ	55.5
S5926	0.07134°2θ	52.5
S6012A	0.0845°2θ	51.5
S6012B	0.0623°2 θ	49.7
S6012C	0.08386°2 θ	49.4
S6012D	0.0617°2 θ	49.1

From table 8.1, no significant relation can be determined between FWHM and crushing strength index values for the samples. The plasma experiment was conducted on the first sample part (S5902) in a hydrogen- air mixture (Tables 4.8 and 4.9). Hydrogen was pumped in continuously throughout the experiment. The Crushing Strength Index (CSI) from Figure 7.3 shows a higher percentage than the average result. In order to check the reliability of the plasma experiment and CSI, both plasma and CSI was performed on the second part of the sample (S5926). The hydrogen pump was turned off accidentally. Thus, the plasma test on second sample part was conducted with air as inlet gas due to leaks. But, CSI from Figure 7.7 indicates a higher percentage of second sample than the average value. Comparing the CSI results of the first and second samples (Figure 7.7),

indicate a higher CSI for the hydrogen- air mixture plasma test sample than the sample tested in air by 3%.

Repeated tests confirmed that the pressure in the vacuum chamber rose due to rapid air leaks from 200 mTorr to 600 mTorr as compared from 600 mTorr to 2 Torr. Plasma tests were conducted for four other sample parts in Table 7.6, with pressures ranging from 600 mTorr to 2 Torr. In order to retain the gas in the chamber, after reaching the desired pressure, the vacuum pump and gas were cut off. Direct current (DC) voltage was supplied for plasma to form inside the hollow cylinder. During continuous plasma in the chamber, the pressure slowly raised to 2 Torr. At that point, DC voltage was shut down. Gas and vacuum pump valves are opened to pump in hydrogen and get the chamber to the desired pressure. The above procedure was followed for all four sample portions, as shown in Table 7.6.

Sample S6012A was selected for performing plasma tests in hydrogen gas. Hydrogen gas was pumped in, and pressures of 1 and 2 Torr were maintained throughout the experiment to minimize air leaks. Tables 4.15-4.17 show the different values for each parameter. The CSI result from Figure 7.13, shows an increase of 0.4% than the average value. As seen in Figure 7.7, plasma tests performed on samples at lower pressures, Tables 4.7-4.8 and 4.18-4.19, give better crushing strength results. Thus, conducting plasma tests in pure hydrogen gas on diamond powder at pressures below 400 mTorr could result in a higher crushing strength. During the plasma test on the other three samples (S6012B, C, and D), a pressure range of 600 mTorr to 1 Torr was maintained in the chamber. Closing of the vacuum pump and hydrogen gas valve increased the pressure due to leaks. The pressure for each hour is given in Tables 4.9-4.14. Figure 7.13 shows

the CSI for all the three samples. CS is between 49-50%, which is lower than the average value. From Tables 4.7 and 4.8, plasma tests at pressures lower than 400 mTorr yields higher CS in a hydrogen-air mixture.

8.2. Future work

A transmission electron microscopy test on the sample shows a change in defects after the plasma tests. The change in defect concentrations can be determined by tests, such as X-ray spectroscopy, mass spectroscopy, and photo-electron spectroscopy on the plasma treated sample. Plasma experiments would give better results if the following points were taken care of before the start of the experiment.

- Using a tightly sealed vacuum chamber, and not allowing air leaks.

- Having a proper experimental setup, such that the gas entering the chamber is on the other end to the vacuum pump.

- Running pre-sample experiments to determine the optimum pressure range and time duration of the experiment.

APPENDIX

5.1 XRD result before plasma

Diamond Powder with Si-Standard
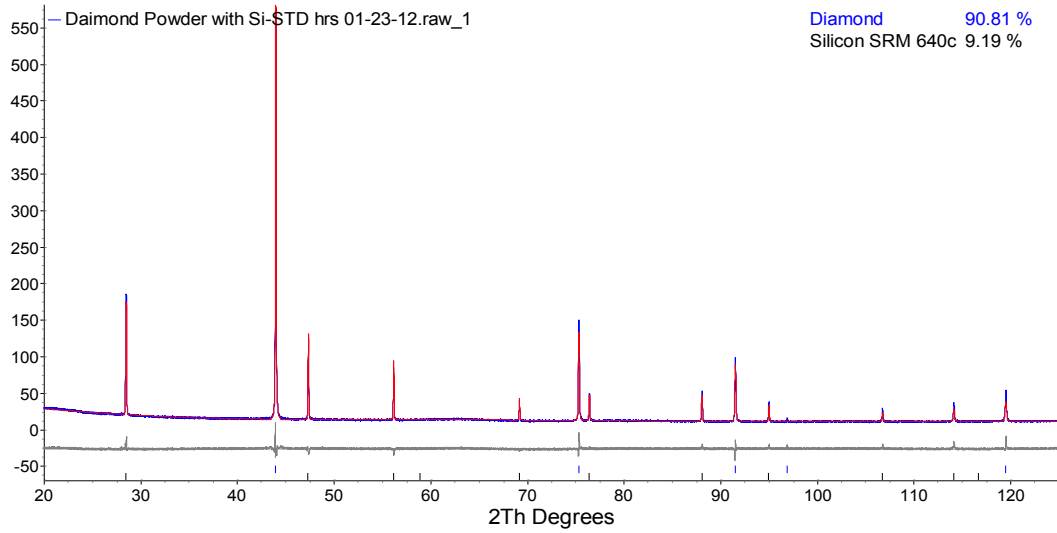
Figure 14: XRD pattern and Rietveld Refinement of Diamond Powder including Si standard (NIST SRM 640c)
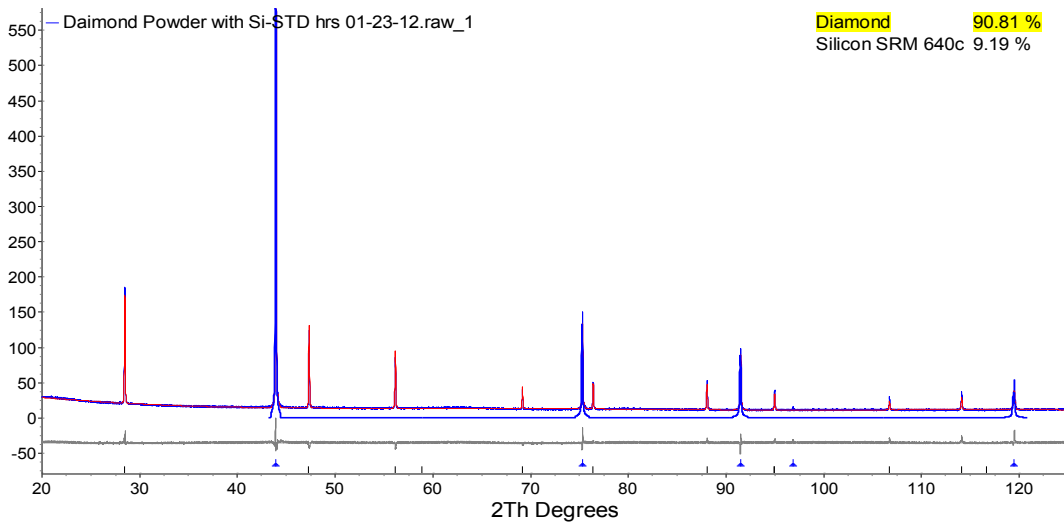
Figure 15: XRD pattern emphasizing on diffracted and calculated intensities for Diamond powder. A simple texture model (texture in (111)) was applied

Analytical Details:

The lattice parameter was refined to 3.567507(9) Å. A texture model (111) was applied.

Range Number : 1

Table 2: Before plasma R-Values

Rexp	**Rwp**	Rp	GOF
4.34	**11.61**	7.88	2.67

Table 3: Before plasma R-Values

Rexp	**Rwp**	Rp	DW
5.70	15.24	12.77	0.34

Table 4: Before plasma Quantitative Analysis –Rietveld

Phase 1	Diamond	90.811(55) %
Phase 2	Silicon SRM 640c	9.189(55) %

Table 5: Before plasma Background

Chebychev polynomial, Coefficient	
0	271.49(53)
1	-228.35(98)
2	155.58(84)
3	-94.68(79)
4	59.79(62)
5	-32.34(57)

Table 6: Before plasma Instrument

Primary radius (mm)	435
Secondary radius (mm)	435
Linear PSD 2Th angular range (°)	3
FDS angle (°)	1
Full Axial Convolution	
Filament length (mm)	12
Sample length (mm)	15
Receiving Slit length (mm)	12
Primary Sollers (°)	2.3
Secondary Sollers (°)	2.5

Table 7: Before plasma Corrections

Zero error	-0.019(16)
Specimen displacement	-0.280(65)
LP Factor	27.3

Table 8: Before plasma Structure 1

Phase name	Diamond
R-Bragg	1.831
Spacegroup	Fd-3mS
Scale	0.2994(11)
Cell Mass	96.088

Cell Volume (Å^3)	45.40404(35)
Wt% - Rietveld	90.811(55)
Crystallite Size	
Cry size Lorentzian (nm)	1255819435000.0(27)
Strain	
Strain L	0.00097(53)
Strain G	0.08713(82)
Crystal Linear Absorption Coeff. (1/cm)	15.89589(12)
Crystal Density (g/cm^3)	3.514195(27)
Preferred Orientation (Dir 1 : 1 1 1)	0.42546(58)

Table 9: Before plasma PVII peak type

FWHM = a + b/Cos(Th) + c Tan(Th)	
a	0.0047(75)
b	0.0069(88)
c	0.0001(49)

Table 10: Before plasma PVII peak type

Exponent m = 0.6+ma+mb/Cos(Th)+mc/Tan(Th)	
ma	0.21(26)
mb	0.18(16)
mc	0.144(35)

Table 11: Before plasma Lattice parameters

a (Å)	3.5675070(92)

Table 12: Before plasma Coordinate values

Site	Np	x	y	z	atom	Occ	Beq
C1	8	0.00000	0.00000	0.00000	C	1	1

Table 13: Before plasma Structure 2

Phase name	Silicon SRM 640c
R-Bragg	11.837
Spacegroup	Fd-3mS
Scale	0.003672(20)
Cell Mass	224.683
Cell Volume (Å^3)	160.20870
Wt% - Rietveld	9.189(55)
Crystallite Size	
Crystallite size Lorentzian (nm)	1612(86)
Strain	
Strain L	0.017(17)
Strain G	0.031(99)
Crystal Linear Absorption Coeff. (1/cm)	148.913
Crystal Density (g/cm^3)	2.329

Table 14: Before plasma PVII peak type

FWHM = a + b/Cos(Th) + c Tan(Th)	
a	0.016(13)
b	0.008(14)
c	0.0001(69)

Table 15: Before plasma PVII peak type

Exponent m = 0.6+ma+mb/Cos(Th)+mc/Tan(Th)	
ma	20(630)
mb	5(470)
mc	5(56)

Table 16: Before plasma Lattice parameters

a (Å)	**5.4311946**

Table 17: Before plasma Coordinate values

Site	Np	x	y	z	atom	Occ	Beq
Si1	8	0.00000	0.00000	0.00000	Si	1	3.402(33)
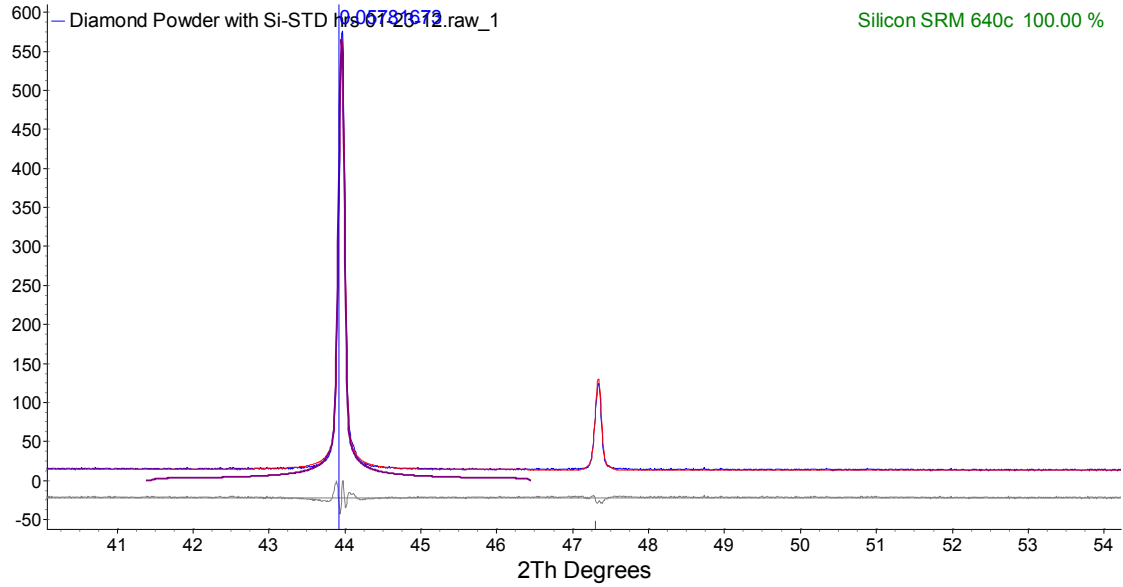
Figure 16: Full Width Half Maximum (FWHM)

FWHM = 0.05782°2theta

5.2 S5902 Result

Diamond Powder (S5902) after Plasma with Silicon Standard (03-14-12)
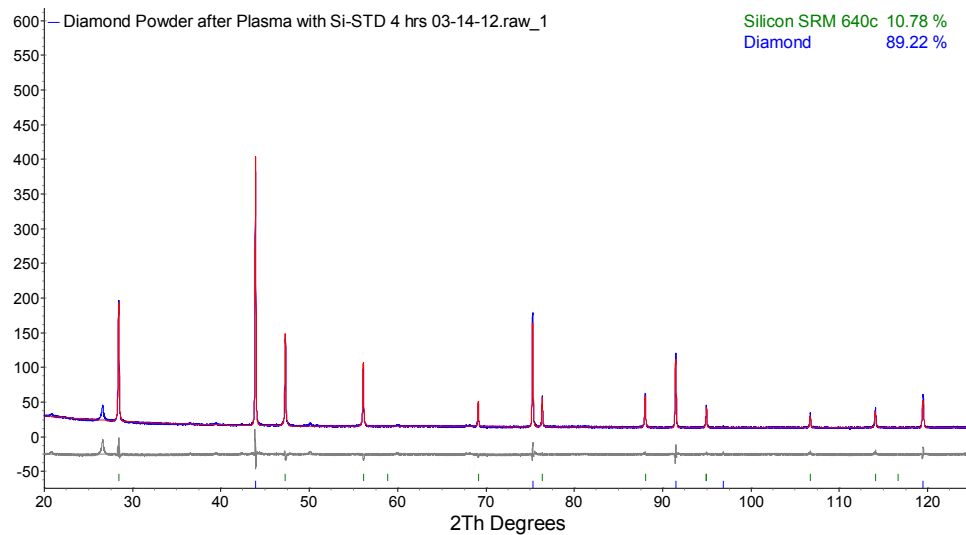
Figure 17: XRD-Rietveld Analysis of Diamond Powder – Plasma-treated
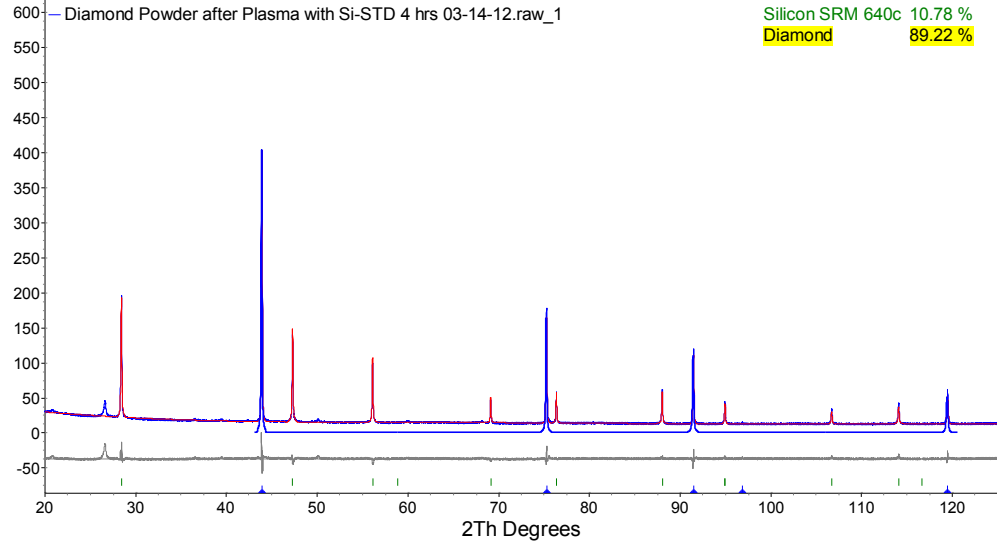
Figure 18: XRD Rietveld Analysis of Diamond Powder calculated intensities of the Diamond phase is highlighted as blue pattern

Blue: measurement intensities, red calculated, grey: measured-calculated intensities

Range Number : 1

Table 18: S5902 R-Values

Rexp	**Rwp**	Rp	GOF
4.39	**14.08**	10.11	3.21

Table 19: S5902 R-Values

Rexp	**Rwp**	Rp	DW
6.35	**20.36**	19.09	0.25

Table 20: S5902 Quantitative Analysis –Rietveld

Phase 1	Diamond	89.22 (19) %
Phase 2	Silicon SRM 640c	10.78 (19) %

Table 21: S5902 Background

Chebychev polynomial, Coefficient	
0	316.74 (68)
1	-248.8 (13)
2	159.3 (11)
3	-93.6(10)
4	57.09(80)
5	-32.34(75)

Table 22: S5902 Instrument

Primary radius (mm)	435
Secondary radius (mm)	435
Linear PSD 2Th angular range (°)	3
FDS angle (°)	1
Full Axial Convolution	
Filament length (mm)	12
Sample length (mm)	15
Receiving Slit length (mm)	12
Primary Sollers (°)	2.3
Secondary Sollers (°)	2.5

Table 23: S5902 Corrections

Zero error	-0.004 (21)
Specimen displacement	-0.003 (83)
LP Factor	27.3

Table 24: S5902 Structure 1

Phase name	Diamond
R-Bragg	2.885
Spacegroup	Fd-3mS
Scale	0.3648 (69)
Cell Mass	96.088
Cell Volume (Å^3)	45.40192 (57)
Wt% - Rietveld	89.22(19)
Crystallite Size	
Cry size Lorentzian (nm)	1620 (310)
Strain	
Strain L	0.0002 (25)
Strain G	0.0700 (21)
Crystal Linear Absorption Coeff. (1/cm)	15.89589(20)
Crystal Density (g/cm^3)	3.514195(44)
Preferred Orientation (Dir 1 : 1 1 1)	0.5980 (40)

Table 25: S5902 PVII peak type

FWHM = a + b/Cos(Th) + c Tan(Th)	
a	0.0083 (70)
b	0.0095 (82)
c	0.0010 (47)

Table 26: S5902 PVII peak type

Exponent m = 0.6+ma+mb/Cos(Th)+mc/Tan(Th)	
ma	0.38 (45)
mb	0.36 (30)
mc	0.114(60)

Table 27: S5902 Lattice parameters

a (Å)	**3.567452 (15)**

Table 28: S5902 Coordinate values

Site	Np	x	y	z	atom	Occ	Beq
C1	8	0.00000	0.00000	0.00000	C	1	1.084 (57)

Table 29: S5902 Structure 2

Phase name	Silicon SRM 640c
R-Bragg	8.902

Spacegroup	Fd-3mS
Scale	0.005340 (28)
Cell Mass	224.683
Cell Volume (Å^3)	160.20870
Wt% - Rietveld	10.78 (19)
Crystallite Size	
Crystallite size Lorentzian (nm)	398 (24)
Strain	
Strain L	0.0139 (36)
Strain G	0.0404 (44)
Crystal Linear Absorption Coeff. (1/cm)	148.913
Crystal Density (g/cm^3)	2.329

Table 30: S5902 PVII peak type

FWHM = a + b/Cos(Th) + c Tan(Th)	
a	0.020 (14)
b	0.004 (16)
c	0.0001 (80)

Table 31: S5902 PVII peak type

Exponent m = 0.6+ma+mb/Cos(Th)+mc/Tan(Th)	
ma	20(580)
mb	5(490)

mc	0(30)

Table 32: S5902 Lattice parameters

a (Å)				5.4311946			
Site	Np	x	y	z	atom	Occ	Beq
Si1	8	0.00000	0.00000	0.00000	Si	1	2.663(30)
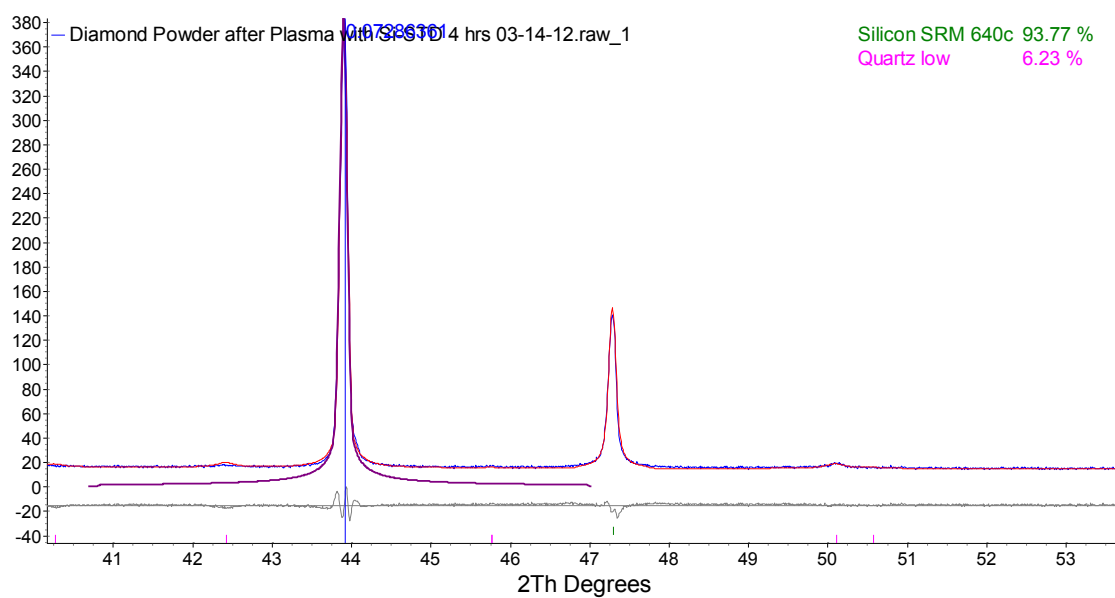
Figure 19: Full Width Half Maximum (FWHM)

FWHM = 0.07286°2theta

5.3 S5926 Result

Diamond Powder (S5926) Plasma treated on 03-25-12
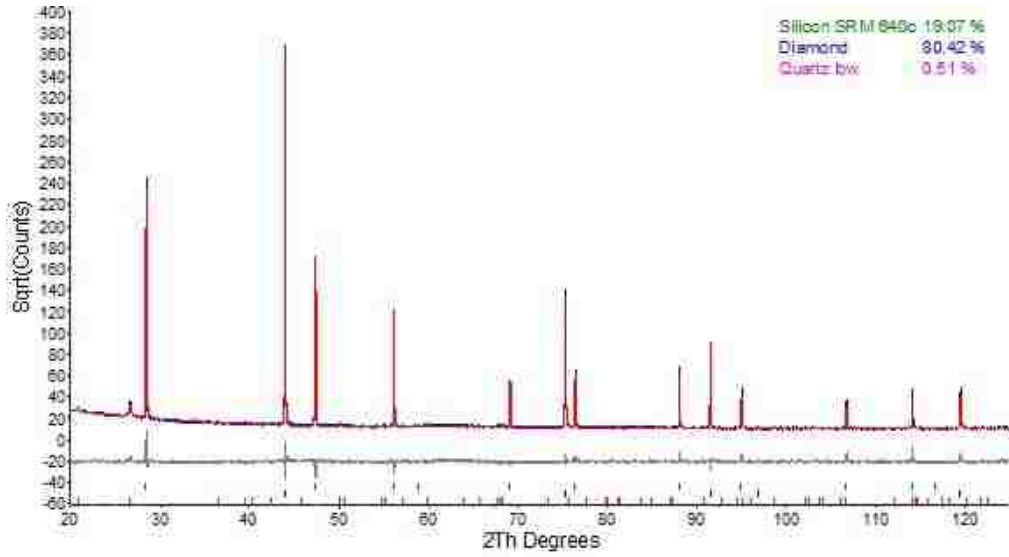
Figure 20: XRD Rietveld Analysis of Diamond Powder

Range Number : 1

Table 33: S5926 R-Values

Rexp	**Rwp**	Rp	GOF
4.89	**13.51**	10.04	2.77

Table 34: S5926 R-Values

Rexp	**Rwp**	Rp	DW
6.82	18.85	17.97	0.32

Table 35: S5926 Quantitative Analysis –Rietveld

Phase 1	Diamond	80.42 (35) %

118

| Phase 2 | Silicon SRM 640c | 19.07 (34) % |
| Phase 3 | Quartz low | 0.508 (18) % |

Table 36: S5926 Background

Chebychev polynomial, Coefficient	
0	244.35 (57)
1	-216.1 (10)
2	145.16 (85)
3	-87.15 (78)
4	49.74 (61)
5	-22.57 (56)

Table 37: S5926 Instrument

Primary radius (mm)	435
Secondary radius (mm)	435
Linear PSD 2Th angular range (°)	3
FDS angle (°)	1
Full Axial Convolution	
Filament length (mm)	12
Sample length (mm)	15
Receiving Slit length (mm)	12
Primary Sollers (°)	2.3
Secondary Sollers (°)	2.5

Table 38: S5926 Corrections

Zero error	-0.009 (15)
Specimen displacement	-0.367 (60)
LP Factor	27.3

Table 39: S5926 Structure 1

Phase name	Diamond
R-Bragg	2.030
Spacegroup	Fd-3mS
Scale	0.2491 (54)
Cell Mass	96.088
Cell Volume (Å^3)	45.39397 (52)
Wt% - Rietveld	80.42 (35)
Crystallite Size	
Cry size Lorentzian (nm)	2470 (740)
Strain	
Strain L	0.0004 (17)
Strain G	0.0662 (63)
Crystal Linear Absorption Coeff. (1/cm)	15.89942 (18)
Crystal Density (g/cm^3)	3.514975 (41)
Preferred Orientation (Dir 1 : 1 1 1)	0.5470 (35)

Table 40: S5926 PVII peak type

FWHM = a + b/Cos(Th) + c Tan(Th)	
a	0.0100 (72)
b	0.0081 (85)
c	0.0001 (48)

Table 41: S5926 PVII peak type

Exponent m = 0.6+ma+mb/Cos(Th)+mc/Tan(Th)	
ma	0.35 (57)
mb	0.40 (38)
mc	0.133 (72)

Table 42: S5926 Lattice parameters

a (Å)	**3.567540 (51)**

Table 43: S5926 Coordinate values

Site	Np	x	y	z	atom	Occ	Beq
C1	8	0.00000	0.00000	0.00000	C	1	1.424(67)

Table 44: S5926 Structure 2

Phase name	Silicon SRM 640c
R-Bragg	16.746
Spacegroup	Fd-3mS

Scale	0.007159 (31)
Cell Mass	224.683
Cell Volume (Å^3)	160.20870
Wt% - Rietveld	19.07 (34)
Crystallite Size	
Crystallite size Lorentzian (nm)	652 (32)
Strain	
Strain L	0.0001 (18)
Strain G	0.000 (10)
Crystal Linear Absorption Coeff. (1/cm)	148.913
Crystal Density (g/cm^3)	2.329

Table 45: S5926 PVII peak type

FWHM = a + b/Cos(Th) + c Tan(Th)	
a	0.0160 (78)
b	0.0089 (89)
c	0.0001 (46)

Table 46: S5926 PVII peak type

Exponent m = 0.6+ma+mb/Cos(Th)+mc/Tan(Th)	
ma	20 (350)
mb	5 (250)
mc	5 (41)

Table 47: S5926 Lattice parameters

a (Å)				5.4311845			
Site	Np	x	y	z	atom	Occ	Beq
Si1	8	0.00000	0.00000	0.00000	Si	1	4.097(29)

Table 48: S5926 Structure 3

Phase name	Quartz low
R-Bragg	7.966
Spacegroup	P3221
Scale	0.0002293 (73)
Cell Mass	264.508
Cell Volume (Å^3)	113.138 (48)
Wt% - Rietveld	0.508 (18)
Crystallite Size	
Crystallite size Lorentzian (nm)	43.1 (23)
Crystal Linear Absorption Coeff. (1/cm)	174.346 (74)
Crystal Density (g/cm^3)	3.8822 (16)

Table 49: S5926 Lattice parameters

a (Å)				4.91402 (78)			
c (Å)				5.4101 (15)			
Site	Np	x	y	z	atom	Occ	Beq
Si1	6	0.4630	0.00000	0.66670	Si+4	1	0.8

| O1 | 6 | 0.40900 | 0.27900 | 0.77400 | O-2 | 1 | 0.9 |

FWHM= $0.07134^0$2theta.

5.4 S6012A Result

Diamond Sample 1 (S6012A) Plasma-treated 4H 05-20-12
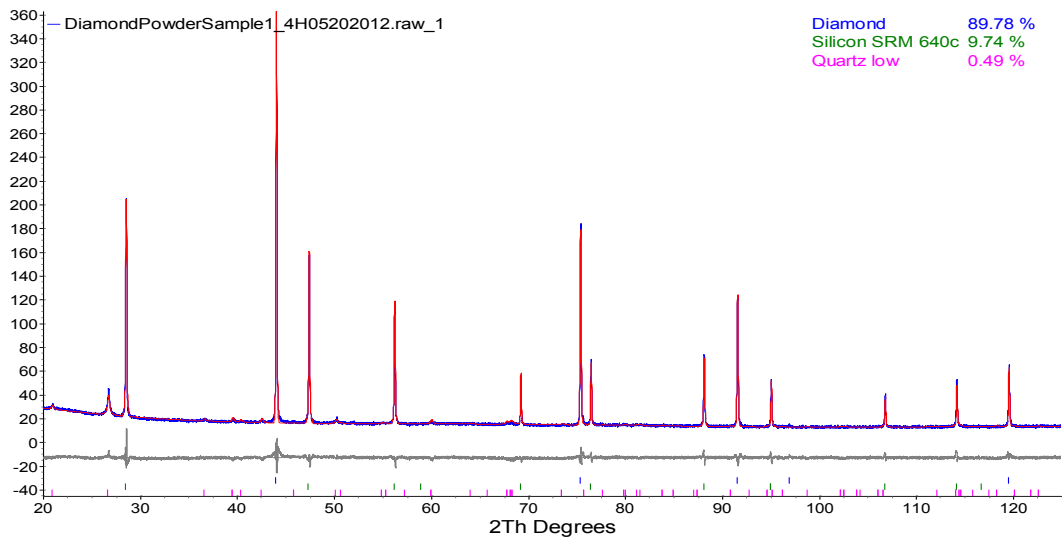
Figure 21: XRD Rietveld Analysis of Diamond Powder

Range Number : 1

Table 50: S6012A R-Values

Rexp	**Rwp**	Rp	GOF
4.23	**10.00**	7.43	2.36

Table 51: S6012A R-Values

Rexp	**Rwp**	Rp	DW
6.01	14.19	13.64	0.41

124

Table 52: S6012A Quantitative Analysis –Rietveld

Phase 1	Diamond	89.78 (14) %
Phase 2	Silicon SRM 640c	9.74 (13) %
Phase 3	Quartz low	0.486 (11) %

Table 53: S6012A Background

Chebychev polynomial, Coefficient	
0	313.28 (54)
1	-224.82(95)
2	141.41 (81)
3	-78.05 (75)
4	54.20 (60)
5	-25.80 (56)

Table 54: S6012A Instrument

Primary radius (mm)	435
Secondary radius (mm)	435
Linear PSD 2Th angular range (°)	3
FDS angle (°)	1
Full Axial Convolution	
Filament length (mm)	12
Sample length (mm)	15
Receiving Slit length (mm)	12

Primary Sollers (°)	2.3
Secondary Sollers (°)	2.5

Table 55: S6012A Corrections

Zero error	-0.021(24)
Specimen displacement	-0.334 (94)
LP Factor	27.3

Table 56: S6012A Structure 1

Phase name	Diamond
R-Bragg	1.502
Spacegroup	Fd-3mS
Scale	0.4812 (71)
Cell Mass	96.088
Cell Volume (Å^3)	45.40587 (39)
Wt% - Rietveld	89.78(14)
Crystallite Size	
Cry size Lorentzian (nm)	3700 (1400)
Strain	
Strain L	0.0005 (22)
Strain G	0.0150 (77)
Crystal Linear Absorption Coeff. (1/cm)	15.89525 (20)
Crystal Density (g/cm^3)	3.514054 (30)

Preferred Orientation (Dir 1 : 1 1 1)	0.6759 (47)

Table 57: S6012A PVII peak type

FWHM = a + b/Cos(Th) + c Tan(Th)	
a	0.0223 (33)
b	0.0126 (39)
c	0.0001 (22)

Table 58: S6012A PVII peak type

Exponent m = 0.6+ma+mb/Cos(Th)+mc/Tan(Th)	
ma	1.16 (51)
Mb	0.38 (34)
Mc	0.451 (82)

Table 59: S6012A Lattice parameters

a (Å)	**3.567555 (10)**

Table 60: S6012A Coordinate values

Site	Np	x	y	z	atom	Occ	Beq
C1	8	0.00000	0.00000	0.00000	C	1	1.577(44)

Table 61: S6012A Structure 2

Phase name	Silicon SRM 640c

R-Bragg	4.735
Spacegroup	Fd-3mS
Scale	0.006326 (21)
Cell Mass	224.683
Cell Volume (Å^3)	160.20870
Wt% - Rietveld	9.74 (13)
Crystallite Size	
Crystallite size Lorentzian (nm)	451 (17)
Strain	
Strain L	0.001 (19)
Strain G	0.0320 (30)
Crystal Linear Absorption Coeff. (1/cm)	148.913
Crystal Density (g/cm^3)	2.329

Table 62: S6012A PVII peak type

FWHM = a + b/Cos(Th) + c Tan(Th)	
a	0.0343 (65)
b	0.0001 (74)
c	0.0001 (40)

Table 63: S6012A PVII peak type

Exponent m = 0.6+ma+mb/Cos(Th)+mc/Tan(Th)	
ma	20(250)

mb	5(180)
mc	5(28)

Table 64: S6012A Lattice parameters

a (Å)	5.4311946

Table 65: S6012A Coordinate values

Site	Np	x	y	z	atom	Occ	Beq
Si1	8	0.00000	0.00000	0.00000	Si	1	2.261(18)

Table 66: S6012A Structure 3

Phase name	Quartz low
R-Bragg	8.117
Spacegroup	P3221
Scale	0.0003795 (72)
Cell Mass	264.508
Cell Volume (Å^3)	113.168 (70)
Wt% - Rietveld	0.486 (11)
Crystallite Size	
Crystallite size Lorentzian (nm)	43.8 (14)
Crystal Linear Absorption Coeff. (1/cm)	174.300 (46)
Crystal Density (g/cm^3)	3.8812 (10)

Table 67: S6012A Lattice parameters

a (Å)	4.91548 (48)
c (Å)	5.40830 (94)

Table 68: S6012A Coordinate values

Site	Np	x	y	z	atom	Occ	Beq
Si1	6	0.4630	0.00000	0.66670	Si+4	1	0.8
O1	6	0.40900	0.27900	0.7740	O-2	1	0.9

Table 69: S6012A FWHM

	h	k	l	m	d	Th2	F^2
1	1	1	1	8	2.05973	43.92261	949.546
2	0	2	2	12	1.26132	75.28133	882.666
3	3	1	1	24	1.07566	91.46976	588.611
4	2	2	2	8	1.02986	96.82806	0.000
5	0	0	4	6	0.89189	119.46249	177.305
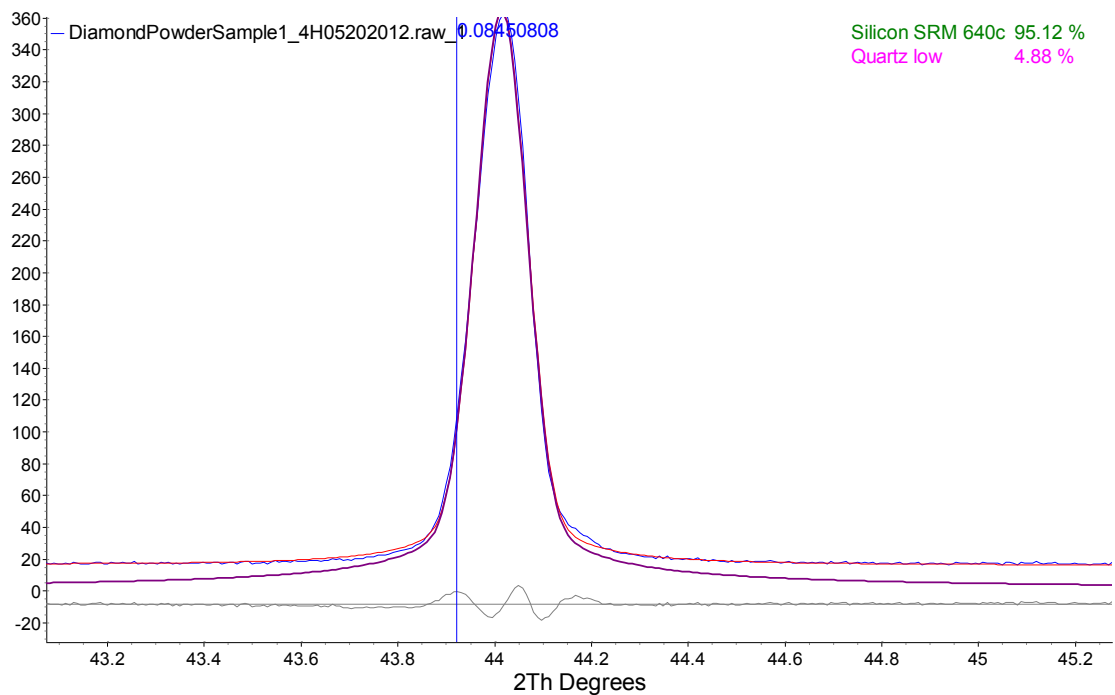
Figure 22: Full width half maximum (FWHM)

Full width half maximum (FWHM) at (111) = 0.0845°2theta

5.5 S6012B Result

Diamond Powder Plasma Treated Sample 2 (S6012B) on 05-22-12
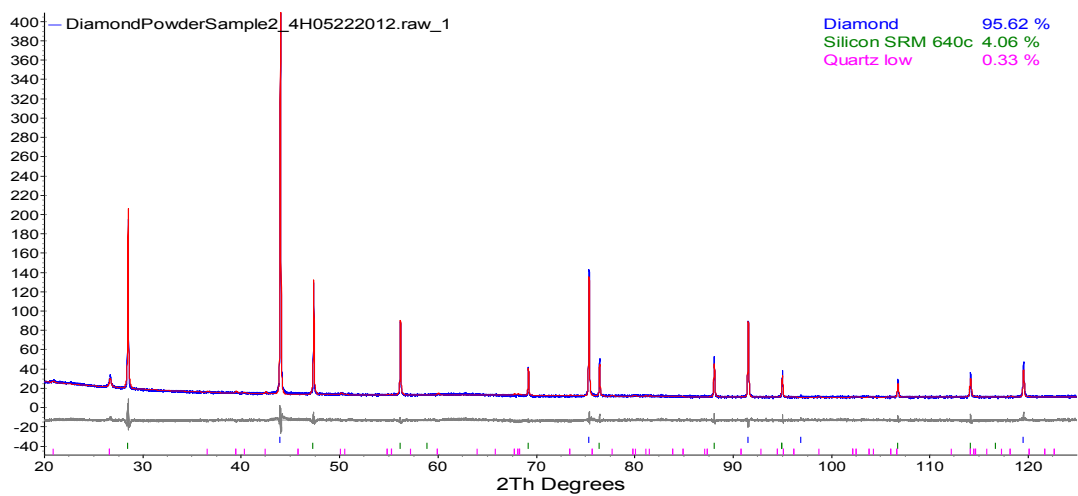
Figure 23: XRD Rietveld Analysis of Diamond Powder

Range Number : 1

Table 70: S6012B R-Values

Rexp	**Rwp**	Rp	GOF
4.95	**10.86**	8.02	2.20

Table 71: S6012B R-Values

Rexp	**Rwp**	Rp	DW
6.97	15.30	14.61	0.51

Table 72: S6012B Quantitative Analysis –Rietveld

Phase 1	Diamond	95.62 (49) %
Phase 2	Silicon SRM 640c	4.06 (49) %
Phase 3	Quartz low	0.328 (13) %

Table 73: S6012B Background

Chebychev polynomial, Coefficient	
0	240.02 (44)
1	-203.32(78)
2	133.40 (66)
3	-74.95 (61)
4	46.85 (48)
5	-22.44 (44)

Table 74: S6012B Instrument

Primary radius (mm)	435
Secondary radius (mm)	435
Linear PSD 2Th angular range (°)	3
FDS angle (°)	1
Full Axial Convolution	
Filament length (mm)	12
Sample length (mm)	15
Receiving Slit length (mm)	12
Primary Sollers (°)	2.3
Secondary Sollers (°)	2.5

Table 75: S6012B Corrections

Zero error	-0.001 (61)
Specimen displacement	-0.31 (23)
LP Factor	27.3

Table 76: S6012B Structure 1

Phase name	Diamond
R-Bragg	1.666
Spacegroup	Fd-3mS
Scale	0.2912 (49)
Cell Mass	96.088

Cell Volume (Å^3)	45.39617 (41)
Wt% - Rietveld	95.62 (49)
Crystallite Size	
Cry size Lorentzian (nm)	1000 (1000)
Strain	
Strain L	0.0001 (23)
Strain G	0.0616 (17)
Crystal Linear Absorption Coeff. (1/cm)	15.89864(14)
Crystal Density (g/cm^3)	3.514804 (32)
Preferred Orientation (Dir 1 : 1 1 1)	0.5211 (24)

Table 77: S6012B PVII peak type

FWHM = a + b/Cos(Th) + c Tan(Th)	
a	0.0128 (60)
b	0.0070 (70)
c	0.0001 (39)

Table 78: S6012B PVII peak type

Exponent m = 0.6+ma+mb/Cos(Th)+mc/Tan(Th)	
ma	0.37 (43)
mb	0.36 (28)
mc	0.172 (56)

Table 79: S6012B Lattice parameters

a (Å)	3.567301 (11)

Table 80: S6012B Coordinate values

Site	Np	x	y	z	atom	Occ	Beq
C1	8	0.00000	0.00000	0.00000	C	1	1.686(54)

Table 81: S6012B Structure 2

Phase name	Silicon SRM 640c
R-Bragg	3.630
Spacegroup	Fd-3mS
Scale	0.00150 (19)
Cell Mass	224.683
Cell Volume (Å^3)	160.20870
Wt% - Rietveld	4.06 (49)
Crystallite Size	
Crystallite size Lorentzian (nm)	407 (10)
Strain	
Strain L	0.0001 (19)
Strain G	0.0803 (13)
Crystal Linear Absorption Coeff. (1/cm)	148.913
Crystal Density (g/cm^3)	2.329

Table 82: S6012B PVII peak type

FWHM = a + b/Cos(Th) + c Tan(Th)	
a	0.0001 (62)
b	0.0001 (65)
c	0.0042 (29)

Table 83: S6012B PVII peak type

Exponent m = 0.6+ma+mb/Cos(Th)+mc/Tan(Th)	
ma	0(43)
mb	1 (28)
mc	2.1 (74)

Table 84: S6012B Lattice parameters

a (Å)				5.4311946			
Site	Np	x	y	z	atom	Occ	Beq
Si1	8	0.00000	0.00000	0.00000	Si	1	1.03 (22)

Table 85: S6012B Structure 3

Phase name	Quartz low
R-Bragg	6.473
Spacegroup	P3221
Scale	0.0001456 (50)
Cell Mass	264.508

Cell Volume (Å^3)	113.129 (45)
Wt% - Rietveld	0.328 (13)
Crystallite Size	
Crystallite size Lorentzian (nm)	53.2 (32)
Crystal Linear Absorption Coeff. (1/cm)	174.359 (70)
Crystal Density (g/cm^3)	3.8825(16)

Table 86: S6012B Lattice parameters

a (Å)				4.91301 (74)			
c (Å)				5.4119 (14)			
Site	Np	x	y	z	atom	Occ	Beq
Si1	6	0.4630	0.00000	0.66670	Si+4	1	0.8
O1	6	0.40900	0.27900	0.7740	O-2	1	0.9
	h	k	l	m	d	Th2	F^2
1	1	1	1	8	2.05958	43.92590	567.243
2	0	2	2	12	1.26123	75.28762	516.078
3	3	1	1	24	1.07558	91.47813	339.745
4	2	2	2	8	1.02979	96.83725	0.000
5	0	0	4	6	0.89183	119.47647	100.165
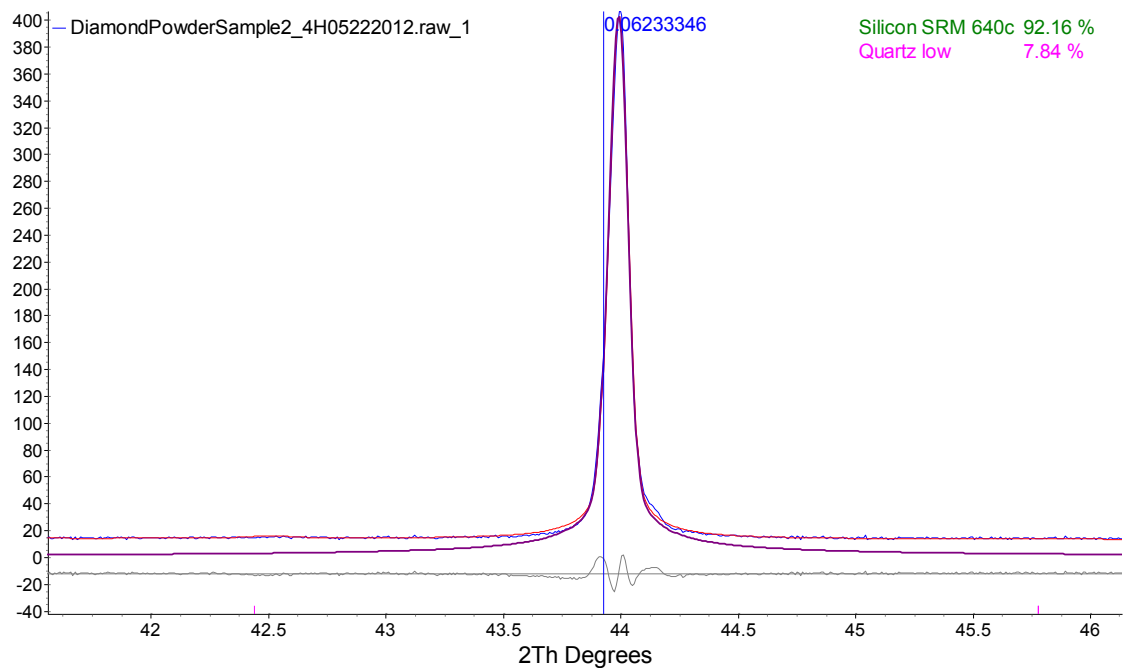
Figure 24: Full width half maximum (FWHM)

FWHM (111) = 0.0623°2theta

5.6 S6012C Result

Sample 3 Diamond Powder (S6012C) after Plasma treatment 05-24-2012.
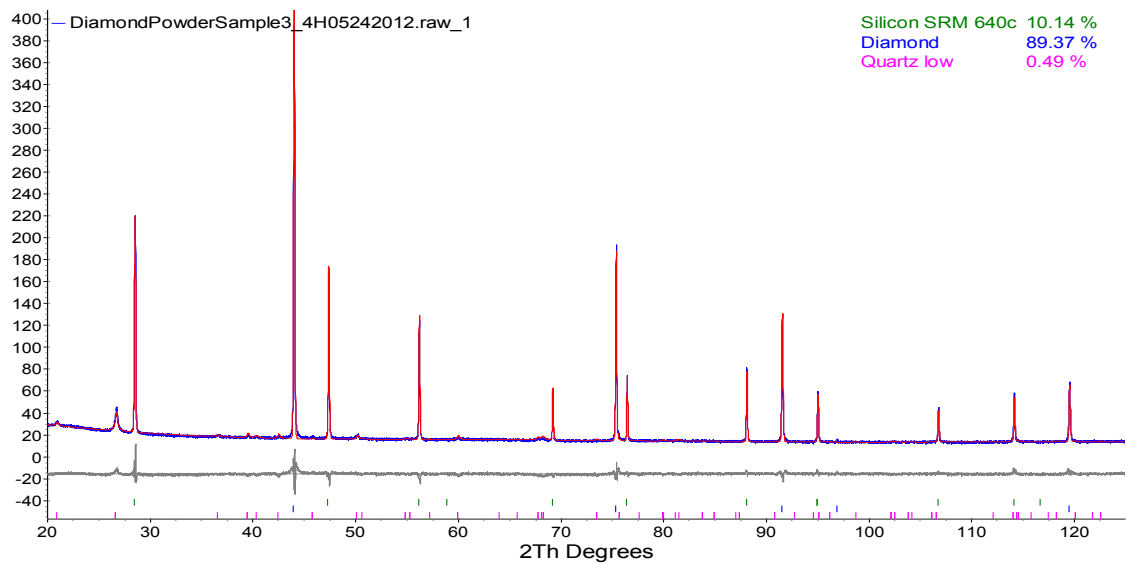
Figure 25: XRD Rietveld Analysis of Diamond Powder

Range Number : 1

Table 87: S6012C R-Values

Rexp	**Rwp**	Rp	GOF
4.06	**10.50**	7.73	2.59

Table 88: S6012C R-Values

Rexp	**Rwp**	Rp	DW
5.58	14.43	13.46	0.38

Table 89: S6012C Quantitative Analysis –Rietveld

Phase 1	Diamond	89.37 (14) %
Phase 2	Silicon SRM 640c	10.14 (13) %
Phase 3	Quartz low	0.488 (11) %

Table 90: S6012C Background

Chebychev polynomial, Coefficient	
0	322.50 (60)
1	-231.3 (11)
2	148.53 (66)
3	-82.04 (83)
4	52.70 (66)
5	-24.99 (44)

Table 91: S6012C Instrument

Primary radius (mm)	435
Secondary radius (mm)	435
Linear PSD 2Th angular range (°)	3
FDS angle (°)	1
Full Axial Convolution	
Filament length (mm)	12
Sample length (mm)	15
Receiving Slit length (mm)	12
Primary Sollers (°)	2.3
Secondary Sollers (°)	2.5

Table 92: S6012C Corrections

Zero error	-0.000 (18)
Specimen displacement	-0.420 (67)
LP Factor	27.3

Table 93: S6012C Structure 1

Phase name	Diamond
R-Bragg	1.821
Spacegroup	Fd-3mS
Scale	0.5157 (73)
Cell Mass	96.088

Cell Volume (Å^3)	45.39612 (44)
Wt% - Rietveld	89.37 (14)
Crystallite Size	
Cry size Lorentzian (nm)	3090 (910)
Strain	
Strain L	0.0031 (20)
Strain G	0.0208 (67)
Crystal Linear Absorption Coeff. (1/cm)	15.89866 (15)
Crystal Density (g/cm^3)	3.514808 (34)
Preferred Orientation (Dir 1 : 1 1 1)	0.6407 (37)

Table 94: S6012C PVII peak type

FWHM = a + b/Cos(Th) + c Tan(Th)	
a	0.0220 (36)
b	0.0120 (42)
c	0.0001 (24)

Table 95: S6012C PVII peak type

Exponent m = 0.6+ma+mb/Cos(Th)+mc/Tan(Th)	
ma	1.03 (59)
mb	0.45 (39)
mc	0.52 (10)

Table 96: S6012C Lattice parameters

a (Å)	3.567300 (11)

Table 97: S6012C Coordinate values

Site	Np	x	y	z	atom	Occ	Beq
C1	8	0.00000	0.00000	0.00000	C	1	1.397(43)

Table 98: S6012C Structure 2

Phase name	Silicon SRM 640c
R-Bragg	6.780
Spacegroup	Fd-3mS
Scale	0.007093 (24)
Cell Mass	224.683
Cell Volume (Å^3)	160.20870
Wt% - Rietveld	10.14 (13)
Crystallite Size	
Crystallite size Lorentzian (nm)	661 (29)
Strain	
Strain L	0.0001 (15)
Strain G	0.000 (12)
Crystal Linear Absorption Coeff. (1/cm)	148.913
Crystal Density (g/cm^3)	2.329

Table 99: S6012C PVII peak type

FWHM = a + b/Cos(Th) + c Tan(Th)	
a	0.0323 (47)
b	0.0043 (54)
c	0.0001 (31)

Table 100: S6012C PVII peak type

Exponent m = 0.6+ma+mb/Cos(Th)+mc/Tan(Th)	
ma	20 (150)
mb	5 (99)
mc	5 (20)

Table 101: S6012C Lattice parameters

a (Å)	**5.4311946**

Table 102: S6012C Coordinate values

Site	Np	x	y	z	atom	Occ	Beq
Si1	8	0.00000	0.00000	0.00000	Si	1	2.272(18)

Table 103: S6012C Structure 3

Phase name	Quartz low
R-Bragg	8.562
Spacegroup	P3221

Scale	0.0004103 (82)
Cell Mass	264.508
Cell Volume (Å^3)	113.151 (32)
Wt% - Rietveld	0.488 (11)
Crystallite Size	
Crystallite size Lorentzian (nm)	42.3 (14)
Crystal Linear Absorption Coeff. (1/cm)	174.325 (49)
Crystal Density (g/cm^3)	3.8818 (11)

Table 104: S6012C Lattice parameters

a (Å)				4.91534 (52)			
c (Å)				5.4078 (10)			
Site	Np	x	y	z	atom	Occ	Beq
Si1	6	0.4630	0.00000	0.66670	Si+4	1	0.8
O1	6	0.40900	0.27900	0.77400	O-2	1	0.9

Table 105: S6012C FWHM

	h	k	l	m	d	Th2	F^2
1	1	1	1	8	2.05958	43.92591	1039.248
2	0	2	2	12	1.26123	75.28765	1000.768
3	3	1	1	24	1.07558	91.47817	681.666
4	2	2	2	8	1.02979	96.83730	0.000

5	0	0	4	6	0.89182	119.47654	212.716
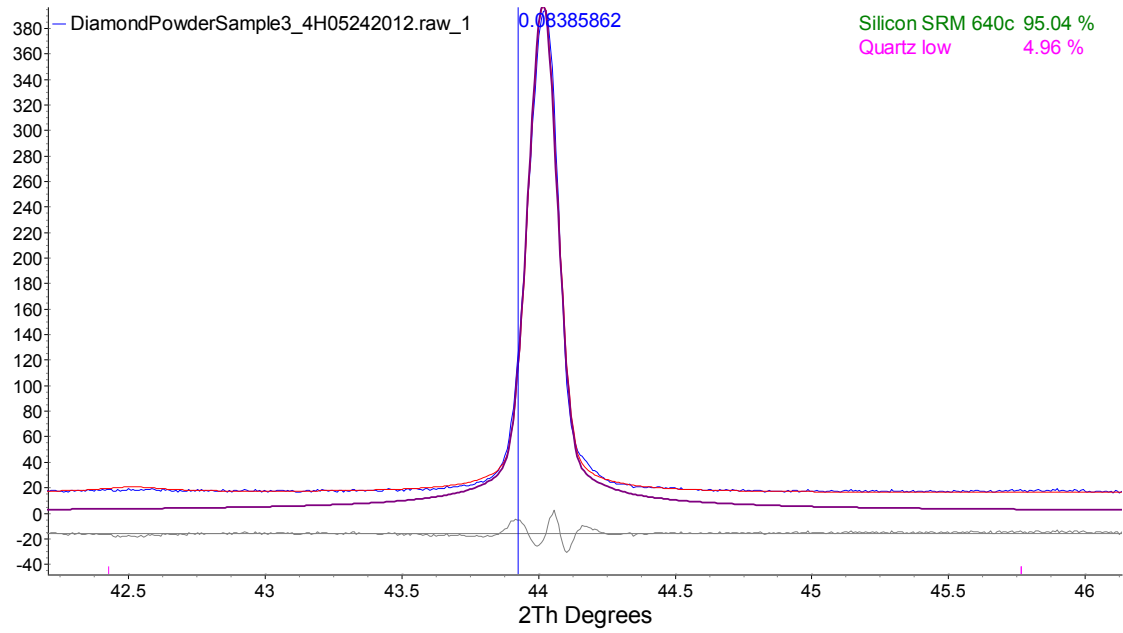
Figure 26: Full width half maximum (FWHM)

FWHM = 0.08386°2theta

5.7 S6012D Result

Diamond Powder (S6012D) Plasma treated Sample 4 05-25-12
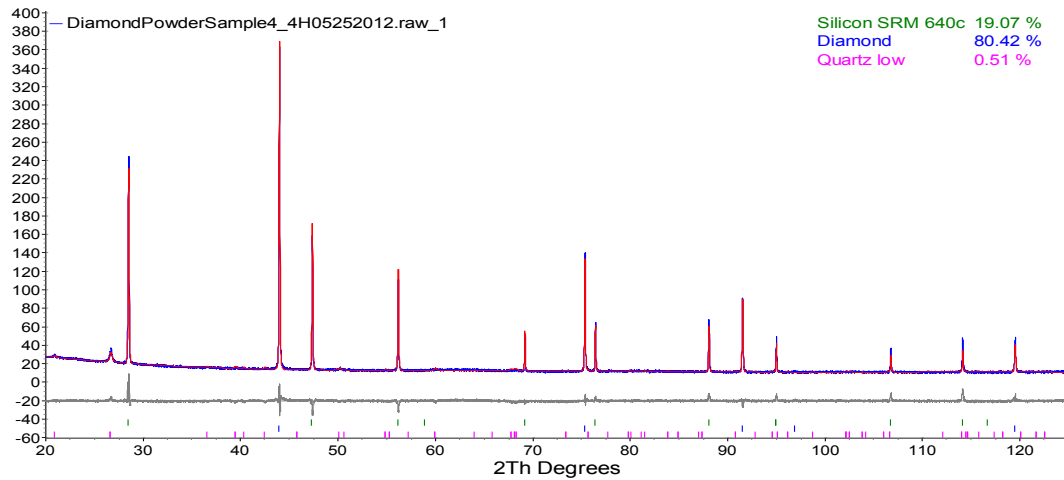
Figure 27: XRD Rietveld Analysis of Diamond Powder

145

Range Number : 1

Table 106: S6012D R-Values

Rexp	**Rwp**	Rp	GOF
4.89	**13.51**	10.04	2.77

Table 107: S6012D R-Values

Rexp	**Rwp**	Rp	DW
6.82	18.85	17.97	0.32

Table 108: S6012D Quantitative Analysis –Rietveld

Phase 1	Diamond	80.42 (35) %
Phase 2	Silicon SRM 640c	19.07 (34) %
Phase 3	Quartz low	0.508 (18) %

Table 109: S6012D Background

Chebychev polynomial, Coefficient	
0	244.35 (57)
1	-216.1 (10)
2	145.16 (85)
3	-87.15 (78)
4	49.74 (61)
5	-22.57 (56)

Table 110: S6012D Instrument

Primary radius (mm)	435
Secondary radius (mm)	435
Linear PSD 2Th angular range (°)	3
FDS angle (°)	1
Full Axial Convolution	
Filament length (mm)	12
Sample length (mm)	15
Receiving Slit length (mm)	12
Primary Sollers (°)	2.3
Secondary Sollers (°)	2.5

Table 111: S6012D Corrections

Zero error	-0.009 (15)
Specimen displacement	-0.367 (60)
LP Factor	27.3

Table 112: S6012D Structure 1

Phase name	Diamond
R-Bragg	2.030
Spacegroup	Fd-3mS
Scale	0.2491 (54)
Cell Mass	96.088

Cell Volume (Å^3)	45.39397 (52)
Wt% - Rietveld	80.42 (35)
Crystallite Size	
Cry size Lorentzian (nm)	2470 (740)
Strain	
Strain L	0.0001 (27)
Strain G	0.0584 (22)
Crystal Linear Absorption Coeff. (1/cm)	15.89942 (18)
Crystal Density (g/cm^3)	3.514975 (41)
Preferred Orientation (Dir 1 : 1 1 1)	0.5470 (35)

Table 113: S6012D PVII peak type

FWHM = a + b/Cos(Th) + c Tan(Th)	
a	0.0100 (72)
b	0.0081 (85)
c	0.0001 (48)

Table 114: S6012D PVII peak type

Exponent m = 0.6+ma+mb/Cos(Th)+mc/Tan(Th)	
ma	0.35 (57)
mb	0.40 (38)
mc	0.133 (72)

Table 115: S6012D Lattice parameters

a (Å)	3.567243 (14)

Table 116: S6012D Coordinate values

Site	Np	x	y	z	atom	Occ	Beq
C1	8	0.00000	0.00000	0.00000	C	1	1.424(67)

Table 117: S6012D Structure 2

Phase name	Silicon SRM 640c
R-Bragg	16.746
Spacegroup	Fd-3mS
Scale	0.007159 (31)
Cell Mass	224.683
Cell Volume (Å^3)	160.20870
Wt% - Rietveld	19.07 (34)
Crystallite Size	
Crystallite size Lorentzian (nm)	652 (32)
Strain	
Strain L	0.0001 (18)
Strain G	0.000 (10)
Crystal Linear Absorption Coeff. (1/cm)	148.913
Crystal Density (g/cm^3)	2.329

Table 118: S6012D PVII peak type

FWHM = a + b/Cos(Th) + c Tan(Th)	
a	0.0160 (78)
b	0.0089 (89)
c	0.0001 (46)

Table 119: S6012D PVII peak type

Exponent m = 0.6+ma+mb/Cos(Th)+mc/Tan(Th)	
ma	20 (350)
mb	5 (250)
mc	5 (41)

Table 120: S6012D Lattice parameters

a (Å)	**5.4311946**

Table 121: S6012D Coordinate values

Site	Np	x	y	z	atom	Occ	Beq
Si1	8	0.00000	0.00000	0.00000	Si	1	4.097(29)

Table 122: S6012D Structure 3

Phase name	Quartz low
R-Bragg	7.966
Spacegroup	P3221

Scale	0.0002293 (73)
Cell Mass	264.508
Cell Volume (Å^3)	113.138 (48)
Wt% - Rietveld	0.508 (18)
Crystallite Size	
Crystallite size Lorentzian (nm)	43.1 (23)
Crystal Linear Absorption Coeff. (1/cm)	174.346 (74)
Crystal Density (g/cm^3)	3.8822 (16)

Table 123: S6012D Lattice parameters

a (Å)				4.91402 (78)			
c (Å)				5.4101 (15)			
Site	Np	x	y	z	atom	Occ	Beq
Si1	6	0.4630	0.00000	0.66670	Si+4	1	0.8
O1	6	0.40900	0.27900	0.77400	O-2	1	0.9

Table 124: S6012D FWHM

	h	k	l	m	d	Th2	F^2
1	1	1	1	8	2.05955	43.92665	500.363
2	0	2	2	12	1.26121	75.28905	479.267
3	3	1	1	24	1.07556	91.48003	325.405
4	2	2	2	8	1.02977	96.83934	0.000

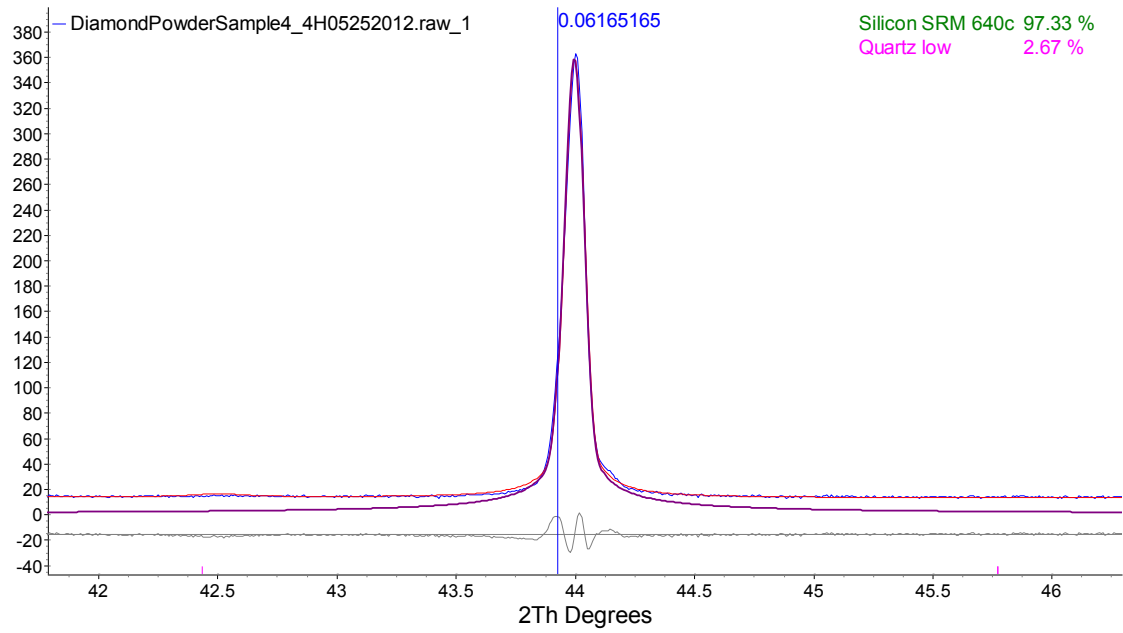| 5	0	0	4	6	0.89181	119.47964	101.002

Figure 28: Full width half maximum (FWHM)

FWHM = 0.0617 °2theta

REFERENCES

[1]   Hershey J. W., 2004, The Book Of Diamonds: Their Curious Lore, Properties, Tests And Synthetic Manufacture 1940, Kessinger Publishing.

[2]   Fan W. d., Chen X., Jagannadham K., and Narayan J., 1994, "Diamond-ceramic composite tool coatings," Journal of Materials Research, **9**(11), pp. 2850–2867.

[3]   Matthias T. R., Griffin N. D., and Hughes P. R., 2003, "Polycrystalline diamond cutters with working surfaces having varied wear ..."

[4]   Metals and Mining - Bain & Company - Publications, from http://www.bain.com/publications/articles/global-diamond-industry-lifting-veil-of-mystery.aspx.

[5]   Diamond Production Map - Gem-Quality Diamond Mining Countries, from http://geology.com/articles/gem-diamond-map/.

[6]   Kurin R., 2007, Hope Diamond: The Legendary History of a Cursed Gem, Harper Collins.

[7]   Time, Inc., 1955, "LIFE," Vol. 38, No. 8, pp.123.

[8]   Davis L.G, 1955, "Manufacture of Synthetic Diamonds," v66(n3240), pp. 91, 93, 95.

[9]   Benea I., Griffin S., and Doyle R., 2007, "Apparatus for measuring the crushing strength of micron superabrasives."

[10] Anthony T. R., 1995, "Stresses generated by impurities in diamond," Diamond and Related Materials, 4(12), pp. 1346–1352.

[11] Bovenkerk et.al, 1959, "Preparation of diamond," V 184, pp. 1094–1098.

[12] "Chemistry of Diamond," About.com Chemistry.

[13] Sumiya H., Toda N., and Satoh S., 1997, "Mechanical properties of synthetic type IIa diamond crystal," Diamond and Related Materials, 6(12), pp. 1841–1846.

[14] Meng Y., Newville M., Sutton S., Rakovan J., and Mao H. K., 2003, "Fe and Ni impurities in synthetic diamond," American Mineralogist, 88(10), pp. 1555–1559.

[15] "Synthetic diamonds still a rough cut - CNET News," CNET.

[16] De S., Heaney P. J., Hargraves R. B., Vicenzi E. P., and Taylor P. T., 1998, "Microstructural observations of polycrystalline diamond: a contribution to the carbonado conundrum," Earth and Planetary Science Letters, 164(3), pp. 421–433.

[17] Inspektor A., Oles E. J., and Bauer C. E., 1997, "Theory and practice in diamond coated metal-cutting tools," International Journal of Refractory Metals and Hard Materials, 15(1–3), pp. 49–56.

[18] Sung C. M., 1999, "Brazed diamond grid: a revolutionary design for diamond saws," Diamond and Related Materials, 8(8), pp. 1540–1543.

[19] Wentorf R. H., 1973, "Diamond tools for machining."

[20] Martin F. D., and Martin F. D., 1946, "Diamond Tool and Method of Making."

[21] Wapler H., Spooner T. A., and Balfour A. M., 1980, "Diamond coatings for increased wear resistance," Tribology International, 13(1), pp. 21–24.

[22] Zeren M., and Karagöz Ş., 2006, "Defect characterization in the diamond cutting tools," Materials Characterization, 57(2), pp. 111–114.

[23] Karagöz Ş., and Zeren M., 2001, "The microstructural design of diamond cutting tools," Materials Characterization, 47(2), pp. 89–91.

[24] Bremner I., and Bremner I., 1946, "Industrial Diamond Tool and Method Op Producing Same."

[25] Ikawa N., Donaldson R. R., Komanduri R., König W., Mckeown P. A., Moriwaki T., and Stowers I. F., 1991, "Ultraprecision metal cutting–the past, the present and the future," CIRP Annals-Manufacturing Technology, 40(2), pp. 587–594.

[26] Scott D. E., 2006, "The history and impact of synthetic diamond cutters and diamond enhanced inserts on the oil and gas industry," Proceedings.

[27] Sozer E., 2008, "GASEOUS DISCHARGES AND THEIR APPLICATIONS AS HIGH POWER PLASMA SWITCHES."

[28] Plasma, Plasma, Everywhere - NASA Science, from http://science.nasa.gov/science-news/science-at-nasa/1999/ast07sep99_1/.

[29] Chen F. F., 1984, Introduction to Plasma Physics and Controlled Fusion, Springer.

[30] Bittencourt J. A., 2004, Fundamentals of Plasma Physics, Springer.

[31] Moon P. K., Krick D. T., and Spurgin K. L., 2000, "Trench isolation process using nitrogen preconditioning to reduce crystal ..."

[32] Muenzer A., 1992, "Method for the passivation of crystal defects in polycrystalline silicon ..."

[33] All about the Sun, from http://www.extremescience.com/sun.htm.

[34] The Solar Atmosphere, from http://www.windows2universe.org/sun/solar_atmosphere.html.

[35] Genesis : Search for Origins | JPL | NASA, from http://genesismission.jpl.nasa.gov/science/mod3_SunlightSolarHeat/SolarStructure/.

[36] Pictures of the Solar Atmosphere, from http://cseligman.com/text/sun/sunatmosphere.htm.

[37] http://dsc.discovery.com/space/gallery/space-images/sun-solar-loop-625x450.jpg.

[38] Major characteristics of the sun, from

http://elearning.stkc.go.th/lms/html/earth_science/LOcanada9/901/3_2en.htm.

[39] Bogaerts A., Neyts E., Gijbels R., and van der Mullen J., 2002, "Gas discharge

plasmas and their applications," Spectrochimica Acta Part B: Atomic Spectroscopy,

57(4), pp. 609–658.

[40] Chapman B. N., 1980, Glow discharge processes: sputtering and plasma etching,

Wiley.

[41] Electric glow discharge - (The Plasma Universe Wikipedia-like Encyclopedia), from

http://www.plasma-universe.com/Electric_glow_discharge.

[42] Fridman A. A., and Kennedy L. A., 2004, Plasma Physics and Engineering, Taylor

& Francis.

[43] Hiraki A., and Miyasato T., 1988, "Process of depositing diamond-like thin film by

cathode sputtering."

[44] Veronis G., Inan U. S., and Pasko V. P., 2000, "Fundamental properties of inert gas

mixtures for plasma display panels," IEEE Transactions on Plasma Science, 28(4),

pp. 1271 –1279.

[45] Zhao J. W., Wang Z., and Catabay W. G., 1997, "Plasma clean with hydrogen gas."

[46] XRD, from http://www.bccmeteorites.com/XRD.PDF.

[47] Dinnebier R. E., 2008, Powder Diffraction: Theory and Practice, Royal Society of

Chemistry.

[48] Klein C., Hurlbut C. S., and Dana J. D., 1993, Manual of mineralogy, Wiley New

York.

[49] Brown A., and Suit H., 2004, "The centenary of the discovery of the Bragg peak," Radiotherapy and Oncology, 73(3), pp. 265–268.

[50] XRD-Intro, from http://epswww.unm.edu/xrd/xrdclass/01-XRD-Intro.pdf.

[51] DIFFRACTION AND RFLECTION, from http://www.tufts.edu/as/tampl/projects/micro_rs/theory.html.

[52] Description of crystal lattice structures, from http://departments.kings.edu/chemlab/animation/.

[53] Lattice Planes and Miller Indices - Parallel lattice planes, from http://www.doitpoms.ac.uk/tlplib/miller_indices/lattice.php.

[54] Sirajuddeen M. S., 2011, "Crystal Physics, from http://msheiksirajuddeen.blogspot.com/2011/08/crystal-physics.html," Mohamed sheik sirajuddeen.

[55] Lattice Planes and Miller Indices - Worked examples, from http://www.doitpoms.ac.uk/tlplib/miller_indices/worked_examples.php.

[56] Bragg's Law and Diffraction, from http://www.eserc.stonybrook.edu/projectjava/bragg/.

[57] Powder Diffraction, from http://pd.chem.ucl.ac.uk/pdnn/diff2/kinemat2.htm.

[58] Xray_diffraction_2004, from http://physics.usask.ca/~bzulkosk/modphyslab/phys381manual/xray_diffraction_2004.pdf.

[59] A brief history of X-rays — ESRF, from http://www.esrf.eu/AboutUs/AboutSynchrotron/XRays.

[60] Kreyssig_1, from http://cmp.physics.iastate.edu/canfield/course/Kreyssig_1.pdf.

[61] X-Ray Generation Notes, from http://xrayweb.chem.ou.edu/notes/xray.html.

[62] SR history, from http://www.aps.anl.gov/asd/diagnostics/uspas03/SR_history.pdf.

[63] History of Synchrotron Radiation Sources, from http://xdb.lbl.gov/Section2/Sec_2-2.html.

[64] Yu P., and Mei X., 2012, "The Stability Analysis of the Relativity Motion of Charged Particles in Electromagnetic Fields and the Possibility to Establish Synchrocyclotron without Radiation Losses," Applied Physics Research, 4(2).

[65] History of Synchrotron light, from http://www.odec.ca/projects/2005/shar5a0/public_html/history_of_synchrotron_light.htm.

[66] X-ray sources, from http://www.ruppweb.org/Xray/x-ray_sources.html.

[67] Basics of X-Ray Powder Diffraction, from http://prism.mit.edu/xray/Basics%20of%20X-Ray%20Powder%20Diffraction.pdf.

[68] X-ray Detectors, from http://pd.chem.ucl.ac.uk/pdnn/inst1/detects.htm.

[69] Sample Holders, from http://pd.chem.ucl.ac.uk/pdnn/inst1/mounts.htm.

[70] X_ray_diffraction, from http://203.199.213.48/1745/1/x_ray_diffraction.pdf.

[71] Monochromators, from http://pd.chem.ucl.ac.uk/pdnn/inst1/monoc.htm.

[72] Instrument X-ray Optics: Reflection Geometry, from http://pd.chem.ucl.ac.uk/pdnn/inst1/optics1.htm.

[73] USGS Information Handout: X-Ray Powder Diffraction, from http://pubs.usgs.gov/info/diffraction/html/index.html.

[74] X-ray Powder Diffraction (XRD), from http://serc.carleton.edu/research_education/geochemsheets/techniques/XRD.html.

[75] Fundamentals of 2- D x ray diffraction, from

http://www.icdd.com/resources/axa/vol43/v43_037.pdf.

[76] Diamond Lapping, Honing, Grinding, Superabrasives – Engis Corp., from

http://www.engis.com/.

[77] Particle Size and Particle Size Distribution - The Measurement and Modelling for

Ceramic Casting Sli, from http://www.azom.com/article.aspx?ArticleID=2794.

VITA

Graduate College
University of Nevada, Las Vegas

Rohit Asuri Sudharshana Chary

Degrees:

Bachelor of Technology, Mechanical Engineering, 2009
Jawaharlal Nehru Technological University, Hyderabad

Thesis title: Plasma test on Industrial Diamond Powder in Hydrogen and Air for Fracture Strength Study

Thesis Examination Committee:
Chairperson, Zhiyong Wang, Ph.D.
Committee Member, Brendan O'Toole, Ph.D.
Committee Member, V.C.Venkatesh, Ph.D.
Graduate Faculty Representative, Venkatesan Muthukumar, Ph.D.